

**Some pages of this thesis may have been removed for copyright restrictions.**

If you have discovered material in AURA which is unlawful e.g. breaches copyright, (either yours or that of a third party) or any other law, including but not limited to those relating to patent, trademark, confidentiality, data protection, obscenity, defamation, libel, then please read our [Takedown Policy](#) and [contact the service](#) immediately

# Use of Imaging Technology to Better Understand Soft Contact Lens Fit Dynamics

**LEE ANTHONY HALL**

Doctor of Philosophy

**ASTON UNIVERSITY**

AUGUST 2014

©Lee Anthony Hall, 2014

Lee Anthony Hall asserts his moral right to be identified as the author of this thesis

This copy of the thesis has been supplied on condition that anyone who consults it is understood to recognise that its copyright rests with its author and that no quotation from the thesis and no information derived from it may be published without appropriate permission or acknowledgement.

ASTON UNIVERSITY

## OPHTHALMIC RESEARCH GROUP

Use of Imaging Technology to Better Understand Soft Contact Lens Fit Dynamics

LEE ANTHONY HALL

Doctor of Philosophy

AUGUST 2014

### Thesis Summary

The principal theme of this thesis is the identification of additional factors affecting, and consequently to better allow, the prediction of soft contact lens fit. Various models have been put forward in an attempt to predict the parameters that influence soft contact lens fit dynamics; however, the factors that influence variation in soft lens fit are still not fully understood. The investigations in this body of work involved the use of a variety of different imaging techniques to both quantify the anterior ocular topography and assess lens fit.

The use of Anterior-Segment Optical Coherence Tomography (AS-OCT) allowed for a more complete characterisation of the cornea and corneoscleral profile (CSP) than either conventional keratometry or videokeratoscopy alone, and for the collection of normative data relating to the CSP for a substantial sample size. The scleral face was identified as being rotationally asymmetric, the mean corneoscleral junction (CSJ) angle being sharpest nasally and becoming progressively flatter at the temporal, inferior and superior limbal junctions. Additionally, 77% of all CSJ angles were within  $\pm 5^\circ$  of  $180^\circ$ , demonstrating an almost tangential extension of the cornea to form the paralimbal sclera. Use of AS-OCT allowed for a more robust determination of corneal diameter than that of white-to-white (WTW) measurement, which is highly variable and dependent on changes in peripheral corneal transparency. Significant differences in ocular topography were found between different ethnicities and sexes, most notably for corneal diameter and corneal sagittal height variables.

Lens tightness was found to be significantly correlated with the difference between horizontal CSJ angles ( $r = +0.40$ ,  $P = 0.0086$ ). Modelling of the CSP data gained allowed for prediction of up to 24% of the variance in contact lens fit; however, it was likely that stronger associations and an increase in the modelled prediction of variance in fit may have occurred had an objective method of lens fit assessment have been made.

A subsequent investigation to determine the validity and repeatability of objective contact lens fit assessment using digital video capture showed no significant benefit over subjective evaluation. The technique, however, was employed in the ensuing investigation to show significant changes in lens fit between 8 hours (the longest duration of wear previously examined) and 16 hours, demonstrating that wearing time is an additional factor driving lens fit dynamics.

The modelling of data from enhanced videokeratoscopy composite maps alone allowed for up to 77% of the variance in soft contact lens fit, and up to almost 90% to be predicted when used in conjunction with OCT.

The investigations provided further insight into the ocular topography and factors affecting soft contact lens fit.

**Keywords/Phrases:** Corneoscleral Topography; Corneal Diameter; Optical Coherence Tomography (OCT); Objective Lens Fit Assessment; Soft Contact Lens Fit.

## **Acknowledgments**

There are many people I would like to thank who have helped me on the journey to the submission of this thesis. Firstly, my supervisor Professor James Wolffsohn, for his extensive guidance, unwavering kindness, enthusiasm and support throughout the duration of my studies.

I would also like to thank my associate supervisor Dr Graeme Young, the inspiration for this work and with whom I have spent many hours discussing and debating the nature of contact lens fit.

Mr Chris Hunt for his advice and support in the production of the statistical modelling undertaken in this thesis. I would also like to thank Louise Nicklin for her help in the collection of data for Chapter 3.

My colleagues and friends in the academic field, especially Dr's Eef van der Worp and Amit Jinabhai for their support, mentoring and encouragement throughout the duration of my PhD studies.

To all of those at Aston University, especially: Dr Leon Davies for agreeing to be my first year viva examiner; Professor Bernard Gilmartin and Dr Hetal Patel for their kind input and reflections as to the nature of the development of the eye as a biological structure; and Dr Thomas Drew for his extensive technical advice, guidance and good humour, all given in full and without reserve – thank you.

Finally, I would like to thank the LHS post-graduate support staff, Gill Pilfold and Matt Richards for gently keeping me on the administrative straight and narrow throughout the duration of my research.

On a personal note, I would also like to thank my friends for their help and support. In no particular order, they are as follows: Cameron, Cath, Linda, Martin, Rachel, David, Lisa and Simon, and many more too numerous to mention, all who have enlightened my path with their friendship and support over the years – thank you.

“Per aspera ad astra”

# Table of Contents

<b>Acknowledgments</b> .....	<b>3</b>
<b>Table of Contents</b> .....	<b>5</b>
<b>List of Tables</b> .....	<b>8</b>
<b>List of Figures</b> .....	<b>10</b>
<b>List of Acronyms</b> .....	<b>12</b>
<b>Chapter 1: Thesis Introduction</b> .....	<b>14</b>
1.0 Vision Impairment and the Soft Contact Lens Market.....	14
1.1 Soft Contact Lens Fit Theory .....	15
1.1.1 Lens Movement.....	15
1.1.2 Squeeze Pressure .....	17
1.1.3 Rubber Band Theory .....	18
1.1.4 Sagittal Depth.....	19
1.2 The Ocular Topography and Soft Contact Lens Fit.....	25
1.2.1 Soft Contact Lens Fit.....	25
1.2.2 Corneoscleral Topography .....	26
1.3 Imaging, Measuring and Mapping the Anterior Ocular Surface .....	28
1.3.1 Imaging.....	28
1.3.2 Slit Lamp Biomicroscopy and Photography.....	28
1.3.3 Keratometry .....	29
1.3.4 Keratoscopy.....	31
1.3.5 Reflection-Based Systems - Videokeratoscopy .....	33
1.3.6 Projection-Based Systems .....	34
1.3.7 Anterior Segment Optical Coherence Tomography.....	39
1.3.8 Summary of Imaging Techniques .....	42
1.4 Thesis Aims and Objectives .....	44
<b>Chapter 2: The Influence of Corneoscleral Topography on Soft Contact Lens Fit</b> .....	<b>46</b>
2.1 Introduction .....	46
2.2 Method.....	47
2.2.1 Statistical Analysis .....	55
2.3 Results .....	56
2.3.1 Biometric Data .....	56
2.3.2 Ocular Dimensions .....	56
2.3.3 Repeatability and Reliability.....	58

2.3.4 Lens Fit .....	59
2.3.5 Lens Fit Correlations.....	59
2.4 Discussion.....	62
2.5 Conclusion .....	64
<b>Chapter 3: Factors Affecting Corneoscleral Topography .....</b>	<b>66</b>
3.1 Introduction .....	66
3.2 Method.....	67
3.2.1 Statistical Analysis .....	72
3.3 Results .....	74
3.3.1 Biometric Data .....	74
3.3.2 Ocular Dimensions .....	78
3.3.3 Correlations between Ocular Topography Variables .....	84
3.3.4 Factors Affecting Ocular Topography Variables.....	86
3.4 Discussion.....	90
3.5 Conclusion .....	93
<b>Chapter 4: Subjective versus Objective Contact Lens Fit Assessment .....</b>	<b>95</b>
4.1 Introduction .....	95
4.2 Method.....	96
4.2.1 Subjective Lens Fit Analysis.....	97
4.2.2 Objective Lens Fit Analysis .....	97
4.2.3 Statistical Analysis .....	100
4.3 Results .....	102
4.3.1 Validity.....	102
4.3.2 Repeatability .....	107
4.4 Discussion.....	108
4.5 Conclusion .....	110
<b>Chapter 5: The Influence of End of Day Fit .....</b>	<b>112</b>
5.1 Introduction .....	112
5.2 Method.....	113
5.2.1 Statistical Analysis .....	115
5.3 Results .....	116
5.3.1 Lens Fit .....	116
5.3.2 Ocular Comfort.....	119
5.3.3 Ocular Physiology .....	119

5.3.4 Lens Wettability .....	124
5.4 Discussion.....	125
5.5 Conclusion .....	127
<b>Chapter 6: Prediction of Soft Contact Lens Fit Using Enhanced Corneal Topography.....</b>	<b>129</b>
6.1 Introduction .....	129
6.2 Method.....	130
6.2.1 Statistical analysis .....	134
6.3 Results .....	134
6.3.1 Biometric Data .....	134
6.3.2 Maximum Chord Width Obtained Using Single versus Composite Scans.....	134
6.3.2 Lens Fit .....	139
6.4 Discussion.....	141
6.5 Conclusion .....	142
<b>Chapter 7: Thesis Discussion.....</b>	<b>144</b>
7.1 Introduction .....	144
7.2 Lens Fit and Variation.....	144
7.3 Instrumentation and Technology.....	147
7.4 Clinical Implications.....	148
7.5 Conclusion .....	149
<b>Bibliography .....</b>	<b>150</b>
<b>Appendix 1: Published Papers .....</b>	<b>164</b>

## List of Tables

Table		Page
<b>Chapter 1</b>		
<b>1.1</b>	Summary of corneal diameter measurements and techniques used from the existing literature	<b>21/22</b>
<b>Chapter 2</b>		
<b>2.1</b>	Abbreviations of ocular measurement variables	<b>53</b>
<b>2.2</b>	Ocular topography measurements by videokeratoscopy and slit-lamp	<b>56</b>
<b>2.3</b>	Ocular topography variables by AS-OCT	<b>57</b>
<b>2.4</b>	Repeatability and reliability of ocular topography results by AS-OCT	<b>58</b>
<b>2.5</b>	Lens fit results	<b>59</b>
<b>2.6</b>	Significant lens fit correlations with corneoscleral shape parameters	<b>60</b>
<b>2.7</b>	Stepwise multiple regression analysis with keratometry, keratometry and videokeratoscopy, and keratometry, videokeratoscopy (VK) and anterior segment optical coherence tomography (AS-OCT) variables	<b>61</b>
<b>Chapter 3</b>		
<b>3.1</b>	Abbreviations of ocular measurement values	<b>69</b>
<b>3.2</b>	Sample size calculations, assuming a power of 80% and alpha value of 0.01	<b>73</b>
<b>3.3</b>	Summary of correlations between right and left eyes for all ocular variables	<b>75</b>
<b>3.4</b>	Summary of Shapiro-Wilk Tests for deviations from normality	<b>76</b>
<b>3.5</b>	Mean spherical equivalent refractive error by age and sex	<b>77</b>
<b>3.6</b>	Ocular topography variables	<b>79</b>
<b>3.7</b>	Classifications of corneoscleral profile according to corneoscleral junction angle	<b>83</b>
<b>3.8</b>	Significant correlations between ocular variables	<b>84</b>
<b>3.9</b>	Significant correlations with subject age, height and refractive error	<b>87</b>
<b>3.10</b>	Summary of multivariate analysis	<b>88</b>
<b>3.11</b>	Ocular topography variables by ethnicity and sex	<b>89</b>
<b>Chapter 4</b>		
	No tables	
<b>Chapter 5</b>		
<b>5.1</b>	Study lens specifications	<b>114</b>
<b>5.2</b>	Relationship in fit variables between lens brands with time	<b>117</b>
<b>5.3</b>	Effect of lens fit (correlations coefficients) on comfort and relationship between lens brands	<b>120</b>

<b>5.4</b>	Relationship in ocular comfort, physiology and lens wettability between lens brands	<b>121</b>
<b>5.5</b>	Effect of lens fit (correlations coefficients) on ocular physiology and relationship between lens brands	<b>122</b>
<b>5.6</b>	Effect of lens fit (correlations coefficients) on ocular physiology and relationship between lens brands	<b>123</b>

### **Chapter 6**

<b>6.1</b>	Medmont videokeratometry measurements	<b>133</b>
<b>6.2</b>	AS-OCT ocular topography measurements	<b>133</b>
<b>6.3</b>	Summary of maximum chord lengths acquired with single vs. composite Medmont scans (right eye)	<b>135</b>
<b>6.4</b>	Summary of maximum chord lengths acquired with single vs. composite Medmont scans (left eye)	<b>136</b>
<b>6.5</b>	Comparison of maximum chord length by meridian for the single, composite of five and composite of nine scans, respectively	<b>139</b>
<b>6.6</b>	Stepwise multiple regression analysis with keratometry; keratometry and single scan videokeratometry (VK); composite of five videokeratometry; composite of nine videokeratometry; composite of five videokeratometry and anterior segment OCT (AS-OCT); composite of nine videokeratometry and anterior segment OCT variables	<b>140</b>

## List of Figures

Figure		Page
<b>Chapter 1</b>		
<b>1.1</b>	Schematic showing the Pre-Lens Tear Film (PLTF) and Post-Lens Tear Film (PoTLF) with a soft contact lens	<b>17</b>
<b>1.2</b>	Change in sagittal depth with diameter/chord length	<b>20</b>
<b>1.3</b>	Tomographs showing variation in limbal transparency between subjects. <b>(a)</b> Tomograph showing well-defined limbal junctions <b>(b)</b> Tomograph showing marked loss of transparency, and thus poorly defined limbal junctions in the peripheral cornea	<b>23</b>
<b>1.4</b>	Change in sagittal depth with corneal eccentricity	<b>24</b>
<b>1.5</b>	Classification of corneoscleral transition profile, according to Gaggioni and Meier	<b>27</b>
<b>1.6</b>	Data measurement and presentation by projection-based and reflection-based corneal topography systems	<b>32</b>
<b>1.7</b>	Slit beam projected from the right during the Orbscan's corneal scan	<b>35</b>
<b>1.8</b>	Scheimpflug image of the anterior segment in cross-section	<b>36</b>
<b>1.9</b>	Overview of OCT devices commercially available	<b>40</b>
<b>1.10</b>	<b>(a)</b> Ocular imaging coverage with keratometric and keratoscopic imaging techniques <b>(b)</b> Additional ocular imaging coverage with scanning-slit/Scheimpflug and OCT imaging techniques	<b>43</b>
<b>Chapter 2</b>		
<b>2.1</b>	<b>(a)</b> Zeiss Visante AS-OCT device with external fixation markers seen from the subject's perspective <b>(b)</b> Zeiss Visante AS-OCT device with external fixation markers seen from the operator's perspective	<b>48/49</b>
<b>2.2</b>	<b>(a)</b> Schematic of OCT ocular topography measurements <b>(b)</b> Zeiss Visante OCT scan showing ocular topography measurements	<b>51/52</b>
<b>Chapter 3</b>		
<b>3.1</b>	OCT ocular topography measurements	<b>68</b>
<b>3.2</b>	<b>(a)</b> Concave corneoscleral profile <b>(b)</b> Flat corneoscleral profile <b>(c)</b> Convex corneoscleral profile	<b>70/71</b>
<b>3.3</b>	Frequency distribution of mean spherical equivalent	<b>77</b>
<b>3.4</b>	Frequency distribution of <b>(a)</b> horizontal and <b>(b)</b> vertical corneal diameter	<b>80</b>
<b>3.5</b>	Frequency distribution of <b>(a)</b> horizontal and <b>(b)</b> vertical corneal sagittal height	<b>81</b>
<b>3.6</b>	Frequency distribution of corneoscleral junction angles	<b>82</b>

<b>3.7</b>	Comparison of the horizontal corneal sagittal height measurements of a chord at 10 mm by computerized videokeratography and OCT and the average measurement (right eyes only), showing the 95% limits after Bland-Altman.	<b>85</b>
<b>Chapter 4</b>		
<b>4.1</b>	Determination of lens centration by objective means	<b>98</b>
<b>4.2</b>	Determination of movement on blink using LabVIEW software	<b>99</b>
<b>4.3</b>	Speed of Drop Calculator using purpose-developed LabVIEW software	<b>101</b>
<b>4.4</b>	Bland-Altman plot of the difference in vertical centration compared to the mean for subjective versus objective measurement, interobserver assessment, objective repeatability and subjective repeatability.	<b>102</b>
<b>4.5</b>	Bland-Altman plot of the difference in horizontal centration compared to the mean for subjective versus objective measurement, interobserver assessment, objective repeatability and subjective repeatability.	<b>103</b>
<b>4.6</b>	Bland-Altman plot of the difference in movement on blink compared to the mean for subjective versus objective measurement, interobserver assessment, objective repeatability and subjective repeatability.	<b>104</b>
<b>4.7</b>	Bland-Altman plot of the difference in horizontal lag compared to the mean for subjective versus objective measurement, interobserver assessment, objective repeatability and subjective repeatability.	<b>105</b>
<b>4.8</b>	Box-plot of objective push-up recovery mean (line), standard deviation (box), 95% confidence interval (bars) and outliers (dots) for subjective push-up recovery grades.	<b>106</b>
<b>Chapter 5</b>		
<b>5.1</b>	Summary of study design/wearing schedule	<b>113</b>
<b>5.2</b>	Movement on blink between study lenses with time after insertion	<b>116</b>
<b>5.3</b>	Increase in lag between study lenses with time after insertion	<b>118</b>
<b>5.4</b>	Push-up recovery speed between study lenses with time after insertion	<b>119</b>
<b>Chapter 6</b>		
<b>6.1</b>	Medmont E300 corneal topography scans captured in the four main cardinal directions of gaze	<b>131</b>
<b>6.2</b>	Medmont E300 corneal topography scans captured in the oblique directions of gaze	<b>132</b>
<b>6.3</b>	Plot showing the maximum measurable chord width using single versus composite Medmont scans	<b>137</b>
<b>6.4</b>	Plot showing the maximum measurable chord width using single versus composite Medmont scans.	<b>138</b>

## List of Acronyms

<u>Acronym</u>	<u>Full Format</u>	<u>Acronym</u>	<u>Full Format</u>
AS-OCT	Anterior Segment Optical Coherence Tomography	LZ	Limbal Zone
BOZR	Back Optic Zone Radius	MSE	Mean Spherical Equivalent
CD	Corneal Diameter	NITBUT	Non-invasive Tear Break-Up Time
CS	Corneal Sagittal Height	OCLR	Optical Low-Coherence Reflectometry
CS10	Corneal Sagittal Height of a Chord of 10 mm	OCT	Optical Coherence Tomography
CSJ	Corneoscleral Junction	OS15	Ocular Sagittal Height of a Chord of 15 mm
CSP	Corneoscleral Profile		
CVK	Computerised Videokeratometry	PA	Palpebral Aperture
		PBM	Post Blink Movement
D	Dioptre	PCTF	Pre Corneal Tear Film
DC	Dioptre Cylinder	PEK	Photo-Electric Keratoscope
DPFP	Double Projector Fourier Profilometry	PCI	Partial Coherence Interferometry
DSP	Digital Signal Processing units	PLTF	Pre-Lens Tear Film
		POLTF	Post-Lens Tear Film
e	Corneal Eccentricity		
EBC	Equivalent Base Curve	SD-OCT	Spectral Domain OCT
		SF	Shape Factor
FD-OCT	Fourier Domain OCT	SKI	Standard Keratometric Index
		SLD	Super-luminescent Diode
HCD	Horizontal Corneal Diameter	SR	Scleral Radius
HEMA	Hydroxyethylmethacrylate	SS-OCT	Swept Source OCT
HVID	Horizontal Visible Iris Diameter	SST	Slit Scanning Topography
HWTW	Horizontal White-to-White		
		TD-OCT	Time Domain OCT
ID	Iris Diameter		
IOL	Intra-Ocular Lens	VK	Videokeratometry
$J_0$	Resultant Cylindrical Power at 0°	WTW	White-To-White
$J_{45}$	Resultant Cylindrical Power at 45°		

# Chapter 1

# Chapter 1: Thesis Introduction

## 1.0 Vision Impairment and the Soft Contact Lens Market

It is estimated globally that some 285 million people suffer visual impairment, 43% of which is attributable to uncorrected refractive error (Pascolini and Mariotti, 2012). Contact lenses provide an affordable, convenient and cosmetically acceptable alternative to the correction of refractive error with spectacles, and the contact lens market continues to grow as a result of advances in material science, manufacturing techniques and innovation made by lens companies and researchers worldwide.

In 2000 the expected worldwide contact lens market was valued at an estimated \$3 billion, with approximately 80 million contact lens wearers worldwide and some 33 million in the US alone (Barr, 2000). Today sales are worth approximately \$7.6 billion (Nichols, 2014) and, with an estimated 125 million wearers worldwide, some are predicting global sales of \$11.7 billion by 2015 (Nichols, 2011).

The UK market has undergone similarly rapid growth in the same period. Sales of contact lenses were worth in excess of £234.4 million in the UK in 2012, up 230 % from £101.9 million in 2000, with the sale of some 606 million lenses in 2012 alone. Not surprisingly, the numbers of contact lens wearers also increased, from 2.5 million in 2000 to in excess of 3.7 million in 2012, with lens wearers now representing 9.0 % of the UK adult population (Kerr and McParland, 2013).

The international contact lens market is composed of sales of rigid, soft, scleral and hybrid contact lenses. However, in their annual survey of international prescribing trends for 2013, Morgan et al. (2014) reported that soft contact lens fitting dominated most of the worldwide markets, accounting for close to 100% of new fits in Australia, Canada, China, Denmark, Greece, Indonesia, Norway, Portugal, Russia, Sweden, the UK and US, and some 88% of new fits worldwide overall. Rigid lens fitting by comparison only accounted for 12% of contact lens fits worldwide in the same period.

In light of the overwhelming predominance of soft contact lenses in the marketplace (Naroo, 2011) and, some might say, the terminal decline of rigid lens fitting (Efron, 2010), this thesis will consider the use of imaging technology to better understand soft contact lens fit dynamics only.

## **1.1 Soft Contact Lens Fit Theory**

Despite the size of the soft contact lens market, relatively little is still known to fully account for the variation in contact lens fit in, and between, different soft contact lens wearers. For instance, why is it that a lens of known and fixed parameters may fit the eye of one wearer, but not fit that of the eye of a different wearer of apparently similar geometry? Why do soft lenses show excessive movement on some eyes and not on others, and why do some lenses show perfect centration on some eyes but decentre on another? Various clinical and theoretical models have been developed in an attempt to predict the lens and anterior eye parameters that influence soft contact lens fit dynamics and answer questions like these.

### **1.1.1 Lens Movement**

Lens movement is essential to ensure adequate tear interchange to provide sufficient oxygen levels and to remove trapped debris, inflammatory cells and other tear components that accumulate under the lens (McNamara et al., 1999). Multiple models of lens fit were put forward in the 1970s and 1980s, with many specifically relating to lens movement. Proposing a theoretical model based on clinical observations, Bibby and Tomlinson (1983) related soft contact lens movement in terms of lens design parameters, specifically lens thickness, total diameter and sagittal depth. They concluded that when lens thickness is reduced, the sagittal depth of the base curve must also be reduced, i.e. flattened, in order to maintain a given amount of movement. They also concluded that a smaller range of base curves would be needed to fit the range of sagittal depths normally encountered in the human population when such a reduction in thickness was made. However, their model was generally limited to thicker lenses and could not always account for the movement of relatively thin lenses.

In a review of available literature at the time, Knoll and Conway (1987) subsequently hypothesised the nature of blink-induced vertical movement in both rigid and soft contact lenses, taking into consideration post-lens tear film (PoLTF) characteristics, lens diameter and the geometry of the anterior segment of the eye. For soft lenses they concluded that both the greater lens diameter and thinner PoLTF layer associated with soft lenses resulted in much less movement than with their rigid lenses, although this was not quantified. Following on from the work of Mandell (1962) who described a 'ramp' of approximately 13° between the cornea and sclera, Knoll and Conway further postulated that lens movement was also reduced with soft lenses because additional force is required to overcome interaction of the lens at the corneoscleral junction interface, despite the inherent flexibility of the lens.

The introduction of much thinner, lower-water content, cast-moulded soft contact lenses such as the etafilcon A Acuvue® (Johnson & Johnson, Jacksonville, FL, US) range of lenses in the late 1980s, saw a significant change in observed lens movement compared to that seen with the more traditional lathe cut low or high water content hydroxyethylmethacrylate (HEMA) lenses that had preceded.

Investigating this, Little and Bruce (1994) assessed the movement of mid-water Acuvue lenses in a study conducted over a 6 hour period on each of two consecutive days. Whereas lens movement of thick low water content lenses had previously been found to be (largely) dependent on the relationship between lens diameter and back optic zone radius (BOZR) to the ocular surface contour (Bibby, 1979b, Lowther and Tomlinson, 1981, Garner, 1982), Little and Bruce speculated that an alternative, or complementary, dynamic may occur where thinner (or higher water content) lenses may be 'lubricated' by the pre-lens (PLTF) and PoLTF tear films (Figure 1.1). Since movement could be considered as a product of interaction between the lens and the upper eyelid, they reasoned that movement in such lenses might be modulated by shear forces in the pre-lens and post lens tear films. Having made objective assessments of lens movement, PoLTF status and tear meniscus height, they found that median lens movement of the thinner cast-moulded lenses was close to zero on insertion, increasing to only 0.34 and 0.30 mm one hour post insertion. They also reported that there was covariance in PoLTF and lens movement for some subjects, suggesting that the PoLTF was a significant determinant of hydrogel lens movement.

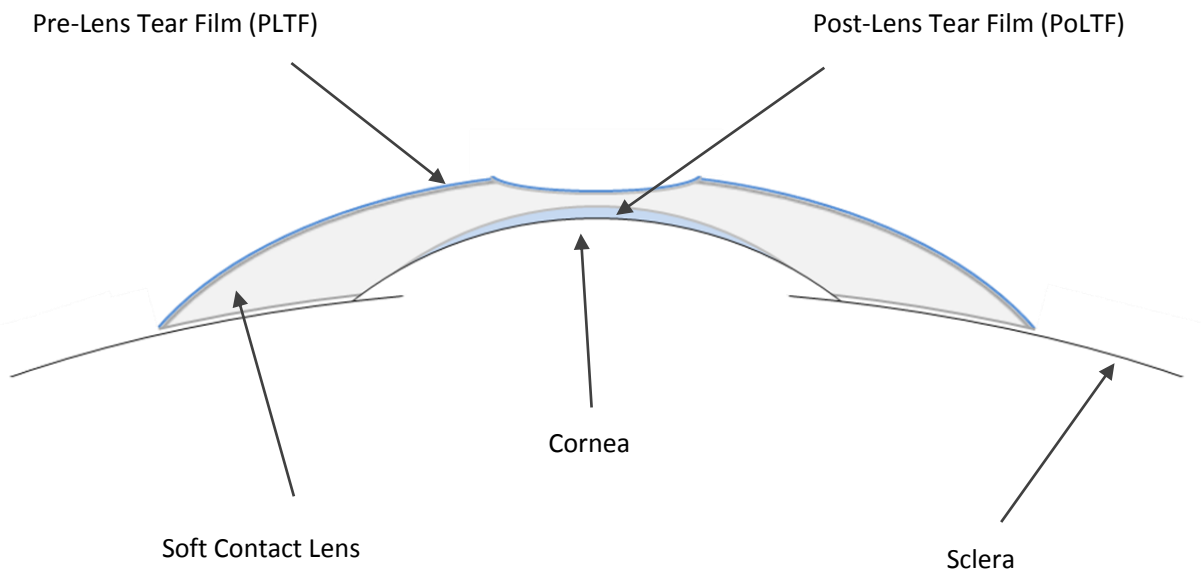


**Figure 1.1:** Schematic showing the Pre-Lens Tear Film (PLTF) and Post-Lens Tear Film (PoLTF) with a soft contact lens (not to scale)

Clearly, lens movement models only partially account for the variance in soft lens fit, and relatively little basic work has been published on the dynamics governing lens movement since the 1970s and 1980s. It is likely that this is due to the change to cast-moulding techniques now largely adopted by manufacturers, resulting in substantially reduced lens movement, and also due to the proprietary nature of the work.

### 1.1.2 Squeeze Pressure

A predominant theory of soft contact lens fit has been that of hydrodynamic squeeze pressure. Hydrogel lenses are typically fitted with a radius of curvature different from that of the patient's corneal and corneoscleral topography. Depending on the modulus of the lens material and the degree of mismatch in lens geometry and ocular profile, varying degrees of lens deformation occur as a patient blinks over the lens. In the time between eyelid blinks, attempted relaxation of the deformed lens towards its previous state induces pressure in the tear film layer trapped beneath it (Jenkins and Shimbo, 1984).

Using an *in vitro* model, Martin and Holden (1986) measured the mechanics of hydrogel lenses over an axisymmetric model eye with the application of a haptic shell to mimic the force of the eyelid on blinking. Using pressure measuring transducers mounted within the model eye, they found that positive squeeze pressure was induced in the tear film layer beneath the lens on application of a deforming force, but that a negative squeeze pressure was then induced on removal of the same force. They hypothesised that the residual negative squeeze pressure remaining after removal of the force was the primary factor responsible for adherence of the lens to the eye, and hence the clinical performance of the lens.

Martin et al. (1989) further assessed the effect of squeeze pressure both *in vitro* and *in vivo* for a range of hydrogel lenses available at the time, assessing squeeze pressure in relation to lens movement (by slit lamp graticule) and “Percentage Tightness” (tightness on push-up) (assessed subjectively using digital pressure). They found that squeeze pressure was significantly related for a variety of lenses over a range of thicknesses, water contents, BOZRs, diameters and back vertex powers. As a result, they concluded that squeeze pressure provided a useful parameter with which to describe and compare the clinical fit of different hydrogel lenses, and a model with which the fit of a lens to an eye could be predicted. They also found there was little or no lens movement when the squeeze pressure was greater than  $-14 \text{ H}_2\text{O}$  ( $-1370 \text{ dynes/cm}^2$ ), and further concluded that the mechanics of lens motion were more likely related to a complicated combination of squeeze pressure and other forces in the eye-lens system when the squeeze pressure was less than this critical pressure. Thus it can be seen that the squeeze pressure model does not account fully for variation in lens fit either.

### **1.1.3 Rubber Band Theory**

Kikkawa (1979) proposed a mechanical model of lens fit in which the peripheral portion of soft contact lenses act like a series of concentric elastic rubber bands and progressively stretch to accommodate changes in the peripheral ocular curvature, influencing both lens centration and also tear pump action beneath the lens. Since the rubber bands are stretched slightly on fitting, elastic force develops in each band. When a lens is dislocated by an external force such as blinking, increased force is induced on the opposing side of the lens to which it is decentred as a result of further stretching to conform to the change in topography, thus creating a state of in-equilibrium. Elastic contraction of the stretched elastic band in this same position then acts against the cornea to push the whole rubber band/lens back to the centre of the cornea and re-equilibrate the system.

### 1.1.4 Sagittal Depth

Another commonly used model for soft contact lens fit relates the sagittal depth of soft contact lenses to the corresponding ocular sagittal height of the eye (Garner, 1982, Snyder, 1984). This is based on the assumption that steeper corneas have greater sagittal height and therefore require a lens of greater sagittal depth in the form of a steeper base curve to fit the cornea (Snyder, 1984). Thus, soft contact lens fitting can be thought of as a process of matching the sagittal depth of the lens to the ocular sagittal height for a given eye, by the selection of an appropriate combination of total lens diameter and back optic zone radius. Consequently, with this model, a tightly fitting lens can be considered as one which has too great a sagittal depth for the eye it is intended to fit and, conversely, a lens that is too loose as having a sagittal depth which is too small (Young, 1992).

Using this model, Young systematically evaluated the effect of typical variations in ocular topography on ocular sagittal height in order to make assessments of the likely effect on soft lens fit. In ranking order, he found that normal variations in corneal diameter and eccentricity, rather than keratometry, resulted in greater variation in sagittal height and concluded that keratometry alone is unhelpful in predicting soft lens fit. Several studies have confirmed that the selection of the optimally fitting base curve does not correlate with central corneal curvature (Gundal et al., 1986, Bruce, 1994). Ultimately, ocular sagittal height is governed not just by central corneal curvature, but also by corneal diameter, corneal shape and peripheral corneoscleral profile (Garner, 1982, Young et al., 2010).

Conversely, in a two-part experiment Cedarstaff et al. (1983) examined the effect of systematically manipulating *lens* sagittal depth and diameter, varying first the sagittal depth of the lens whilst maintaining lens diameter, and then separately, varying the lens diameter whilst maintaining a constant sagittal depth. Using regression analysis, they found that lens movement could be decreased by increasing lens thickness, reducing lens diameter or flattening the base curve of the lens.

#### 1.1.4.1 The Effect of Corneal Diameter on Corneal Sagittal Height

The sagittal depth of a spherical curve may be considered to be the perpendicular distance from the apex of the curve to a chord intersecting the two ends of the curve, where the distance between the two ends represents the *diameter*, and the *radius of curvature* is equal to the radius of the circle that would be formed if the curve were to continue indefinitely. From Figure 1.2 it can be seen that for a given variation in diameter there will be a resultant variation in sagittal depth.

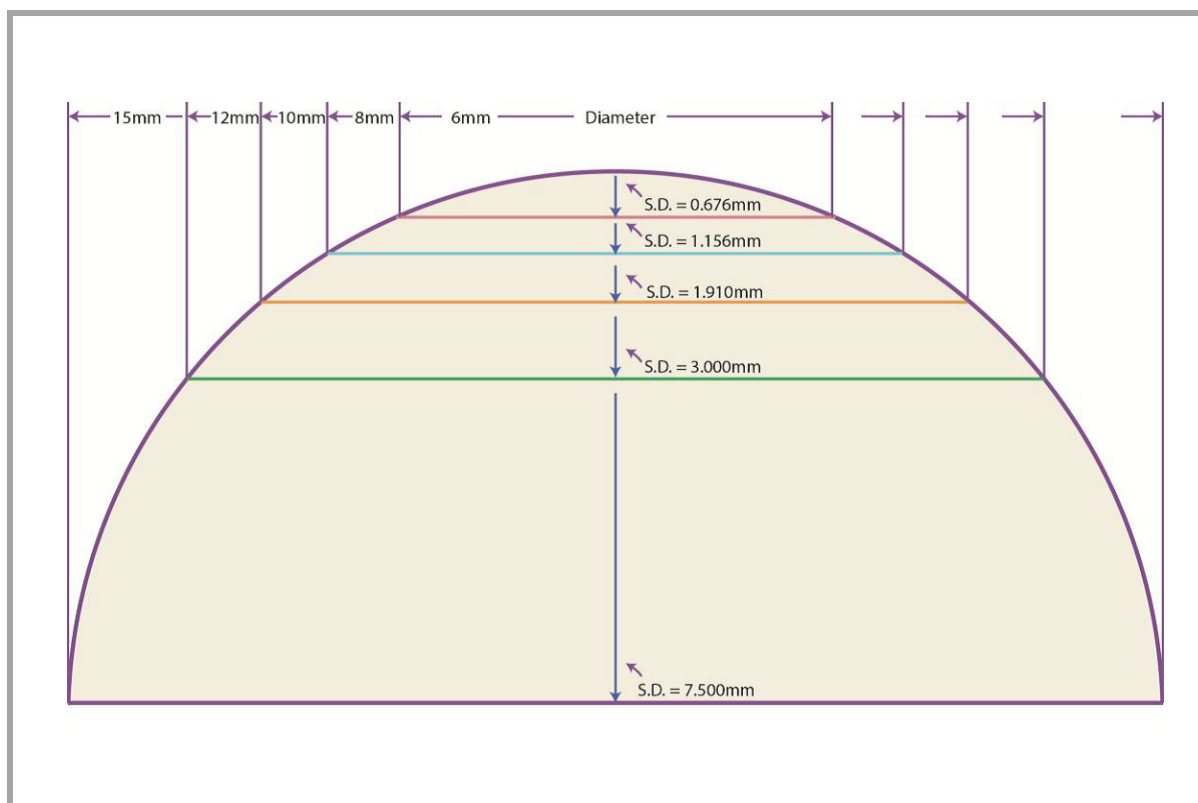


**Figure 1.2:** Change in sagittal depth with diameter/chord length

Consequently, variation in corneal diameter will result in a corresponding variation in ocular sagittal height and, therefore, in the sagittal depth of lens required to fit the cornea.

André and Caroline (2001) examined the effect of variation in corneal diameter on ocular sagittal height. Taking a normal healthy cornea of a radius of 7.85 mm and diameter of 12.9 mm, they predicted an ocular sagittal height of approximately 3.12 mm. By varying the radius of curvature and corneal diameter by 10% in either direction, they established a range of parameters that would encompass a large majority of normal human corneas. Calculation of the sagittal values for all of the permutations found revealed a maximum difference in sagittal height of 2.81 mm between the flattest, smallest segment and the steepest, largest segment. Subsequent numerical analysis showed that 62% of the variance in ocular sagittal height was accounted for by the variation in corneal diameter, whereas less than a third was accounted for by the variation in central corneal curvature.

Various workers have quantified corneal diameter using a variety of measurement techniques (Table 1.1). Even taking into account potential differences due to ethnicity, age, sex or height, there is,

Workers/Publication	n	Mean CD (mm)	Range	Instrumentation	Type	Notes
Martin & Holden <i>Am J Optom Physiol Opt</i> 1982; 59(5):436-441	30 eyes	12.89 ±0.60	-	Closed-circuit video & Photographic techniques	HCD	*HVID 11.64 ±0.49
Pop <i>et al.</i> <i>J Cataract Refract Surg.</i> 2001; 27:1033-1038	34 eyes	11.87 ±0.49	10.85-12.7	Surgical callipers	HWTW	
Baumeister <i>et al.</i> <i>J Cataract Refract Surg.</i> 2004; 30:374-380	100 eyes	11.91 ±0.71 11.8 ±0.60 11.78 ±0.43 12.02 ±0.38 12.12 ±0.65	- - - - -	Callipers Holladay-Godwin gauge Orbscan II (SST) IOLMaster (PCI) Digital Images	HWTW	
Fea <i>et al.</i> <i>J Cataract Refract Surg.</i> 2005; 31:1713-1718	10 eyes	11.69 ±0.40	10.50-12.70	Orbscan II	HWTW	
Potgieter <i>et al.</i> <i>J Cataract Refract Surg.</i> 2005; 31:106-114	29 eyes	11.9 ±0.3	11.5-12.6	AE-1500 ASICO Retinal Calliper	HWTW	
Rufer <i>et al.</i> <i>Cor.</i> 2005; 24(3): 259-261	743 eyes	11.71 ±0.42 (11.77 ± 0.37 males) (11.64 ± 0.47 females)	10.70-12.58 (11.04-12.50 males) (10.70-12.58 females)	Orbscan II	HWTW	
Srivannaboon <i>et al.</i> <i>J Med Assoc Thai.</i> 2005; 88(9): 1222-1227	420 eyes	11.60 ±0.37	10.80-12.9	Orbscan	HWTW	<i>Thai population – myopes only</i>

Key: HWTW =Horizontal White-To-White; HCD = Horizontal Corneal Diameter; OCLR = Optical Low-Coherence Reflectometry; Photo = Photographic technique; PCI = Partial Coherence Interferometry; SST = Slit Scanning Topography. \*HVID shown as an alternate/ 'surrogate' marker for Horizontal Corneal Diameter

**Table 1.1:** Summary of Corneal Diameter Measurements and Techniques from the Existing Literature

Workers/Publication	n	Mean CD (mm)	Range	Instrumentation	Type	Notes
Kim <i>et al.</i> <i>J Cataract Refract Surg.</i> 2008; 34:632-637	10 subjects	11.72 ±0.42	11.3 to 12.6	Orbscan IIz	HWTW	
Pinero <i>et al.</i> <i>J Cataract Refract Surg.</i> 2008; 34:126-131	30 eyes	12.25 ±0.49	11.34-13.16	CSO Corneal Topography System/Digital Calliper	HWTW	
Buckhurst <i>et al.</i> <i>Br J Ophthalmol</i> 2009; 93(7):949-953	112 subjects	12.08 ±0.86 12.15 ±0.95	11.20-12.80 11.06-12.91	Lenstar LS 900(OLCR) IOLMaster	HWTW	
Reinstein <i>et al.</i> <i>J Cataract Refract Surg.</i> 2009; 25:185-194	40 eyes	11.96 ±0.37	11.40-12.70	Orbscan II	HWTW	<i>High myopes only</i>
Kawamorita <i>et al.</i> <i>J Cataract Refract Surg.</i> 2010; 36:617-627	31 eyes	11.65 ±0.32	-	Orbscan II	HWTW	
Nemeth <i>et al.</i> <i>J Cataract Refract Surg.</i> 2010; 36:1862-1866	91 eyes	11.99 ±0.47	11.0-13.30	Lenstar LS 900	HWTW	
Venkataraman <i>et al.</i> <i>Indian J Ophthalmol.</i> 2010; 58(3):219-222	73 eyes	11.737 ±0.32 Observer A 11.739 ±0.32 Observer B	-	Orbscan Automated/Orbscan Eyemetrics	HWTW	Inter-observer comparison
Qin <i>et al.</i> <i>Ophthalmic Surg Lasers Imaging</i> 2012;31:106-114			-	Optical Coherence Tomography		

Key: HWTW =Horizontal White-To-White; HCD = Horizontal Corneal Diameter; OCLR = Optical Low-Coherence Reflectometry; Photo = Photographic technique; PCI = Partial Coherence Interferometry; SST = Slit Scanning Topography. \*HVID shown as an alternate/ 'surrogate' marker for Horizontal Corneal Diameter

**Table 1.1:** Summary of Corneal Diameter Measurements and Techniques from the Existing Literature (continued)

however, a wide variation in reported diameters in the literature (10.5 – 13.3 mm). Assessment of the corneal diameter has largely been through measurement of the white-to-white (WTW) diameter, although determination by this means is confounded by the both the three dimensional transparency profile of the peripheral cornea, and also by the increasing loss of limbal transparency with age.

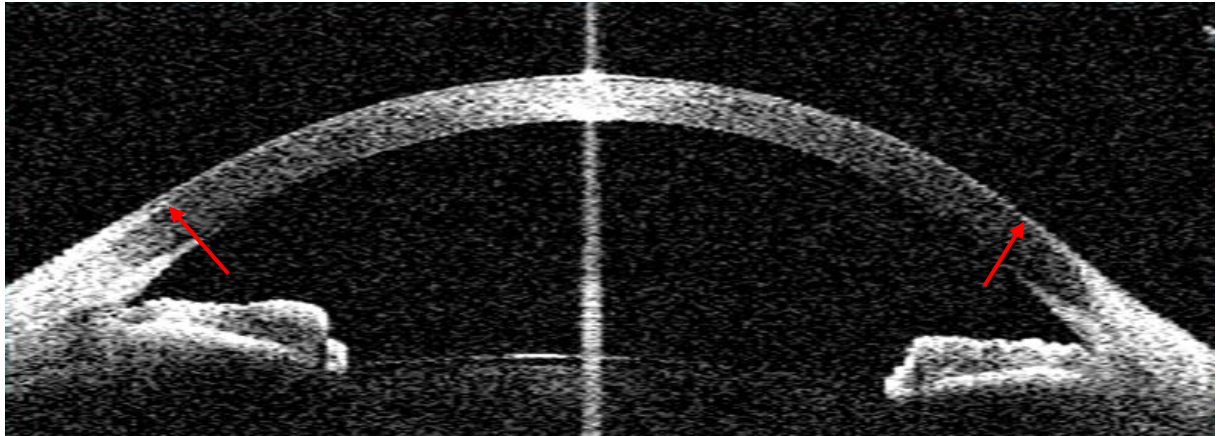


**Figure 1.3 (a):** Tomograph showing well-defined limbal transitions

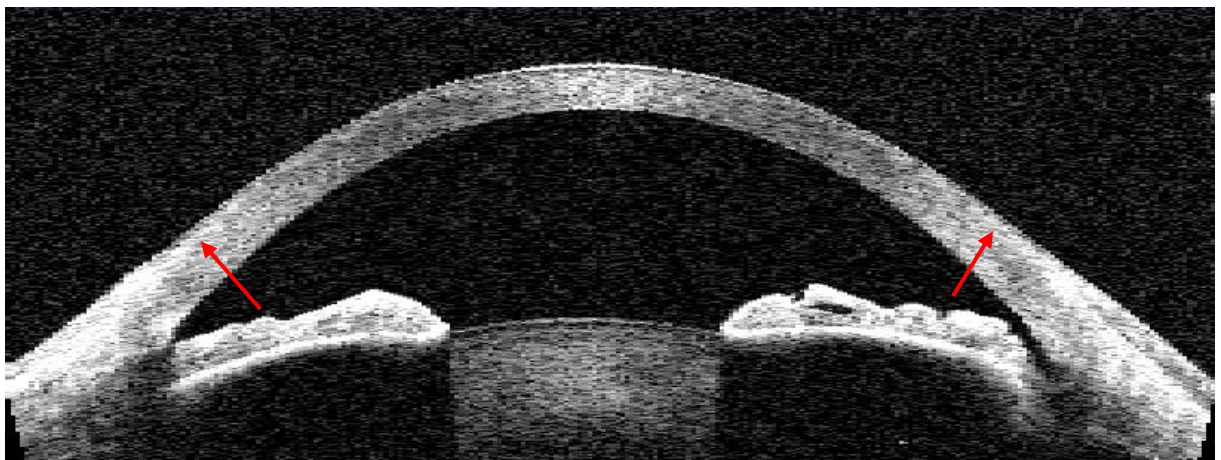


**Figure 1.3 (b):** Tomograph showing marked loss of transparency, and thus poorly defined limbal transition in the peripheral cornea

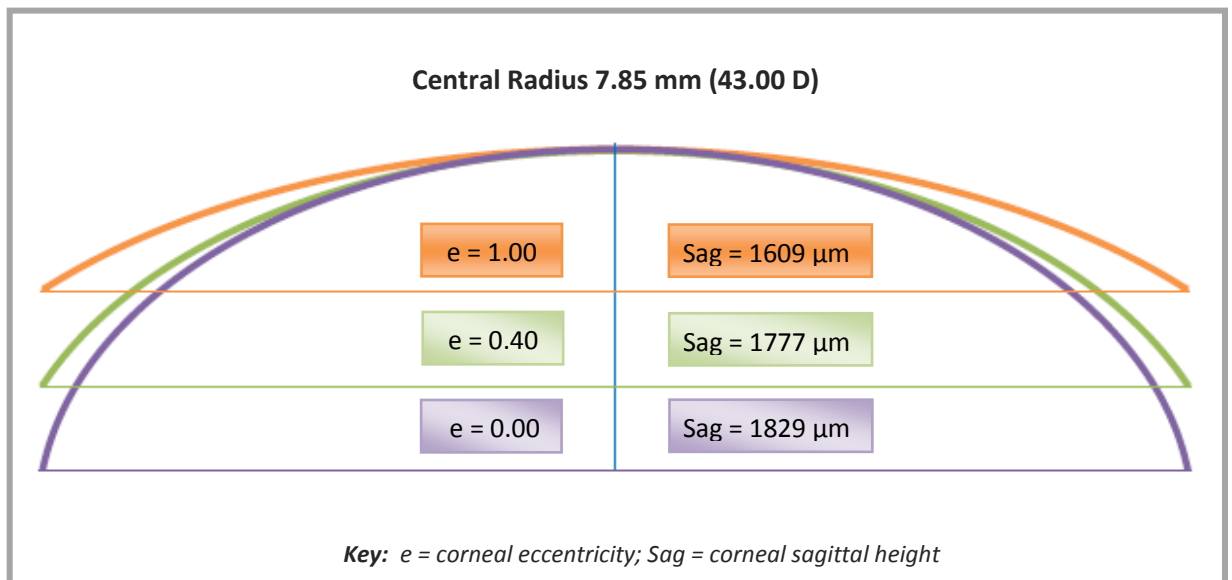
**Figure 1.3:** Tomographs showing variation in limbal transparency between subjects.

A few workers such as Martin and Holden (1982) have used alternative measurement techniques to define the corneal diameter, often with quite different results. How corneal diameter is defined will drive many of the metrics that influence soft contact lens fit, especially corneal sagittal height. Consequently, an alternative and more robust method of corneal diameter measurement is desirable.

### 1.1.4.2 The Effect of Corneal Eccentricity on Corneal Sagittal Height

The contribution of corneal diameter, therefore, is clear - the larger the corneal diameter, the greater the ocular sag and, conversely, the smaller the corneal diameter, the smaller the sag. However, a less well understood parameter is that of corneal eccentricity and its contribution to overall ocular sagittal height.

Caroline and André (2010) highlighted the effect of corneal eccentricity in a recent case study. Taking a normal healthy cornea with a central radius of curvature of 7.85 mm and diameter of 11.8 mm, they calculated the ocular sagittal heights for a range of corneal eccentricities and demonstrated that corneal sagittal height decreases as corneal eccentricity (e-value) increases (Figure 1.4). Consequently, variation in corneal eccentricity will also result in a corresponding variation in ocular sagittal height and, therefore, in the sagittal depth of soft lens required to fit the cornea.



*Reproduced and adapted from Caroline & André, 2010*

**Figure 1.4:** Change in sagittal depth with corneal eccentricity

## **1.2 The Ocular Topography and Soft Contact Lens Fit**

### **1.2.1 Soft Contact Lens Fit**

The effect of corneal topography on soft contact lens fit has been relatively neglected. Of over 2000 papers on soft contact lenses listed in the medical paper database PubMed (US National Library of Medicine), fewer than ten specifically address lens fit in relation to the ocular topography.

One study attempted to relate soft lens fitting characteristics to corneal asphericity, but found no correlation (Bruce, 1994). Another study attempted to relate success with toric soft lenses to corneal topography measurements; however, this study was more concerned with visual performance rather than lens fit, and consequently elicited little about the relationships governing soft lens fit (Szcotka et al., 2002).

The selection of initial base curve has traditionally been based on the central 2-3 mm corneal curvature, as measured by keratometry. This is based on the assumption that steeper corneas have greater sagittal height and therefore require a lens of greater sagittal depth in the form of a steeper base curve to fit the cornea (Young et al., 2010).

Previous work has shown that large changes in lens back optic zone radius (BOZR) are required in order to effect a clinically significant change in lens fit (Lowther and Tomlinson, 1981). As a result, minor variations in corneal curvature are likely to have little effect on soft contact lens fit in a normal population (Young, 1992).

In a separate study, Douthwaite (2002) investigated the influence of apical radius, surface asphericity and horizontal visible iris diameter (HVID) on corneal sagittal height. He concluded that HVID, a surrogate marker of corneal diameter, had the greatest influence in changing corneal sagittal depth and, consequently, was the most appropriate measurement to take to select the optimum soft contact lens specification.

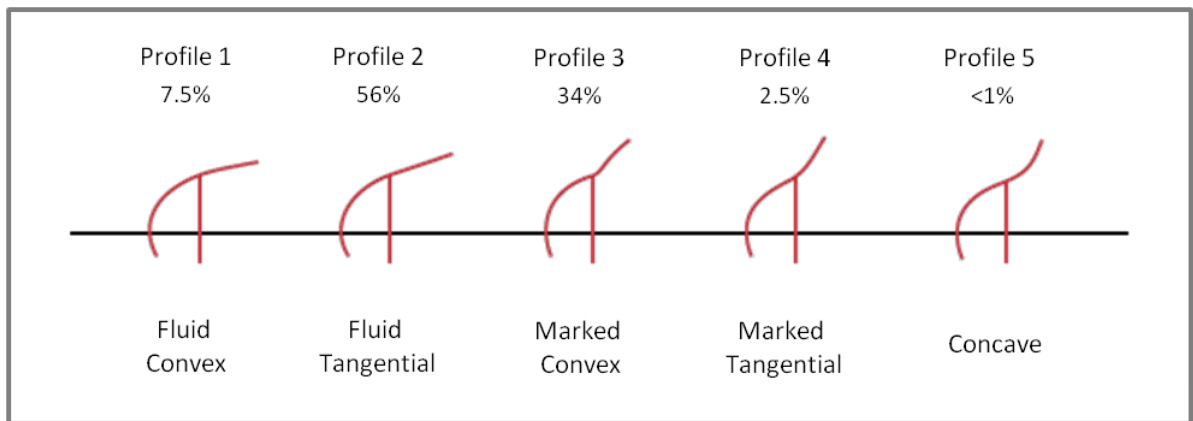
Despite these findings, many of the most popular soft contact lenses on the market are available in one diameter only (and frequently only two base curves, at best) as manufacturers of mass-produced lenses attempt to minimise inventory size in order to remain commercially competitive (Caroline and André, 2002). Even when a choice of lens diameter is available, many manufacturers may still make base curve recommendations based on an assumption of average corneal size (André et al., 2001).

A more recent study, (Young et al., 2010) investigated the effect of corneal topography on the fit of three commonly used frequent-replacement lenses using videokeratoscopy. Some correlations were evident between corneal measurements and lens fit, most notably between corneal sagittal height and lens centration. Young and co-workers concluded, however, that while computerised videokeratoscopy allowed for a better prediction of lens fit than keratoscopy alone, it was not sufficient to enable accurate selection of the best fitting soft lens base curve. They attributed this primarily to the incomplete corneal coverage inherent with Placido-disc instruments and speculated that, even if such instruments were able to characterise the entire cornea, prediction of soft contact lens fit would still prove limited since such techniques fail to take into account the profile of the paralimbal sclera. Although the topography of the peripheral cornea plays little or no role in foveal vision, it does, however, play an important role in peripheral vision and contact lens fitting (Iskander et al., 2007). Information on the topography of the peripheral cornea, corneoscleral junction and limbal sclera, however, is scarce (van der Worp et al., 2010). Consequently, Young and co-workers (Young et al., 2010) further speculated that Optical Coherence Tomography (OCT) might be used to characterise the peripheral cornea and corneoscleral junction in order to gain a better understanding of the corneoscleral topography, particularly in relation to soft contact lens fit.

### **1.2.2 Corneoscleral Topography**

In early work, Marriott (1966) characterised the curvature of the sclera using measurements taken from haptic shells, themselves derived from impressions of multiple eyes. He showed that the nasal portion of the sclera is usually flatter than that of the temporal, superior and inferior scleral faces. His work, however, was limited to scleral contour alone and did not consider the effect of the corneoscleral junction angle on corneoscleral profile (CSP).

Meier and co-workers (Gaggioni and Meier, 1987, Meier, 1992) went on to define the CSP, as an aid to soft contact lens fitting, based on qualitative observations of the limbal transition zone made using the naked eye or slit lamp biomicroscope. They described five different corneoscleral transition models (Figure 1.5): a gradual transition from cornea to sclera, where the scleral portion is either convex (Profile 1) or tangential (Profile 2); a marked transition where again the scleral portion can be either convex (Profile 3) or tangential (Profile 4); and finally a fifth, sinusoidal profile, where the convex cornea blends into a concave sclera (Profile 5). Significantly, ocular sagittal height was found to decrease through the classification scale, with eyes of Type 1 profile exhibiting the greatest sagittal height and eyes of Type 5 profile exhibiting the smallest sagittal height (van der Worp et al., 2010).



*Reproduced and adapted from Gaggioni & Meier, 2007*

**Figure 1.5:** Classification of corneoscleral transition profile, according to Gaggioni and Meier

Meier and co-workers' assessments of corneoscleral profile were, however, restricted to the superior corneoscleral junction and a subsequent study showed that this was neither an accurate nor reproducible means of classifying the CSP (Bokern et al., 2007).

Van der Worp et al. (2010) recently described the use of OCT imaging to try and better identify the corneoscleral profile. Analysing the results of 46 profiles using applied software to draw a forced circle through the periphery of the anterior sclera, they defined the corneoscleral transition profile in terms of either a gradual or marked transition in a similar fashion to Meier. Another recent study (Sorbara et al., 2010) described the use of OCT imaging and scanning-slit technology to obtain anterior segment biometry. This study, however, gathered data from a relatively small sample population of limited ethnicity.

Following on from the findings of Knoll and Conway (1987), and also of those of Young and co-workers (Young, 1992, Young et al., 2010), it seems likely that the peripheral corneoscleral profile might significantly influence soft contact lens fit dynamics.

## **1.3 Imaging, Measuring and Mapping the Anterior Ocular Surface**

### **1.3.1 Imaging**

'Imaging' may be defined as the visual representation of an object typically in the form of an objective recording (Wolffsohn and Peterson, 2006). Imaging of the eye, and the cornea in particular, is critical in the on-going assessment of physiological health and contact lens fit in the contact lens wearer. Technological advances allow clinicians to better evaluate this region of the eye and corneal measurement continues to advance beyond that of traditional keratometry (Swartz et al., 2007). This section presents an overview of the major anterior segment imaging techniques but will be limited to those technologies most relevant to the imaging, measuring and mapping of the cornea and anterior ocular surface. Videokeratoscopy (VK) and Optical Coherence Tomography (OCT) are fundamental to the author's research and, as such, will be considered in detail.

### **1.3.2 Slit Lamp Biomicroscopy and Photography**

The slit lamp biomicroscope is a commonly used instrument in both ophthalmic and medical practice, but is also considered an essential diagnostic tool in the pre-fitting evaluation, fitting and post-fitting follow-up of the contact lens wearing subject (Sellers, 1967). The instrument is composed of an illumination system consisting of a bright light source of variable width and height and a binocular microscope of variable magnification which, when correctly aligned, will result in a coincidental focus of the slit and microscope. Image capture can be achieved by the insertion of a beam splitter in the observation path or by the attachment of a camera to an eyepiece (Wolffsohn and Peterson, 2006). Video footage may be collected by the substitution of a video camera into the same optical path.

The technique allows for a highly magnified view of the external eye, anterior chamber and iris, essential in the on-going management of anterior eye disease. In contact lens practice, however, it allows for qualitative assessment of both contact lens fit and contact lens-related ocular complications and also quantitative assessments of the same when used in conjunction with a graticule or appropriate grading system).

### 1.3.3 Keratometry

The keratometer is an instrument which measures the central 2-3 mm radius of curvature of the anterior corneal surface of the eye and which allows for an assessment as to the extent and axis of corneal astigmatism. Also referred to as an ophthalmometer, the instrument has its origins in the late 1700s after the work of Jesse Ramsden and Everard Home. They proposed that accommodation occurred primarily as a result of changes in the cornea and, in an effort to prove their theory, attempted to measure the corneal curvature using a telescope allowing observation of a doubled image reflected from the cornea (Ramsden, 1779). The keratometer, however, was subsequently invented by the German physiologist Hermann von Helmholtz in 1853 using the ideas of the astronomer Clausen (Clausen, 1841) to create a keratometer that doubled images with two glass plates. In his design, two images were displaced from one another by the tilting of two movable glass plates in opposite directions until the extremities of the images touched one another. The amount of displacement between the plates is equal to the size of the image. Since the doubled images move together in this arrangement, any head or eye movements have an equal effect on both and did not affect the measurement (Gutmark and Guyton, 2010).

Keratometers use the relationship between object size (O), image size (I), the distance reflective between the corneal surface and the object (d), and the radius of the reflective anterior corneal surface. If the three variables O, I and d are known (or fixed), the fourth, (R), can be calculated using the formula:

$$R = \frac{2dI}{O}$$

Keratometers traditionally provided readings of corneal curvature in dioptrical values requiring the use of conversion tables to yield a measurement of radius of curvature in millimetres; however, most keratometers now frequently incorporate both scales for ease of use.

There are two distinct modern-day variants of the keratometer; the Javal-Schiotz type keratometer (generic) and the Bausch & Lomb keratometer (Bausch & Lomb, Rochester, NY, US):

The Javal-Schiotz keratometer is a two-position instrument which uses a fixed *image* and doubling size but adjustable *object* size to determine the central radius of curvature of the anterior corneal surface. It is comprised of two self-illuminated object mires, one typically a red square and the other a green staircase design, which are both mounted on a circumferential track so as to maintain a fixed distance from the eye. However, particular care must be taken with focussing in order to ensure accurate, repeatable results. Consequently, a Scheiner disc with at least two apertures is usually incorporated into the instrument in order to ensure the reflected light rays from the two image sources are viewed correctly in focus.

The Bausch & Lomb keratometer, by contrast, is a one position instrument which has fixed *object* size and where the *image* size is the manipulated variable. The incorporation of a Scheiner disc with four apertures, and also of two prisms each aligned perpendicularly to each other, enables independent measurement of the principal axis without adjusting the orientation of the instrument unlike the Javal-Schiotz keratometer.

The keratometer fulfils a number of different roles in contact lens practice, including aiding in the fitting of contact lenses, the monitoring of changes in both corneal and lens curvature, and confirmation of parameters of a finished contact lens (Sheridan, 1989). The instrument also allows for non-invasive qualitative assessment of the pre-corneal tear film (Hirji et al., 1989).

The selection of initial contact lens base curve has traditionally been based on central corneal curvature, as measured by keratometry. However, measurement of the corneal radius by keratometry is limited to the central corneal cap, an area approximately 2-3 mm in diameter and does not take into account the corneal eccentricity ( $e$ ). Various studies have shown that keratometry alone is a poor predictor of soft contact lens fit (Young, 1992, Roseman et al., 1993). Consequently, alternative imaging techniques allowing measurement of the wider corneal, or corneoscleral, profile are more likely to allow better prediction of soft contact lens fit.

### **1.3.4 Keratometry**

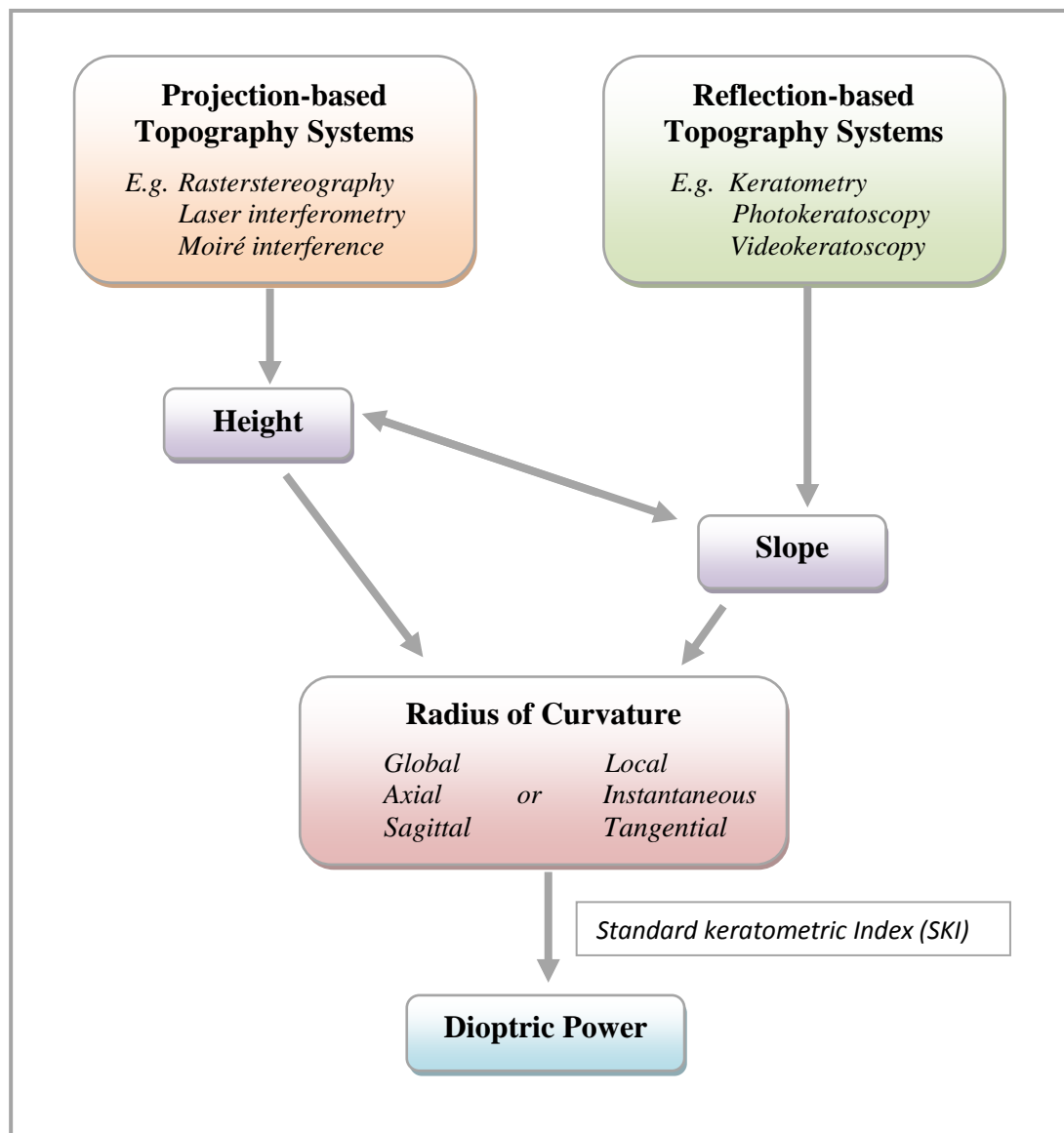
Corneal topography, or keratometry, is a non-invasive medical imaging technique for mapping the surface curvature of the cornea. Its origins lie in the Placido disk, a device developed by the Portuguese ophthalmologist, Antonio Plácido, who produced a painted disc of alternating black and white rings, the reflected image of which showed as contour lines in the corneal epithelium (Goss and Gerstman, 2000), allowing for qualitative assessment of the corneal contour.

The principle was expanded upon in 1896 by Gullstrand who incorporated a Placido disc into his ophthalmoscope, together with a camera, to form a photokeratoscope. Extracting data from the images acquired using a measuring microscope, he then went on to manually calculate the corneal curvature, by means of a numerical algorithm, and thus quantify photokeratometry for the first time. However, the flat field of the Placido disc reduced the accuracy of measurements taken close to the corneal periphery. The introduction of instruments such as the Photo-Electronic Keratoscope (PEK) (Reynolds, 1958), marketed as an aid to rigid contact lens fitting, and successors, such as the Corneoscope (Rowsey et al., 1981), saw the introduction of bowl targets to help overcome this effect and, as such, laid the foundation for the modern videokeratoscope.

Clinically, keratometry has been used to assist in the diagnosis and management of corneal ectasia (Maguire and Bourne, 1989); the monitoring of corneal disease (Maguire et al., 1987a); the planning (Gatinel et al., 2007) and post-operative assessment (Lumba and Hersh, 2000) of refractive surgery; assessment of tear film stability (Iskander and Collins, 2005) and rigid contact lens fitting (Lester et al., 1994, Szczotka, 2003). The extra contour data provided by corneal topography, however, is also of significant interest to the modern day contact lens practitioner, especially in research and in the fitting and management of orthokeratology patients and other complex contact lens fitting cases.

Previously, methods for assessing corneal topography have been based solely on the principle of reflection, and the majority of commercially available corneal topography instruments still rely on this principle today. Instruments using projection techniques have, however, been developed in more recent years (Corbett, 2000). Projection-based systems measure the true shape of the cornea in terms of the height, or elevation, above a reference plane, the data from which can be used to calculate the surface slope, curvature or power of the corneal surface. Reflection-based systems, by contrast, calculate the slope of the corneal surface, then the curvature and finally the power of the refractive surface. The slope in this instance, however, cannot be converted to height without additional measurements (and certain assumptions) being made. In each case the radius of

curvature is then calculated either on a global or local basis and converted to dioptric power using the standard keratometric index (SKI = 1.3375) (Corbett, 2000) (Figure 1.6).



Reproduced and adapted from Corbett, 2000

**Figure 1.6:** Data measurement and presentation by projection-based and reflection-based corneal topography systems

### **1.3.5 Reflection-Based Systems - Videokeratoscopy**

Computerised videokeratoscopy (CVK) is based on the 'Reflection' principle and is considered the current standard in the measurement of corneal surface topography (Alonso-Caneiro et al., 2008). A Placido disc target in the form of a bowl or cone is projected onto the corneal surface and the reflected image, the first Purkinje image, captured using a video camera and automatically digitised (Busin et al., 1989). Computerised image analysis is then undertaken to determine the position of up to 38 circular mires, in 360 separate semi-meridians, to provide a theoretical maximum of 11,000 data points across the corneal surface. Proprietary algorithms are used to calculate the corneal curvature at each of these points (Corbett, 2000). The corneal topography data obtained is then displayed graphically (Maguire et al., 1987b) in a variety of colour-coded topography maps representing different aspects of corneal curvature (Wilson et al., 1993). The two most commonly used topography maps are the axial and tangential maps:

- Axial maps, also referred to as 'power' or 'sagittal' maps, are the simplest of all the topographical displays and show variations in corneal curvature using a colour-scale to represent dioptric values. Warm colours such as red and orange represent steeper areas whilst cool colours such as blue and green denote flatter areas (Sowka et al., 2000). The axial map gives a global view of the corneal curvature as a whole; however, axial maps are limited by the assumption that all light rays are refracted to a focal point along the optical axis (Schafer and Berntsen, 2006), resulting in an overall 'smoothing' of the surface in which more subtle changes in corneal curvature may be lost.

- Tangential maps, sometimes referred to as 'instantaneous', 'local', or 'true' maps, also make use of colours to represent changes in dioptric value. The fact that all light rays are not refracted perfectly along the optical axis is taken into account in tangential maps, with the topographer calculating the curvature based on the tangent to the normal for a particular point on the cornea (Schafer and Berntsen, 2006). As a result the tangential map is more sensitive to sudden changes in corneal curvature, eliminating the 'smoothing' appearance that occurs with axial maps. This is of particular importance in the detection of corneal ectasia such as keratoconus and may result in an earlier diagnosis than when using an axial map alone (Rabinowitz, 1996).

An additional map, the elevation map, shows the height of the cornea relative to a best-fit reference sphere. Warm colours are used to depict points higher than the reference surface, and cool colours are used to show lower points. This map is of most use in predicting rigid contact lens fluorescein patterns and most modern videokeratoscopes now offer contact lens fitting modules that generate

simulated fluorescein patterns which aid in the design of rigid contact lens for patients (Lester et al., 1994). In these, areas of the cornea with negative elevation values show areas of fluorescein pooling, whereas areas with positive elevation values will show touch or bearing. These systems also assess apical clearance and tear exchange between the cornea and posterior lens surface, allowing for a more accurate and accommodating lens fit that decreases the risk of potential contact lens related ocular complications.

Reflection-based imaging has a number of important limitations. Placido-based videokeratometry measures the anterior corneal curvature and derives the curvature map from the data assuming a prolate corneal geometry. This assumption can lead to errors when attempting to map the surface of irregular corneas or those of patients that have undergone refractive surgery (Koch et al., 1989). An inability to measure the true power of the posterior corneal surface also remains a weakness of such systems. Perhaps the greatest limitation though, and of most relevance to the author's work, is that of limited corneal coverage. For videokeratoscopes based on the Placido disc principle, it is evident corneal coverage is limited by the fact that the instrument is based on specular reflection. It may further be limited by obscuration of the mire image by the subjects' nose, brow, and eyelashes (Read *et al.*, 2006). This may, in part, be alleviated by small cone Placido-based systems such as the Medmont E300 (Medmont, Camberwell, Australia) and Keratron Scout (Optikon, Roma, Italy) devices.

### **1.3.6 Projection-Based Systems**

A more accurate way to measure curvature is to determine the true shape of the cornea: projection-based systems derive corneal shape directly by means of scanning slits or rectangular grids and then determine power from that shape. Projection-based videokeratoscopes also have the potential to measure larger corneal areas than Placido-based systems (Mejia-Barbosa and Malacara-Hernandez, 2001). The predominant technologies include; slit photography (scanning slit); rasterstereography (grid), Moiré interference (grating) and laser Interferometry (coherent wavefronts). This discussion will be limited to currently available technology, namely scanning-slit, Scheimpflug and gratings systems.

#### **1.3.6.1 Slit-Scanning Systems**

Slit-scanning devices utilise three-dimensional slit scanning triangulation to measure both the anterior and posterior corneal curvature. Advantages of this approach include the direct measurement of corneal elevation (without conversion from the curvature values obtained) and the ability to measure convex surfaces, which often defy the algorithms used in Placido-based systems

(Srinivas and Subramaniam, 2008). The only commercially available instrument to utilise this approach, the Orbscan (Bausch & Lomb Surgical Inc, San Dimas, CA, USA), was first introduced in 1995. This instrument scans the cornea from limbus to limbus (Figure 1.7) through the sequential projection of 40 vertical optical slits (20 from the left and 20 from the right) at an angle of 45°.

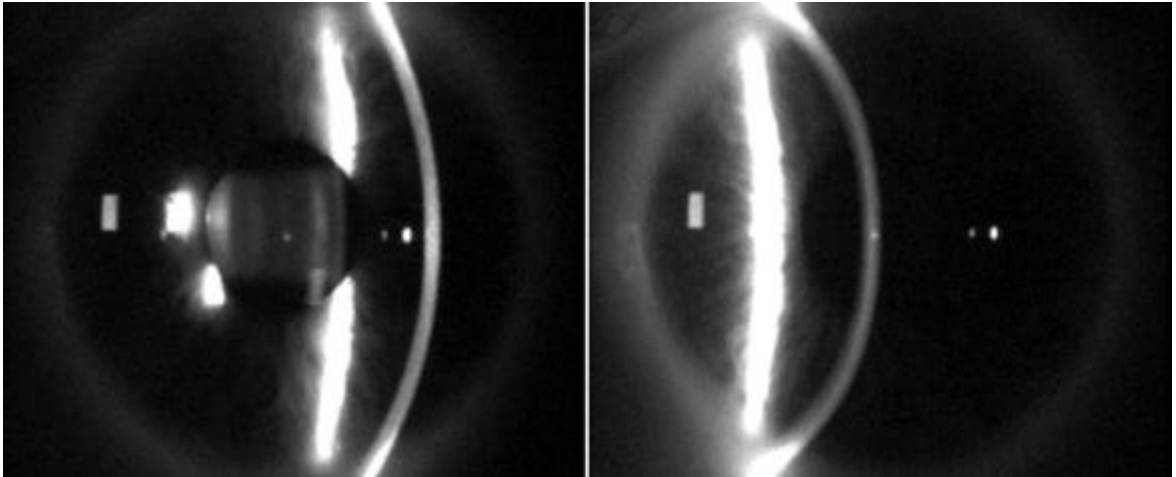


**Figure 1.7:** Slit beam projected from the right during the Orbscan's corneal scan

Back-scattered light from the slits is captured by a high resolution video camera and the instrument's software analyses 240 points per slit to independently determine the x, y, and z locations of approximately 9000 points across the cornea. The resulting data points are used to reconstruct the true topography of each anterior segment surface along with the thickness of the cornea and anterior chamber analysis (Lattimore et al., 1999). The data obtained is then represented graphically, most typically in the form of the 'quad map' presentation which includes curvature, anterior and posterior elevation, and pachymetric maps (Hashemi et al., 2005).

When using the Orbscan, anterior surface curvature was initially derived through calculation. A newer version, the Orbscan II, incorporated Placido disc technology to improve the accuracy of the topographical data over the optical slit data alone. The latest hardware upgrade, the Orbscan IIz, can be integrated with a Shack-Hartmann aberrometer allowing wavefront analysis through the 5th order to identify the total aberrations of the eye (Konstantopoulos et al., 2007).

Several studies have tested the validity of measurements achieved with the Orbscan (Maldonado et al., 2006, Jonuscheit and Doughty, 2007). The accuracy and repeatability of the instrument is reported to be below 10  $\mu\text{m}$ , and in the range of 4  $\mu\text{m}$  in the central cornea and 7  $\mu\text{m}$  in the peripheral cornea under optimal conditions (Liu et al., 1999).

An inability to detect interfaces (e.g. after LASIK flap formation) and longer image acquisition, and processing times in comparison with those of Placido-based videokeratoscopy, remain limitations of the current optical slit scanning technology.

### 1.3.6.2 Scheimpflug Imaging

Scheimpflug imaging is based on the Scheimpflug principle, which occurs when a planar subject is not parallel to the image plane. In this situation, an oblique tangent can be drawn from the image, object and lens planes, and the point of intersection, the Scheimpflug intersection, is where the image will be in best focus. Using this principle, Scheimpflug-based devices image the anterior eye, using a camera perpendicular to a slit-beam, to create an optic section of the cornea and lens (Wolffsohn and Davies, 2007b).

A major advantage of Scheimpflug based systems is the ability to measure the entire anterior segment of the eye and provide cross-sectional views of the anterior ocular surface beyond the limbus. In addition to measuring anterior surface corneal curvature the technology also allows the measurement of posterior corneal surface curvature, total corneal pachymetry and anterior segment depth.

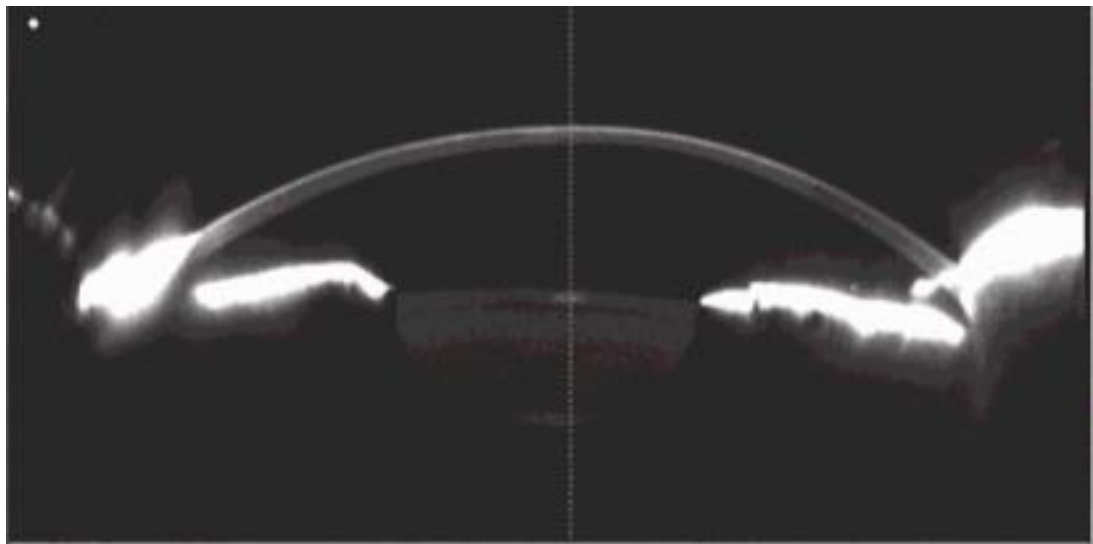


**Figure 1.8:** Scheimpflug image of the anterior segment in cross-section

Clinically, Scheimpflug imaging has been used in the assessment of keratoconus (Mihaltz et al., 2009); cataract (Tkachov et al., 2006); intraocular lens implant tilt and decentration (de Castro et al., 2007); posterior sub-capsular opacification after intraocular lens implantation (Wolffsohn and Peterson, 2006); corneal thickness (Morgan et al., 2002); corneal topography (Abad et al., 2007); anterior chamber depth (Buehl et al., 2006, Feng et al., 2011) and the measurement of the crystalline lens surface curvature (Dubbelman and Van der Heijde, 2001).

The four commercially available devices that utilise the Scheimpflug principle are the Pentacam (Oculus, Germany, Inc.), the Galilei (Ziemer USA, Inc.), Sirius (CSO, Scandicci, Italy) and TMS-5 (Tomey Corporation, Nagoya, Japan) systems. The Pentacam is able to image the cornea such that it can visualise anterior and posterior surface topography to provide curvature, tangential, and axial maps. Utilising one camera for detection and measurement of the pupil (which helps with orientation and fixation) and a second 360° rotating Scheimpflug camera to visualise the anterior segment, the Pentacam is able to capture 50 Scheimpflug images in less than 2 seconds. Each image yields 500 true elevation points for a total of 25,000 points, providing true elevation data for both anterior and posterior corneal surfaces. Like the Orbscan, the output of the Pentacam is most typically presented in the form of a 'quad map' displaying front and posterior corneal curvature, elevation and thickness, amongst other variables.

Advantages of the Pentacam system include high resolution imaging of the entire cornea and the facility to calculate pachymetry from limbus to limbus. The provision of true anterior corneal elevation data also allows more accurate prediction of the lens/cornea fitting relationship, especially in cases of corneal irregularities (Davis and Barry Eiden, 2011), and to the apply contact lens fitting designs through the Oculus Pentacam contact lens fitting software and simulated fluorescein patterns. The Pentacam's expanded diagnostic capabilities also include the measurement of densitometry values of media opacities and analysis of corneal aberrometry.

The Galilei, Sirius and TMS-5 dual Scheimpflug systems all provide similar diagnostic capabilities to those of the Pentacam, but also integrate a Placido disc for corneal topography and three dimensional analysis of the anterior segment.

Scheimpflug measures of central corneal thickness and anterior chamber depth have been shown to be accurate and repeatable in comparison with other technologies such as Orbscan slit-scanning topography, partial coherence interferometry, ultrasonography and MRI (Koretz et al., 2004, Hashemi et al., 2005). However, Scheimpflug images in their raw unprocessed form are subject to distortions due to the tilt of the camera and refraction as light passes through the preceding optical surface, such

that the image is decreased in size perpendicular to the direction of the optical axis (Wolffsohn and Davies, 2007b). Consequently, the curvatures of subsequent radii are reduced and axial lengths are increased (Fink, 2005), and this may lead to the underestimation of the anterior chamber depth in pseudophakic eyes (Wolffsohn and Davies, 2007b). Despite the ability to *physically* image the entire anterior segment, practical measurement of the ocular topography is also limited to that of limbus to limbus due to saturation of the optical sensor as a result of the high reflectivity of the sclera.

#### **1.3.6.3 Moiré Fringe Interferometry**

Moiré fringe imaging is a non-contact imaging technique in which a moiré fringe pattern is formed by the superimposition of two gratings of very fine step, one distorted and one undistorted, and from which height or deformation data can be obtained. Moiré topography in particular is a widely used means for the shape contouring of three-dimensional objects and has multiple applications in the field of mechanical engineering.

The application of this principle in the measurement of the ocular topography was first described by Jongsma et al. (1998) following the development of the experimental Maastricht Shape Topographer. This instrument allowed for an assessment of the cornea and peripheral topography which could be displayed in a two-dimensional profile map.

The only device that currently utilises this principle is the newly released Eye Surface Profiler (Eaglet-Eye, Utrecht, NL). This employs an updated implementation of moiré fringe interferometry, Double Projector Fourier Profilometry (DPFP), from which standard topographical and three-dimensional height maps may be produced.

### **1.3.7 Anterior Segment Optical Coherence Tomography**

Optical Coherence Tomography (OCT) is a technique developed for the non-invasive, cross-sectional imaging of biological systems (Huang et al., 1991). OCT itself is based upon conventional low coherence interferometry. In conventional interferometry, with long coherence length, interference of light is measured over a distance of metres. In OCT this interference is shortened to a distance of micrometres. A number of different OCT technologies exist, Time Domain OCT (TD-OCT), Spectral (or Fourier) Domain OCT (SD-OCT) and Swept Source (SS-OCT).

In Time Domain OCT (TD-OCT) systems, low-coherence interferometry light from a super-luminescent diode (SLD) light source is split into a reference beam, which undergoes reflection by a semi-silvered mirror, and also a sample beam, the latter of which is reflected by the ocular structures of the eye (Wolffsohn, 2008). If the light from the reference and sample beams travel identical optical distances before being recombined at a photo-detector, (positive) coherent interference occurs, which is measured by an interferometer (Wolffsohn and Davies, 2007a). Having acquired point data in this way, depth data are then acquired by varying the optical length of the reference arm by the physical movement of the mirror, and an image analogous to an ultrasound A-scan is formed. Moving the scanning spot laterally across the eye allows for the acquisition of multiple A-scans before processing takes place to create a cross-sectional image, a tomograph, itself analogous to an ultrasound B-scan. In contrast, Spectral Domain (SD-OCT) and Swept Source OCT systems negate the need to oscillate the reference mirror by the spectral separation of the detectors, either by encoding the optical frequency in time with a spectrally scanning or 'swept' source, respectively, or with a dispersive detector such as a grating and a linear detector array. The depth scan is then ascertained by means of Fourier transform calculations without movement of the reference arm (Wolffsohn and Davies, 2007b). Axial resolution is determined as a function of spectral bandwidth, and allows imaging resolutions as low as 3-5 microns to be achieved (Bigelow et al., 2007).

The most notable application has been in the field of ophthalmology where the technique has been used extensively in imaging the retina and anterior segment. Since the first device became commercially available in 1995 its use has become widespread in the evaluation and diagnosis of posterior segment retinal disease, including diabetic eye disease (Al-latayfeh et al., 2010); macular hole pathologies (Wang et al., 2010) and macular degeneration (Pieroni et al., 2006). The introduction of Anterior Segment OCT (AS-OCT) technology (Izatt et al., 1994) has allowed for imaging of the cornea and anterior segment structures with a range of applications, including: determination of corneal thickness (Ishibazawa et al., 2011); imaging of the Canal of Schlemm (Usui et al., 2011); evaluation of implanted intraocular lenses (Baikoff, 2006) and assessment of posterior capsular

opacification (Kaluzny et al., 2006b). Previous workers have described the use of AS-OCT as an adjunct to contact lens fitting, most notably Gemoules (2008) with the fitting of scleral lenses. Up until recently though, relatively few workers have used AS-OCT in the assessment of soft contact lens fit.

A number of OCT systems are currently commercially available (Figure 1.9). Amongst these are a number of instruments optimised for posterior segment imaging, but which also allow imaging of the anterior segment through the incorporation of a high powered condensing lens into the optical path. These devices are frequently limited in the anterior scan width that they can achieve and also exhibit reduced depth of field in comparison with dedicated AS-OCT systems. The Visante™ (Carl Zeiss Meditec, Dublin, CA) AS-OCT system, however, is one of the few commercially available and validated (Dunne et al., 2007) AS-OCT devices capable of capturing full corneal depth and width in one scan at this present time.

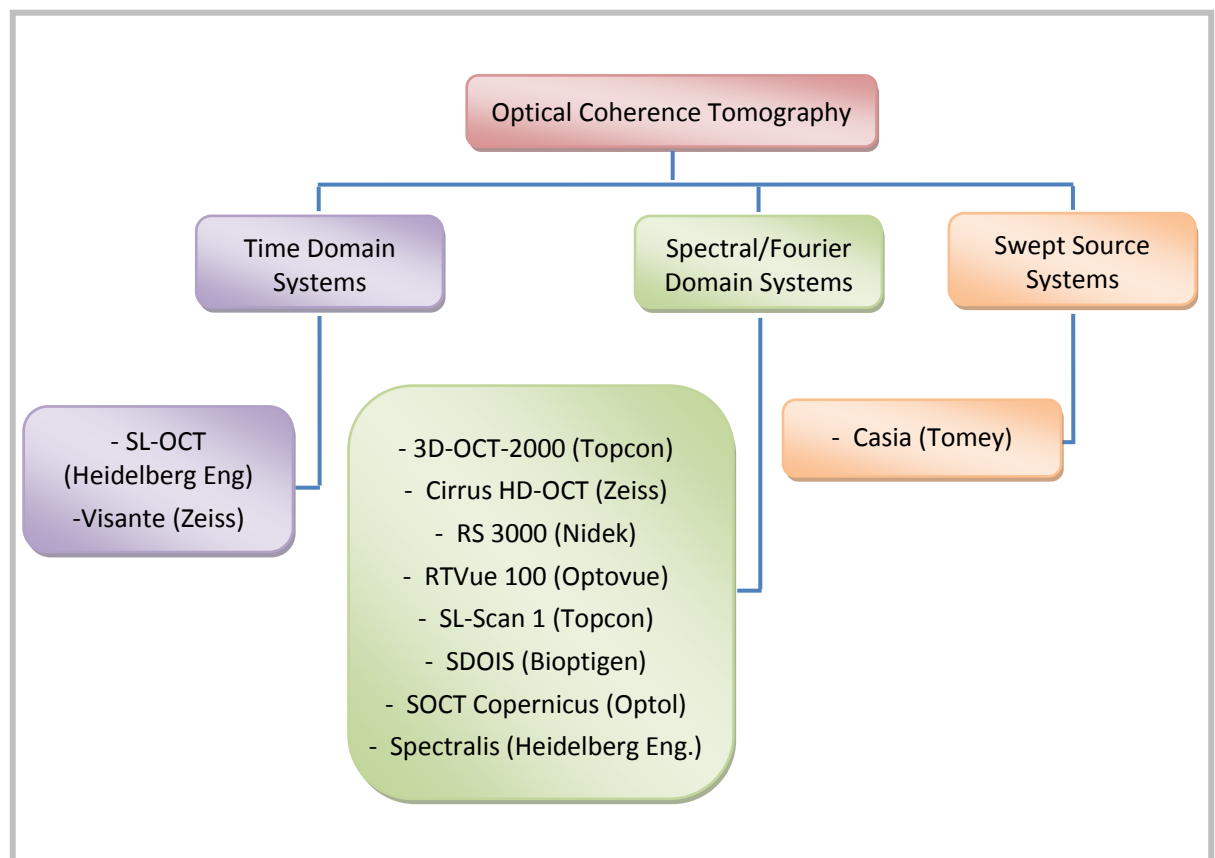


**Figure 1.9:** Overview of OCT devices commercially available

The Visante AS-OCT allows high-speed (Sakata et al., 2010), high-resolution (Leung et al., 2010), non-invasive, and non-contact (Leung et al., 2007a) cross-sectional imaging of the anterior segment. The

incorporation of on-board measurement tools allows for post-acquisition analysis of images. Additionally the instrument offers automated pachymetric mapping of the cornea, a feature which has been used extensively in the management and planning of both refractive (Ho et al., 2007, Kouassi et al., 2012), and restorative (Lim et al., 2008) surgical procedures.

Posterior segment OCT systems employ short wavelength (820 nm) light sources that allows for excellent penetration through to the level of the retina. The Visante AS-OCT system, by contrast, uses longer 1310 nm wavelength light which has greater absorption resulting in more limited penetration. This allows the light source to be intensified since decreased amounts reach the retina and, as such, the light is 20 times the strength, giving a much greater signal to noise ratio. This increased intensity in turn allows for faster image acquisition resulting in reduced motion artefacts (Goldsmith et al., 2005). The longer wavelength light employed in the Visante system is also less prone to scattering making penetration through opaque tissues such as the sclera possible. This results in better evaluation of the anterior segment and visualisation of the angle and, to a lesser degree, the ciliary body (Konstantopoulos et al., 2007). Pigmentation of the iris, however, blocks the light of the sampling beam, restricting imaging to 'line of sight' and thus preventing imaging of the lens equator and zonules (Wolffsohn and Peterson, 2006).

The Visante AS-OCT offers two primary imaging modes, 'Anterior Segment Mode' (standard resolution imaging) and 'High Resolution Mode' (High Res Mode). In 'Anterior Segment Mode' (standard resolution) 256 A-scan per line sampling is utilised, yielding an image 16 mm wide and 6 mm deep, to provide a full overview of the anterior segment including the cornea, anterior chamber, iris and both angles and, of most importance to the author, the anterior corneoscleral profile. In 'High Res Mode', 512 A-scan per line sampling is undertaken to provide a more detailed image 10 mm wide and 3 mm deep and, as such, this mode is more suited to detailed imaging of the cornea albeit over a smaller area. The resolution of Visante images overall is limited by the spacing between the scans performed, although resolutions of up to 18  $\mu\text{m}$  axially and 60  $\mu\text{m}$  in the transverse are quoted by the manufacturer (Carl Zeiss Meditech, 2009).

The updated version 2.0 operating software also incorporated an 'Enhanced Mode' for the 'Anterior Segment' and 'High Res Mode' scans. In the Enhanced Mode four consecutive scans are performed and summed into a single image, resulting in reduced signal noise to produce a higher density, higher contrast image. Additional software tools have also been added to produce a phakic IOL template and measurement tools for endothelial clearance and lens vault distance, along with more sophisticated angle measurement tools (Amin, 2013).

The latest hardware incarnation of the Visante, the Visante *Omni*, incorporates v3.0 software which allows for integration with the ATLAS corneal topography system (Carl Zeiss Meditec, Dublin, CA, USA), a Placido-disk based videokeratoscope. In this integrated system the vertex of the ATLAS scans and the Visante pachymetric scans are superimposed to represent the same location. By using the pachymetric data obtained with the Visante AS-OCT and the known anterior surface curvature data from the ATLAS posterior corneal curvature data may be calculated.

Clinically, the Visante has been used to assist in the diagnosis of angle-closure glaucoma (Tahiri et al., 2010); the diagnosis of dry eye (Ibrahim et al., 2010); the management of hydrops (Kucumen et al., 2010); the analysis of bleb morphology following trabeculectomy (Leung et al., 2007b) and the determination of LASIK flap depth (Kouassi et al., 2012). The Visante is equipped with a Badal optical system capable of changing focus over a range of -35 to +20 dioptres. By altering the Badal system power, accommodation can be induced and dynamic changes of the anterior segment and crystalline lens measured (Sheppard and Davies, 2011). A recent study has also employed the Visante system to determine the metrics of the normal cornea (Sorbara et al., 2010).

The Visante AS-OCT has been shown to exhibit excellent repeatability and reproducibility (Fukuda et al., 2010). It is subject, however, to optical distortion in the same manner as any other technique involving the passage of light through media with curved surfaces and varying refractive indices (Wolffsohn, 2008). Whilst the Visante's proprietary curvature correction software has been shown to improve accuracy in comparison to using uncorrected images, it is still prone to underestimation errors in its measurement of curvature and axial depth; however, this may be correct with the use of suitable algorithms (Dunne et al., 2007).

### **1.3.8 Summary of Imaging Techniques**

Determination of the anterior ocular topography has traditionally been undertaken using keratometry, and more recently keratoscopic techniques, with limited corneal coverage (Figure 1.10 a). Newer technologies such as projection imaging and AS-OCT allow for even greater imaging width, with that of AS-OCT extending out beyond the limbus to enable imaging of the corneoscleral periphery (Figure 1.10 b).

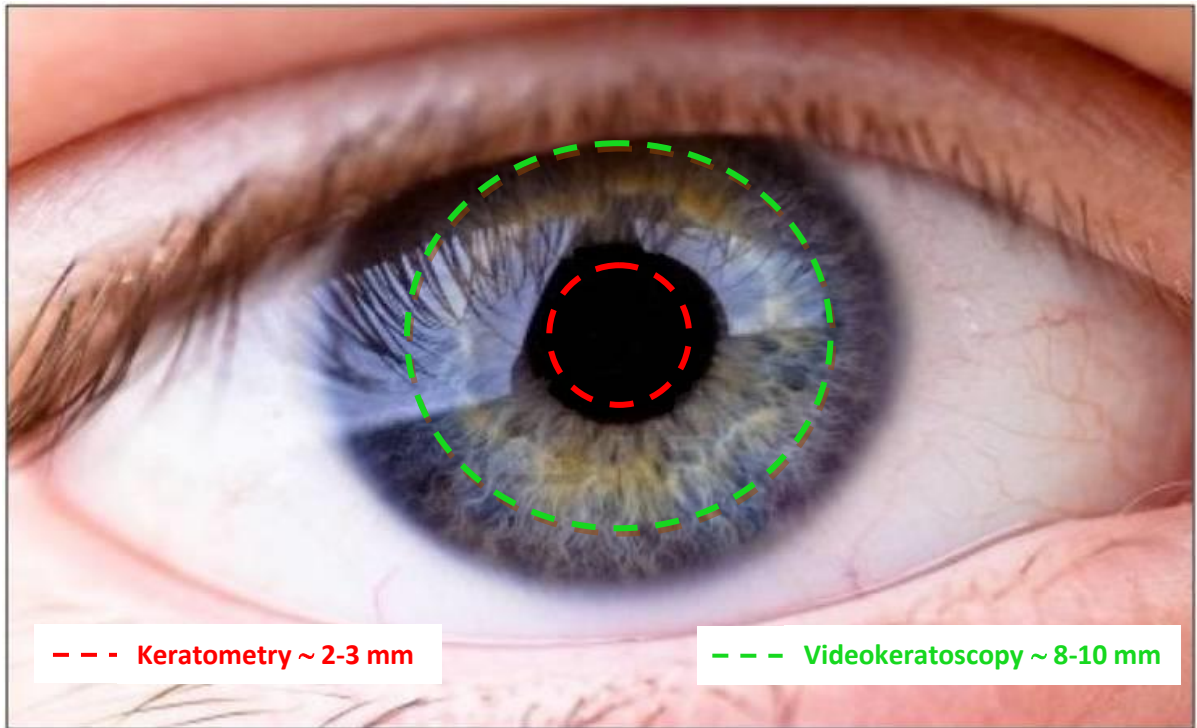


**Figure 1.10 (a):** Ocular imaging coverage with keratometric and keratoscopic imaging techniques

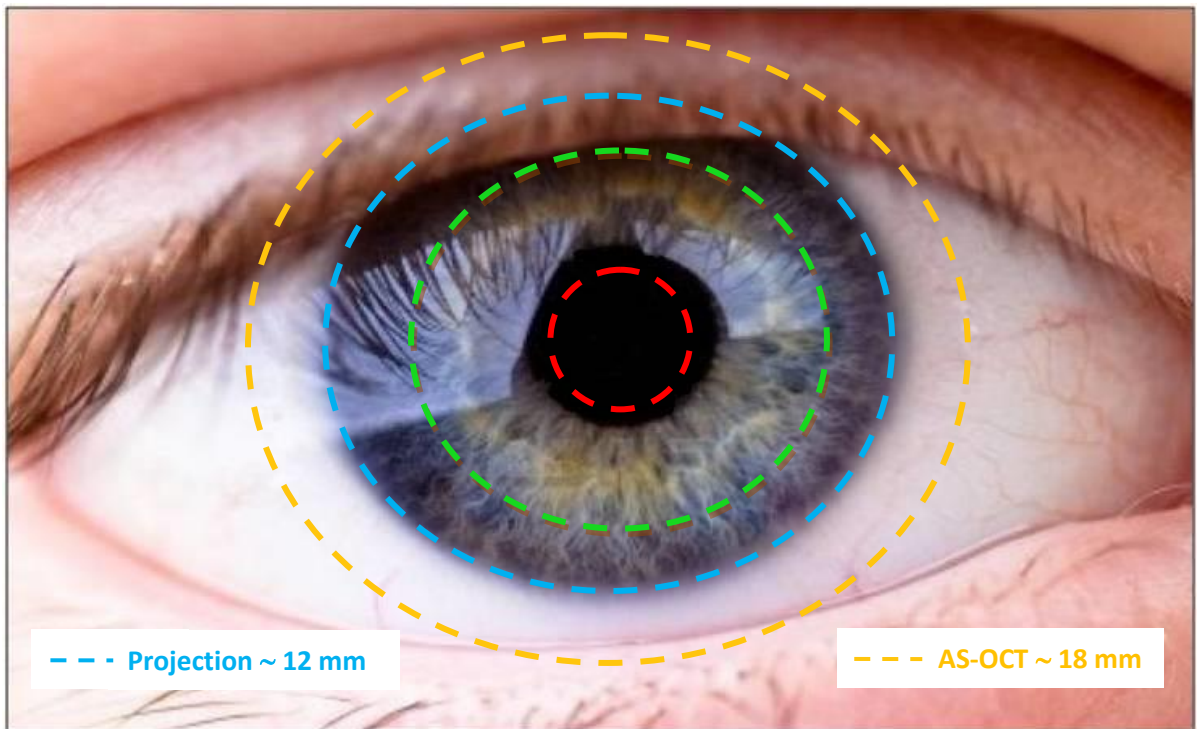


**Figure 1.10 (b):** Additional ocular imaging coverage with scanning-slit/Scheimpflug and AS-OCT imaging techniques

## **1.4 Thesis Aims and Objectives**

The selection of initial contact lens base curve has traditionally been based on central corneal curvature alone, as assessed by keratometry. However, studies have shown that keratometry is a poor predictor of soft contact lens fit. A variety of different models have been put forward in an attempt to predict parameters that influence soft contact lens fit dynamics, although these do not fully account for the total variation in lens fit. Given the limitations of current models, the primary aim of this research was to further identify factors affecting, and thus better predict, the variation in lens fit, particularly factors relating to the peripheral ocular topography. This thesis will demonstrate a range of investigations undertaken to fulfil this aim using a variety of different imaging techniques.

Recent technological advances have allowed for a more complete imaging of the anterior segment and anterior ocular topographies, and also for more objective assessment of lens fit over that previously offered by more traditional imaging techniques. Having identified potential factors affecting lens fit, a sub-aim of this work was to assess those technologies used in this body of work, and their suitability in context of both the research and practice-based environments.

Various workers have quantified corneal diameter using a variety of measurement techniques. Even taking into account potential differences due to ethnicity, age, sex or height though, there is a wide variation in reported diameters in the scientific literature. How corneal diameter is defined, however, will drive many of the metrics that influence soft contact lens fit, especially corneal sagittal height. Consequently a sub-aim of this thesis was to identify a more robust measurement technique of corneal diameter using these technologies.

It is hoped this work will lead to further studies examining factors that influence soft contact lens dynamics, especially as new imaging technologies become available to researchers and eye care practitioners alike.

## Chapter 2

## **Chapter 2: The Influence of Corneoscleral Topography on Soft Contact Lens Fit**

### **2.1 Introduction**

Suboptimal soft contact lens fit has been associated with discomfort (Young, 1996), poor vision (Young, 1996), physiological changes (Knop and Brewitt, 1992, Young and Coleman, 2001) and drop out from wear (Young, 2004). Accurate predictors of soft lens fit to explain why lens fit varies between eyes would therefore be desirable aids to the fitting process. The selection of initial base curve has traditionally been based on central corneal curvature, as measured by keratometry. The underlying assumption behind this is that steeper corneas have greater sagittal height and therefore require a lens of greater sagittal depth in the form of a steeper base curve to optimally fit the cornea (Snyder, 1984). Ocular sagittal height, though, is governed not just by central corneal curvature, but also by corneal diameter, corneal shape factor and the peripheral corneoscleral profile (Garner, 1982, Young et al., 2010). Most commercially available soft contact lens diameters range from 13.8 to 14.2 mm and hence drape over the limbus onto the sclera by about 1 mm all around. Consequently, keratometry can be considered an over-simplistic predictor of soft lens fit and previous studies have shown that there is no strong correlation between keratometry readings and the best fitting soft contact lens (Gundal et al., 1986, Young et al., 2010).

Computerised videokeratoscopy allows a more complete characterisation of the corneal topography, with modern topographers capturing many thousands of data points across the corneal surface compared to that of only four in conventional keratometry. Their usefulness in the fitting of rigid contact lenses has been well documented (Caroline et al., 1994, Hansen, 2003). However, comparatively little work has been published regarding their application in soft lens fitting, and a recent study of soft lens fit showed only weak correlations (Young et al., 2010).

Although videokeratoscopy measurements have facilitated the collection of accurate data relating to the central and mid-peripheral cornea, information on the topography of the peripheral cornea, corneoscleral junction and limbal sclera is scarce (Marriott, 1966, Meier, 1992). It seems likely, however, that this area has the most influence on soft lens fit since this is where lenses are required to make the greatest flexural changes in order to align to the ocular surface (Bibby, 1979a).

OCT has allowed for more extensive and detailed imaging of the anterior segment and peripheral corneoscleral profile. The imaging of soft contact lenses was first reported by Kaluzny et al. (2006a) using high resolution SD-OCT. Shen et al. (2010) have also described the use of a custom built SD-OCT device to image an entire contact lens both *in vivo* and *in vitro*. However, very few studies have assessed anterior surface topography using OCT, and none have assessed the influence of the peripheral ocular topography on soft contact lens fit.

The purpose of this study was to evaluate the predictive value of peripheral ocular topography, as evaluated with AS-OCT, on soft contact lens fit compared to traditional measures of corneal profile utilizing keratometry and videokeratoscopy. It was expected that the corneoscleral shape profile would have a greater influence on lens fit than that predicted by corneal shape alone, partly explaining why lens fit varies between eyes with similar keratometry values. Also, that lens fit would demonstrate a wider range with a stiffer contact lens material, in turn, contributing to the differences in lens fit seen clinically between soft contact lenses of the same curvature fitted on the same eye.

## **2.2 Method**

The study was prospective and undertaken at a single site, Aston University (Birmingham, UK). Subjects were excluded if they exhibited ocular pathology, dry eye disease, ocular allergy or corneal irregularity, as were those with a history of recent ocular surgery or previous refractive surgery. Subjects gave written informed consent after an explanation of the nature and possible consequences of the study. The research followed the tenets of the Declaration of Helsinki and the study protocol was approved by the University's Research Ethics Committee prior to commencing.

Fifty subjects' eyes were imaged using a TD AS-OCT device (Visante, Carl Zeiss Meditec, Dublin, CA), calibrated daily. This instrument allows high-speed (Sakata et al., 2010), non-invasive and non-contact (Leung et al., 2007a) *in vivo* imaging of the anterior segment, capturing full corneal depth and width in one scan (Dunne et al., 2007), with a resolution of up to 18  $\mu\text{m}$  in the axial and 60  $\mu\text{m}$  in the transverse plane.

OCT images were captured with the eye in the primary-gaze position and also in the four cardinal directions of gaze to give both full sagittal cross-sections of the cornea and cross-sections of the corneoscleral junctions at the superior, inferior, nasal and temporal positions. External fixation targets (Figure 2.1a & 2.1b) were used to ensure consistency of subjects' direction of gaze at an angle



**Figure 2.1 (a):** Zeiss Visante AS-OCT device with external fixation markers seen from the subject's perspective



**Figure 2.1 (b):** Zeiss Visante AS-OCT device with external fixation markers seen from the operator's perspective

of 35° from the normal, which corresponded with the yellow 'No.3' targets, for images taken perpendicularly in the horizontal meridian. Orange dot targets arranged at the same angle from the normal were used to ensure fixation in the vertical plane

Measurements of corneoscleral junction (CSJ) angle, corneal diameter (CD), corneal sagittal height (CS) and scleral radius (SR) were then extracted from the images using the Visante's built-in calliper and protractor tools (Figure 2.2a & 2.2b, Table 2.1). CD was defined as the distance between the two external scleral sulci, where the position of the sulci taken to be the point of 'deflection' in the sclera, determined subjectively with a straight edge. The corneal sagittal height of a chord at 10 mm (CS10), and the ocular sagittal height at 15 mm (OS15), were also taken. Analysis of the OCT images was undertaken using the Visante's proprietary curvature correction software, which has been shown to reduce underestimation errors in its measurement of corneal curvature and axial depth (Dunne et al., 2007).

The OCT measurements were tested for intrasession repeatability and reliability by randomly selecting and analysing 10 different subjects' images sets six times. The principal measurements of CDh, CSh, CSJ angle and SR were recorded for each image six times by the same operator, with each measurement being taken on different days with the operator masked to their previous measurement outcome.

Conventional corneal topography data were collected using a Medmont E300 corneal topographer (Medmont, Camberwell, Australia), an instrument which has been shown to be both accurate and repeatable (Tang et al., 2000, Cho et al., 2002). In addition to providing simulated K's, this also gave corneal height (CS10) and shape factor (SF) data. Subjects' refractions were determined using a validated autorefractor (SRW-5000, Shin-Nippon, Tokyo, Japan)(Mallen et al., 2001).

Measurements of horizontal visible iris diameter (HVID) and vertical palpebral aperture (PA) were also extracted from images acquired with a digital slit lamp and image analysis software (SL 990 Digital Vision System, CSO, Firenze, Italy). Limbal zone (LZ) width, the transition zone between outer edge of the visible iris and the outer corneal sulci, was then determined for each eye as the difference between the horizontal CD and HVID measurements.

From chord diameter and sagittal height measurements, it is possible to calculate the radius of curvature for the equivalent spherical shape which would align the ocular surface. Equivalent base

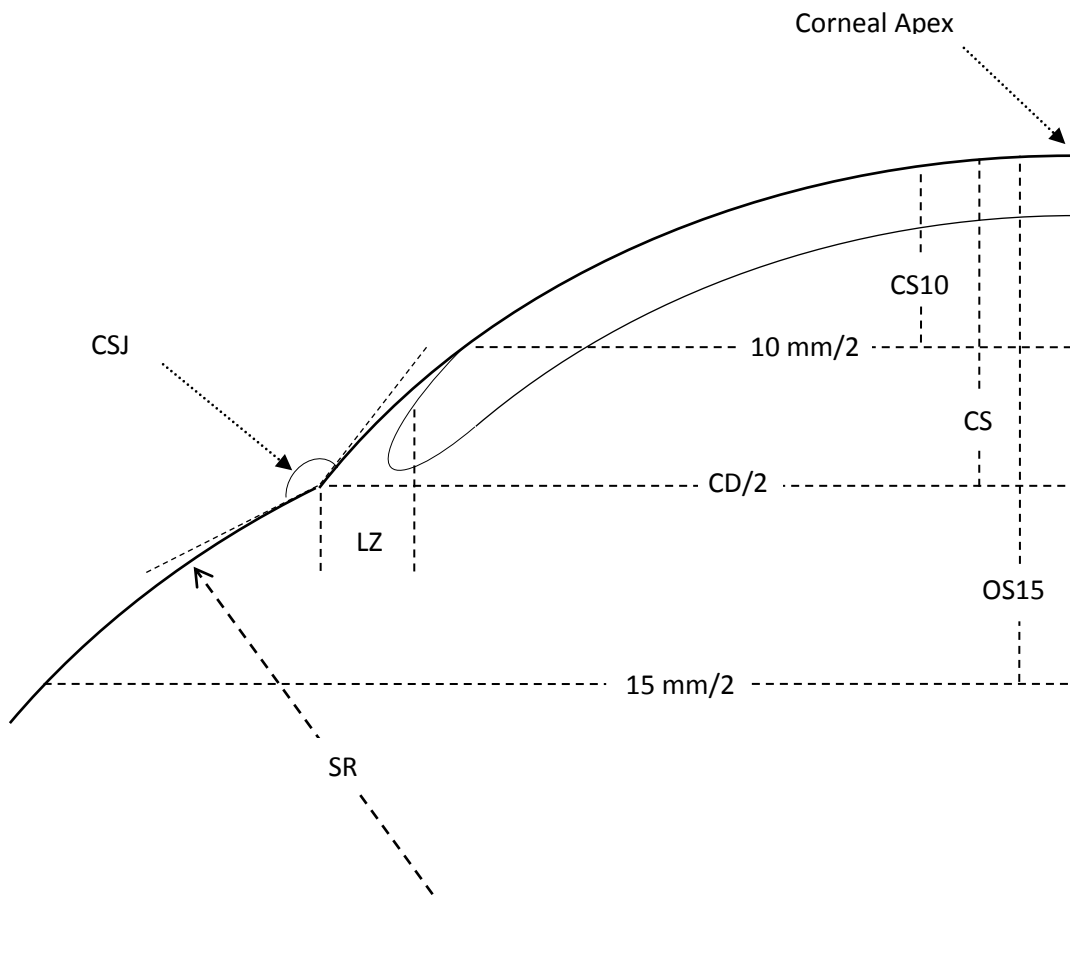


**Figure 2.2 (a):** Schematic of OCT ocular topography measurements (Table 2.1)

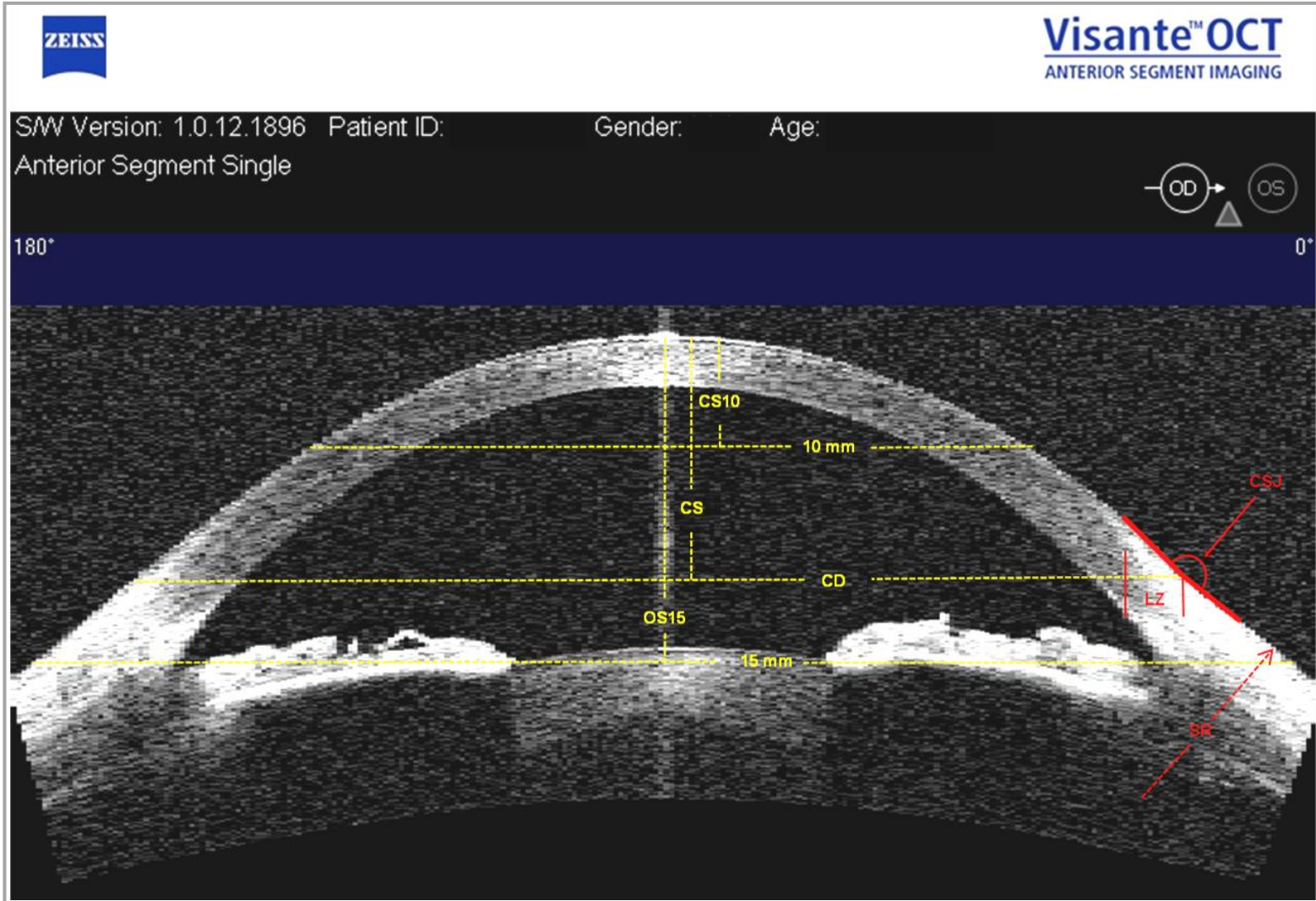


**Figure 2.2 (b):** Typical Zeiss Visante OCT scan showing ocular topography measurements (Table 2.1)

Abbreviation	Description	Instrument
HVID	Horizontal visible iris diameter - synonymous with white-to-white (WTW)	Slit lamp graticule
PA	Palpebral aperture	Slit lamp graticule
K	Simulated keratometry reading	VK
SF	Corneal shape factor ( $SF=e^2$ )	VK
CS10-VK	Corneal sagittal height of a chord at 10 mm	VK
CD	Corneal diameter	OCT
CS	Corneal sagittal height of a chord taken between the anterior corneal sulci	OCT
CS10-OCT	Corneal sagittal height of a chord at 10 mm	OCT
OS15	Ocular sagittal height of a chord at 15 mm	OCT
CSJ	Corneoscleral junction angle	OCT
SR	Scleral radius	OCT
EBC	Equivalent (spherical) base curve	-
LZ	Limbal zone, the transition zone between the outer edge of the visible iris and the outer corneal sulci; where $LZ = (CD-HVID)/2$	-
$\Delta CD$	Difference in corneal diameter between the horizontal and vertical meridians	-
$\Delta CSJ$	Difference between the two corneoscleral junction angles in a given meridian	-
n, t, s, i	Nasal, temporal, superior, inferior	-
h, v	Horizontal, vertical	-

**Table 2.1:** Abbreviations of ocular measurement variables

curves (EBCs) were calculated for each subject using the horizontal CD and CS measurements with the appropriate formula:

$$\frac{CS^2 + \left(\frac{CD}{2}\right)^2}{2CS}$$

In similar fashion, the EBC was also calculated for subject's individual topographies for a chord diameter of 15 mm.

Two daily wear soft contact lens types, of power -2.50 D, were evaluated; a conventional hydrogel design (Acuvue® 2 [Vistakon]; etafilcon A material, modulus 0.30 MPa) and a silicone hydrogel design (Acuvue® Advance® [Vistakon]; galyfilcon A material, modulus 0.43 MPa). These lenses were chosen for their similar geometries and identical base curve (8.3 mm) and diameter (14.0 mm). Subjects were randomly assigned to wear one lens design in each eye, i.e. contralaterally. The steepest available base curve (8.30 mm) was selected for dispensing in each case and lens blister packs were re-labelled by a clinical assistant so as to ensure both investigator and subject were masked to lens type.

Lenses were inserted by an investigator and allowed to settle. Comfort and lens fit were then assessed after 30 minutes of wear, representative of a lens settled after several hours (Brennan et al., 1994, Golding et al., 1995). Comfort on settling was graded by subjects on a 0-10 scale. Four main lens fit variables (Young, 1996), the primary endpoints - decentration (mm), post-blink movement (mm) (PBM), tightness on push-up (%) and overall fit (acceptable/unacceptable) - were assessed by a single, experienced investigator to maintain consistency.

Lens centration was measured with respect to the limbus in both the horizontal and vertical meridians, with the eyelids in situ, and summated in the post-study analysis to give total decentration. The post-blink movement (PBM) was measured immediately after the blink, with the subject fixating in primary gaze. Measurement was made by observation of the inferior lens edge and, where necessary, the lower lid was gently displaced to obtain a good view while ensuring minimal displacement of the lens. Lens tightness on push-up was graded on a continuous scale from 0 to 100, where 50 corresponds to the optimum tightness and values above and below 50 signify relatively tighter or looser fits, respectively. Overall fit acceptance was graded as being either acceptable or unacceptable, dependant on the investigator's overall assessment of the lens fit.

### 2.2.1 Statistical Analysis

Pearson's correlation coefficients were used to test for associations between selected clinical, ocular and lens fit variables. Spearman's correlation coefficients were used to assess the association of these variables with subjective ratings. In view of the risk of Type I errors with multiple comparisons of association, only those with a  $P \leq 0.01$  are presented. Repeated measure analysis of variance was used to assess the difference in parameters between ocular quadrants.

Multiple regression analysis (forward stepwise method; entry  $P = 0.05$ , removal  $P = 0.10$ ) was undertaken to determine the predictive values for key fit variables when measured using keratometry alone, keratometry and videokeratoscopy and, finally, keratometry, videokeratoscopy and OCT in combination. Ocular topography variables were tested for entry into the model sequentially, based on the significance level of the score statistic. After each entry, variables that were already in the model were tested for possible removal, and variables not included thus far were tested for inclusion. This was repeated until no more variables met entry or removal criteria, or until the model remained unchanged.

For the repeatability and reliability analysis, the OCT results were analysed using one-way ANOVA with subject as the factor. From this the repeatability and reliability were calculated as follows:

$$\text{Measurement error } (s_w) = \sqrt{RMS} \quad \text{Repeatability} = 1.96 \times \sqrt{(2RMS)}$$

Intraclass correlation coefficients (ICC) were calculated as follows:

$$\text{Intraclass correlations (ICC)} = \frac{mSSB - SST}{(m-1)SST}$$

Where: RMS = Residual mean square; m = number of observations per subject;

SSB = sum of square between subjects; SST = total sum of squares.

The analysis was undertaken using PASW Statistics V.18 statistical software (SPSS Inc., Chicago, IL, USA). Missing data were excluded from the analysis and not extrapolated from the collected data.

#### **Sample Size Calculation:**

Since this was an exploratory study using a previously unused methodology to determine both the ocular topography, and to test for associations between these values and lens fit variables, no sample size calculation was made prior to subject enrolment. However, taking 0.35 as the minimal critical correlation coefficient value to demonstrate moderate (or better) correlative strength and,

assuming a two-tailed test, the sample size required to achieve the required statistical significance level ( $P \leq 0.01$ ) was found to be 50, as determined using a statistical look-up table (Zar, 1984).

## 2.3 Results

### 2.3.1 Biometric Data

Fifty subjects (70% female) were enrolled and completed the study. The mean age of subjects was 22.8 yrs (SD  $\pm 5.0$ , range 18 to 43). The mean spectacle sphere on auto-refraction was -1.97 D (SD  $\pm 2.36$ , range -7.87 to +2.50) and the mean spectacle cylinder -0.64 DC (SD  $\pm 0.50$ , range 0.00 to -2.12).

The ethnicity of subjects was 68% British Asian (individuals of Indian, Pakistani or Bangladeshi descent) and 18% Caucasian. Three were also identified as Asian/Oriental, three as Afro-Caribbean and one as mixed race.

### 2.3.2 Ocular Dimensions

A wide range of corneal shapes was measured across the study population (Table 2.2). The corneal topography results, as assessed by AS-OCT imaging, are summarised in (Table 2.3)

Ocular Variable		Mean	SD	Median	Range
K (mm)	Flat	7.85	0.26	7.80	7.41 - 8.73
	Steep	7.65	0.25	7.63	7.12 - 8.51
SF	Flat	0.43	0.16	0.44	0.00 - 0.77
	Steep	0.21	0.12	0.20	0.00 - 0.66
CS10-VK (mm)	Horz.	1.74	0.08	1.73	1.51 - 1.89
	Vert.	1.81	0.09	1.83	1.57 - 1.99
PA (mm)		10.89	1.36	11.00	6.6 - 13.43
HVID (mm)		11.86	0.56	11.89	9.26 - 13.22

**Table 2.2:** Ocular topography measurements by videokeratometry and slit-lamp

	Horizontal				Vertical			
Ocular Variable	Mean	SD	Median	Range	Mean	SD	Median	Range
CD (mm)	13.39	0.44	13.37	12.10 - 14.55	13.11	0.57	13.18	11.61 - 14.96
CS (mm)	3.18	0.21	3.17	2.74 - 3.75	3.07	0.24	3.12	2.45 - 3.63
CS10-OCT (mm)	1.76	0.07	1.76	1.53 - 1.94	1.79	0.07	1.80	1.52 - 1.94
OS15 (mm)	3.74	0.16	3.73	3.23 - 4.10	3.77	0.15	3.78	3.31 - 4.16
CSJ (°)	173.7 n	3.1	173.7	149.1 - 179.9	178.3 s	1.7	178.7	167.2 - 181.1*
	177.6 t	1.6	177.7	172.8 - 180.0	177.4 i	1.4	177.4	174.0 - 180.0
SR (mm)	45.0 n	41.4	31.4	7.5 - 312.5	43.1 s	32.2	31.4	-19.7 - 157.5
	25.3 t	14.8	20.7	12.2 - 78.8	42.2 i	30.1	31.3	9.4 - 155.8

See Table 2.1 for Ocular Variable abbreviations. \* Angle of >180° signifies a convex corneoscleral junction profile.

**Table 2.3:** Ocular topography variables by AS-OCT

The only measurement derived from both videokeratometry and AS-OCT was the measurement of corneal sagittal height for a 10mm chord (CS10); this showed a significant correlation between the two measurement techniques ( $r = +0.69$ ,  $P < 0.0001$ ; mean difference  $0.03 \pm 0.01$  mm [95% CI]).

The mean corneoscleral junction (CSJ) angle tended to be sharpest at the nasal CSJ and became progressively flatter at the inferior, temporal and superior junctions ( $F = 102.18$ ,  $P < 0.001$ ; Table 2.3). In many cases, CSJ angles were within  $\pm 1^\circ$  of  $180^\circ$ , indicating almost tangential extensions of the peripheral cornea to form the sclera; this was evident in 44%, 29%, 12% and 1% of eyes at the superior, temporal, inferior and nasal corneoscleral junctions, respectively. The mean differences (95% CI) between opposing corneoscleral junction angles ( $\Delta$ CSJ), e.g. nasal and temporal, were  $4.07^\circ$  ( $\pm 0.65$ ) and  $0.93^\circ$  ( $\pm 0.45$ ) for the horizontal and vertical meridians, respectively. Scleral radii ranged from 7.5 to 312.5 mm (Table 2.3). The mean scleral curvature was steepest in the temporal sclera, but similar to each other in the nasal, superior and inferior scleral planes ( $F = 10.13$ ,  $P < 0.0001$ ).

There was a wide variation in limbal zone (LZ) width (0.09 to 2.04 mm); the mean horizontal LZ width was 0.80 mm (SD  $\pm 0.29$ ). The mean EBC for the cornea was 8.64 mm (SD  $\pm 0.33$ , range: 7.27 to 9.80 mm) and for an ocular chord of 15 mm was 9.38 mm (SD  $\pm 0.26$ , range: 8.91 to 10.32 mm).

### 2.3.3 Repeatability and Reliability

All readings showed a small measurement error and, therefore, good repeatability:  $\pm 0.14$  mm,  $\pm 0.06$  mm,  $\pm 0.60^\circ$  and  $\pm 7.08$  mm for the key ocular variables CD, CS, CSJ angle and SR, respectively. Intrasection reliability was also good, as evidenced by high intraclass correlation coefficients: 0.89, 0.94, 0.96 and 0.83 (95% CI) for the same key ocular variables (Table 2.4).

Variable	Measurement	Repeatability		Reliability		
		Measurement error	Repeatability	ICC	95% CI	P-value
Image Analysis	CDh	0.14	0.40	0.89	0.77 to 0.97	<0.0001
	CSH	0.06	0.16	0.94	0.86 to 0.98	<0.0001
	CSJ angle	0.60	1.66	0.96	0.91 to 0.99	<0.0001
	SR	7.08	19.64	0.83	0.67 to 0.95	<0.0001

**Table 2.4:** Repeatability and reliability of ocular topography measurements by Zeiss Visante AS-OCT

### 2.3.4 Lens Fit

Lens fit was found to be less variable with the hydrogel lens which tended to show a narrower range of fittings when compared with the silicone hydrogel lens (Table 2.5). Some extremes of PBM and tightness on push-up were seen with both lens types. However, most fittings fell within what might be regarded as acceptable ranges. For instance, the proportion of fittings exhibiting PBM in the range 0.2-0.6 mm was 77%. Overall lens fits were rated as successful for 79% and 88% of the galyfilcon A and etafilcon A lenses, respectively.

Lens Fit Variable	etafilcon A lens			galyfilcon A lens		
	Mean	SD	Range	Mean	SD	Range
Total decentration (mm)	0.15	0.13	0.00 to +0.6	0.22	0.17	0.0 to 0.8
Horizontal decentration (mm)	-0.04	0.14	-0.5 to +0.2	-0.03	0.12	-0.3 to +0.2
Vertical decentration (mm)	+0.03	0.13	-0.4 to +0.3	+0.12	0.22	-0.6 to +0.8
Post-blink movement (mm)	0.33	0.17	0.00 to 0.80	0.25	0.14	0.00 to 0.60
Lens tightness (push up test %)	40.7	9.5	20 to 60	41.9	9.9	20 to 65

**Table 2.5:** Lens fit results

### 2.3.5 Lens Fit Correlations

A number of lens fit variables were correlated to corneoscleral variables for the silicone hydrogel lens, but the only assessment that correlated with the hydrogel lens was between post-blink movement and PA (Table 2.6). Modelling of the principal factors of lens fit with corneoscleral measurements showed that central keratometry was a poor predictor of contact lens fit. The addition of videokeratometry data did not improve the prediction in this study; however, incorporation of corneoscleral topography from the AS-OCT data strengthened the predictive power of the model. The combined AS-OCT and slit lamp data, for instance, were able to account for 24% of the variance of post-blink movement for the silicone hydrogel lens (Table 2.7).

<b>Lens Fit Variable</b>	<b>Lens Type</b>	<b>Ocular Variable</b>	<b>Correlation Coefficient (r)</b>	<b>P-Value</b>
Comfort	galyfilcon A	CS10h -VK	-0.39	0.0062
Lens tightness	galyfilcon A	$\Delta$ CSJh	+0.40	0.0041
Post-blink movement	etafilcon A	PA	+0.39	0.0086
Post-blink movement	galyfilcon A	PA	+0.44	0.002
Total decentration	galyfilcon A	Srt	+0.37	0.0091
Horizontal centration	galyfilcon A	CS10h -OCT	-0.38	0.0065
Horizontal centration	galyfilcon A	CS10v -OCT	-0.39	0.0056
Vertical centration	galyfilcon A	Srt	+0.47	0.0005

**Table 2.6:** Significant lens fit correlations with corneoscleral shape parameters

Lens Type	Outcome Variable	Predictor Variables		Regression Model		Predictor Variables		Regression Model		Predictor Variables		Regression Model	
		Variable	P-value	Adjusted R <sup>2</sup>	P-value	Variable	P-value	Adjusted R <sup>2</sup>	P-value	Variable	P-value	Adjusted R <sup>2</sup>	P-value
		Sim. Keratometry				Sim. Keratometry and VK				Sim. Keratometry, VK and AS-OCT			
Etafilcon A	Total Decentration	Constant Kf	0.024 0.043	0.06	0.043	Constant Kf	0.024 0.043	0.06	0.043	Constant SRn	0.0020 0.024	0.08	0.024
	Movement	Constant PA	0.13 0.0020	0.18	0.002	Constant PA	0.13 0.0020	0.18	0.002	Constant PA	0.13 0.0020	0.18	0.002
	Tightness	No significant predictor variables				No significant predictor variables				Constant CS10voct	0.0007 0.022	0.09	0.022
Galyfilcon A	Total decentration	No significant predictor variables				No significant predictor variables				Constant SRt	0.0038 0.0091	0.12	0.009
	Movement	Constant PA	0.32 0.0086	0.13	0.009	Constant PA	0.32 0.0086	0.13	0.009	Constant PA $\Delta$ CSAh	0.63 0.0060 0.014	0.24	0.002
	Tightness	No significant predictor variables				No significant predictor variables				Constant $\Delta$ CSAh	<0.0001 0.0041	0.14	0.004

**Table 2.7:** Stepwise multiple regression analysis with keratometry, keratometry and videokeratoscopy, and keratometry, videokeratoscopy (VK) and anterior segment optical coherence tomography (AS-OCT) variables

## 2.4 Discussion

This study has highlighted a number of interesting findings in relation to the corneoscleral profile. The junction between the cornea and sclera is often portrayed as a sharp transition given that the radius of the sclera is visibly larger than that of the cornea. However, this study has shown a smooth and, in many cases, tangential transition at the CSJ, with median values of 179° and 178° at the superior and temporal junctions, respectively. This apparent contradiction arises because of there being a gradual transition in topography between the cornea and sclera, with the sclera adopting its true radius some millimetres from the limbus.

Meier (1992) also noted a tangential corneoscleral profile in a majority of eyes when visually examining the superior profile in a large proportion of subjects. It was suggested that this assessment of superior CSJ might be used to predict soft contact lens fit; however, this seems optimistic given the variation in CSJ between different meridians noted in this study. The fact that CSJ angles were sharper at the nasal junction is consistent with the findings of Marriott (1966) who noted different scleral topography nasally compared with the other three quadrants and ascribed this to the insertion of the medial rectus muscle being closest to the cornea.

The mean CD as assessed using AS-OCT was greater than the HVID measured using traditional image capture. There was a wide range of CDs amongst the sample and the horizontal meridian was wider than the vertical, as expected ( $P < 0.0004$ ,  $t = 3.70$ ). The mean HVID was similar to that noted in previous studies (Martin and Holden, 1982, Theodorff and Lowther, 1990, Matsuda et al., 1992), but the mean horizontal CD of 13.39 mm (SD  $\pm 0.44$ ), was slightly greater than the measurements of Martin & Holden (1982), who found a mean corneal diameter of 12.9 mm (SD  $\pm 0.6$ ) using a photographic method.

The use of AS-OCT allowed for a characterisation of the limbal transition zone (LZ) based on the difference between HVID and the horizontal CD. There was a wide variation in LZ width which emphasises the poor reliability of HVID measurements in characterising corneal size (Kwok, 1990). This is primarily due to the difficulty in defining visible iris diameter, which itself depends on the rate of loss of transparency of the peripheral cornea.

As hypothesised, lens fit tended to be more variable with the stiffer, silicone hydrogel lens which, despite having a similar profile, showed fewer acceptable fittings than the hydrogel lens. A number of corneoscleral measures were correlated to lens fit variables for the silicone hydrogel lens whereas,

with the lower modulus lens, the only correlation was between post-blink movement and PA. Modelling of the principal components of lens fit confirmed that central keratometry was a poor predictor of contact lens fit. The addition of the videokeratoscopy data did not improve the prediction; however, the incorporation of corneoscleral topography data allowed better prediction of lens fit, especially for the silicone-hydrogel lens. It seems probable that the higher elastic modulus of the silicone material prevents it from wrapping as closely to the corneoscleral shape as a conventional hydrogel contact lens, resulting in less friction and more interaction between the lid and lens profile.

With respect to decentration of the hydrogel lens, the predictive ability of keratometry along the flat meridian was out-performed by the OCT measurement of nasal scleral curvature. The greater influence of the horizontal meridian is probably due to the asymmetry in CSJ angles between the nasal and temporal quadrants. Interestingly, decentration with the stiffer silicone hydrogel lens was less well predicted by corneal shape, but the predictive ability of the scleral radius was greater.

Variance in PA consistently allowed for the prediction of 13-18% of post-blink movement, with the difference in CSJ angles between the nasal and temporal quadrants ( $\Delta\text{CSJh}$ ) also explaining an additional 7% of variance for the silicone hydrogel lens. The influence of PA can be explained by the effect of the area of friction between the eyelids and lens surface and, hence, the speed of post-blink lens recovery. In addition, the eyelid has to travel further to cover a wider PA, resulting in more interaction with the lens surface, increasing the movement during blink and hence PBM.

Differences in nasal and temporal CSJ angle relate to asymmetry of the horizontal sclera. With Acuvue Advance, larger differences in the horizontal CSJ angles ( $\Delta\text{CSJh}$ ) were associated with increased lens tightness on push-up. As difference in CSJ angle increases, it is likely that the lens is forced to undergo greater stretching and flexing in the periphery in order to align with the corneoscleral topography, leading to greater inner elastic forces and increased tightness. The fact that corneal sagittal height in the vertical meridian (as opposed to  $\Delta\text{CSJh}$ ) predicted tightness with the Acuvue 2 lens may be attributable to the lower modulus of etafilcon A, resulting in more forgiving alignment of the lens to the corneoscleral topography.

Although corneoscleral topography accounts for more of the variance in soft lens fit than corneal topography alone, approximately three-quarters of the variance remains unexplained. This may be partly explained by a number of limitations in the present study design. The model compared linear association between the topography and lens fit variables whereas the interactions may be more complex. The ratings of contact lens fit were observational and the variability, even in an experienced

observer, will weaken the associations with corneoscleral topography. The contact lens designs used in this study exhibited a relatively narrow range of fitting behaviours and it is possible that more varied lens designs would have revealed stronger associations. It is also possible that a larger sample may have revealed a wider range of ocular topographies which, in turn, may have revealed stronger relationships.

Kikkawa (1979) described a model where a soft contact lens could be considered as a series of concentric elastic rubber bands, progressively stretching to accommodate changes in peripheral ocular curvature. It is likely that the enforced change in lens radius for a lens to align to the scleral surface may result in raised squeeze pressure at the lens periphery, in turn explaining why some lens fits appear excessively 'tight' or 'loose'. The use of OCT enabled the measurement of CD and CS, but also ocular sagittal height at a chord roughly equivalent to soft contact lens diameter (15 mm). The EBC for the cornea was close to that of a typical soft lens but was appreciably flatter for the wider 15 mm chord (8.6 vs. 9.4 mm). This suggests that most stretching of the type described by Kikkawa (1979) takes place in the lens periphery.

## **2.5 Conclusion**

The measurement of anterior ocular topography using an OCT technique allowed for a more complete characterisation of the cornea and peripheral corneoscleral profile than either conventional keratometry or videokeratoscopy. The extra peripheral corneoscleral data gained from OCT characterisation of the ocular surface architecture also allowed for prediction of some of the variance in soft contact lens fit, providing some insight into soft contact lens fit dynamics.

Since the peripheral ocular topography has been shown to influence lens fit, an understanding of the effect of any potential change in peripheral architecture variables as a result of body size (as dictated by height), and also eye size (as dictated by refractive error size, sex, ethnicity and ageing), may help clinically predict changes in lens fit. Consequently a large-cohort study with the aims of evaluating factors affecting corneoscleral topography, providing data for future modelling of lens fit, and also to provide a better understanding of the true range of parameters therein was undertaken in Chapter 3.

## Chapter 3

## Chapter 3: Factors Affecting Corneoscleral Topography

### 3.1 Introduction

Corneal videokeratometry measurements provide objective data relating to the central and mid-peripheral corneal topography; however, information on the topography of the peripheral cornea, corneoscleral junction and limbal sclera, which form the corneoscleral profile (CSP), is scarce (van der Worp et al., 2010). These data are of particular relevance in scleral contact lens fitting, and have also been shown to influence the fit of soft contact lenses, since this area is where soft contact lenses are required to make the greatest flexural changes in order to align to the ocular surface (Chapter 2) (Hall et al., 2011).

Marriott (1966) first attempted to characterise the anterior ocular profile using haptic shells taken from impressions of eyes; however, his study was limited to scleral contour alone and did not consider the effect of the corneoscleral junction angle (CSJ) on corneoscleral profile. Meier and co-workers (Gaggioni and Meier, 1987, Meier, 1992) later defined the CSP, as an aid to soft contact lens fitting, based on qualitative assessments of the limbal transition zone made using the naked eye or slit lamp biomicroscope. They described five different corneoscleral transition models. Their assessments of CSP, though, were restricted to the superior corneoscleral junction, and a subsequent study (Bokern et al., 2007) found that this was neither an accurate or reproducible means of classification.

More recently, a number of different workers (Feng and Simpson, 2005, van der Worp et al., 2010, Hall et al., 2011) have employed OCT, a technique that allows for more extensive imaging of the anterior segment and peripheral corneoscleral profile. The Zeiss Visante AS-OCT utilises low coherence interferometry to facilitate high-speed, non-invasive and non-contact *in-vivo* imaging of the anterior segment, and is validated in capturing full corneal depth and width in a single scan (Dunne et al., 2007).

Age, height, ethnicity, sex, and manifest refraction have been identified as affecting various anterior eye dimensions such as corneal curvature (Goto et al., 2001), central corneal thickness (Doughty and Zaman, 2000), and anterior chamber depth (Leung et al., 2010, Qin et al., 2011). It is hypothesised, therefore, that they will also influence CSP variables and, hence, could be clinically relevant in contact lens design, the optimisation of surgical procedures involving the cornea or sclera and also

in intraocular lens (IOL) selection. The purpose of this study was to define normative corneoscleral topography data and evaluate the factors affecting the peripheral corneoscleral topography in a healthy, visually-normal population.

### **3.2 Method**

A cross-sectional study was undertaken at two sites in the UK, Visioncare Research Clinic (Farnham) and Aston University (Birmingham). Subjects with pre-existing ocular pathology or a history of previous ocular surgery or refractive surgery were excluded. Subjects gave written informed consent after explanation of study procedures. The study followed the tenets of the Declaration of Helsinki and was approved by the University's Research Ethics Committee prior to commencing.

A majority of subjects identified themselves as belonging to one of two ethnicities, either Caucasian or British Asian (individuals of Indian, Pakistani, or Bangladeshi descent), and provided sufficient sample sizes to make statistical comparison between these two ethnicities. The overall ethnicity of subjects recruited was 67% Caucasian, 28% British Asian, and 5% others.

Two hundred and four subjects (408 eyes) were imaged using the Visante AS-OCT. Vertically and horizontally scanned images were captured with the subject's eye in the primary position, and also perpendicular images in the four cardinal directions of gaze to give full sagittal cross-sections of the cornea and cross-sections of the corneoscleral junctions in the vertical and horizontal meridians. External fixation targets were used to ensure consistency of subject's direction of gaze for images taken perpendicularly in the horizontal and vertical planes, as described in Chapter 2. Images were corrected for distortion using the Visante's built-in, proprietary image-correction algorithm (Software Version 1.0.12.1896).

The Visante's internal fixation target was adjusted by the operator to compensate for the angle between the visual axis and the optical axis (angle  $\alpha$ ) and carefully centred during image acquisition using the Visante's built-in alignment monitor for images acquired in primary gaze. External fixation targets were used to ensure consistency of subjects' direction of gaze for images taken perpendicularly.

Measurements of corneal diameter (CD), corneal sagittal height (CS), iris diameter (ID), corneoscleral junction (CSJ) angle and scleral radius (SR) were extracted from the images using the Visante's built-in calliper and protractor tools (Figure 3.1, Table 3.1). The corneal sagittal height of a chord at 10 mm (CS10), and the ocular sagittal height at 15 mm (OS15), were also taken. CD was defined as the

distance between the two external scleral sulci. These measurements have previously been shown to be both repeatable and reliable (Chapter 2) (Hall et al., 2011).

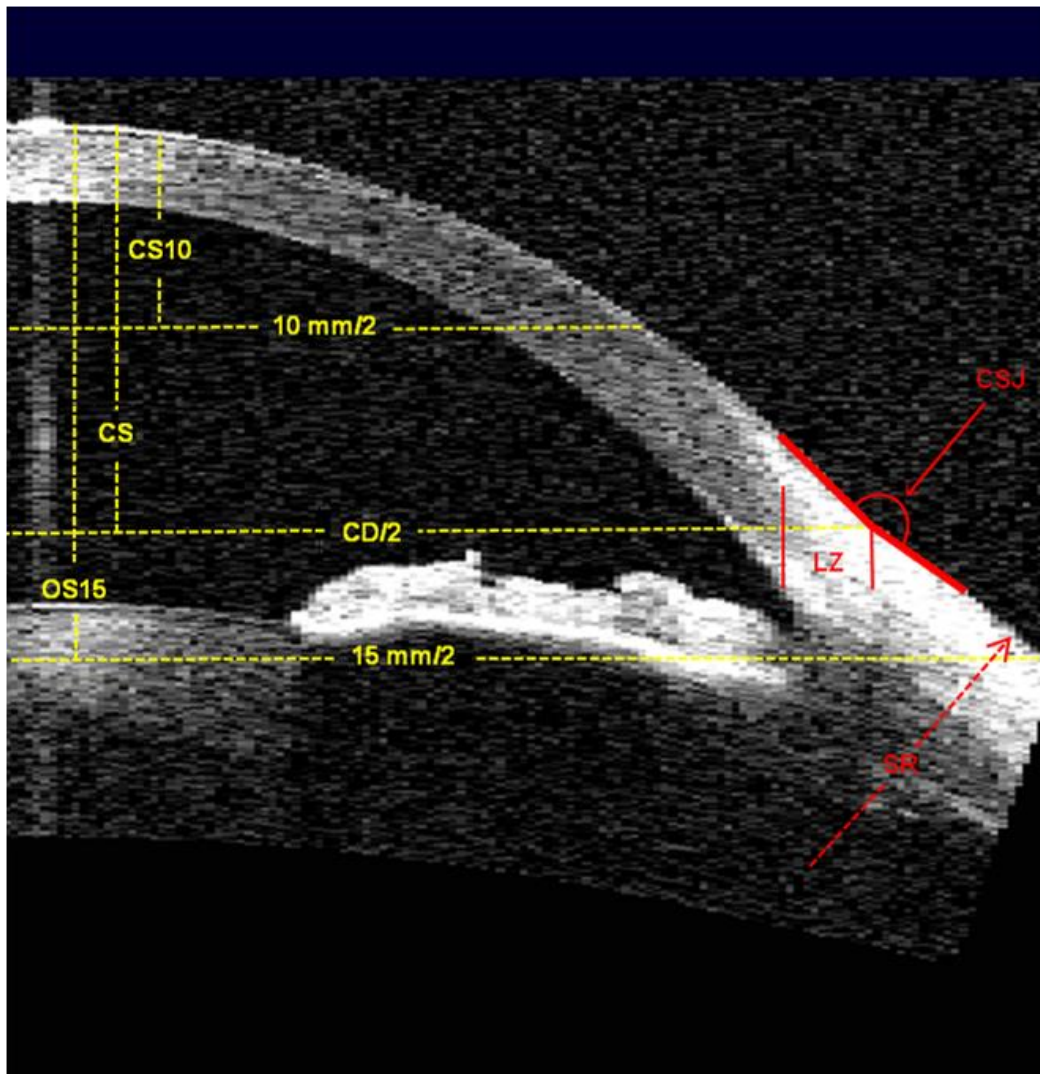


*Figure 3.1 OCT ocular topography measurements (Table 3.1)*

Abbreviation	Description	Instrument
HVID	Horizontal visible iris diameter - synonymous with white-to-white (WTW)	Slit lamp graticule
PA	Palpebral aperture	Slit lamp graticule
K	Simulated keratometry reading	VK
SF	Corneal shape factor ( $SF=e^2$ )	VK
CA	Corneal astigmatism	VK
CS10-VK	Corneal sagittal height of a chord at 10 mm	VK
CD	Corneal diameter	OCT
CS	Corneal sagittal height of a chord taken between the anterior corneal sulci	OCT
CS10-OCT	Corneal sagittal height of a chord at 10 mm	OCT
OS15	Ocular sagittal height of a chord at 15 mm	OCT
ID	Iris diameter	OCT
CSJ	Corneoscleral junction angle	OCT
SR	Scleral radius	OCT
LZ	Limbal zone, the transition zone between the outer edge of the visible iris and the outer corneal sulci; where $LZ = (CD-ID)/2$	-
$\Delta CD$	Difference in corneal diameter between the horizontal and vertical meridians	-
$\Delta CSJ$	Difference between the two corneoscleral junction angles in a given meridian	-
n, t, s, i	Nasal, temporal, superior, inferior	-
h, v	Horizontal, vertical	-

**Table 3.1:** Abbreviations of ocular measurement values

Conventional corneal topography data were collected using the Medmont E300 corneal topographer (Medmont, Camberwell, Australia) (Tang et al., 2000, Cho et al., 2002). In addition to providing simulated keratometry (K) readings, this also provided corneal height (CS) and corneal shape factor (SF) data. Since the Medmont E300 presents SF as  $e^2$  (where  $e$  = conicoidal eccentricity), the results use the convention in which a SF of zero indicates a spherical surface and a negative value indicates an oblate ellipse. Objective refraction was measured using an auto-refractor (SRW-5000; Shin-Nippon, Tokyo, Japan) (Mallen et al., 2001).

In addition to measurement of iris diameter (ID) by OCT, subjects' horizontal visible iris diameter (HVID), equivalent to the measurement of WTW, was measured using a FS2 slit lamp with built-in graticule (Nikon, Tokyo, Japan). This provided a comparison of iris diameter, as determined by OCT, with 'visible' iris diameter, as measured by slit lamp graticule. Measurements of vertical palpebral aperture (PA) were also taken using the slit lamp biomicroscope. The width of the limbal zone (LZ), the transition between the outer edge of the visible iris and the outer corneal sulci, was determined for each eye as the difference between the horizontal CD and HVID measurements. Subjects' body height was measured to test for associations between height and ocular topography variables.

A classification of CSP was made dependent on CSJ angle which was also demarked by the change from smooth cornea to undulating conjunctival profile. Transition zones with CSJ angles of  $<179^\circ$  were classified as concave (negative) zones, with angles of between  $179-181^\circ$  classified as 'flat' and those with angles of  $>181^\circ$  classified as convex (positive) (Figure 3.2).

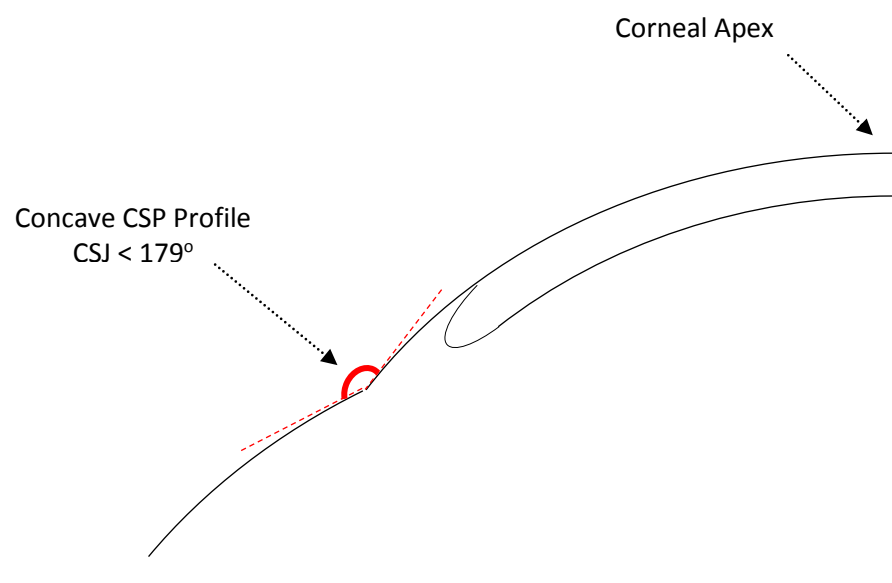


**Figure 3.2 (a):** 'Concave' corneoscleral profile

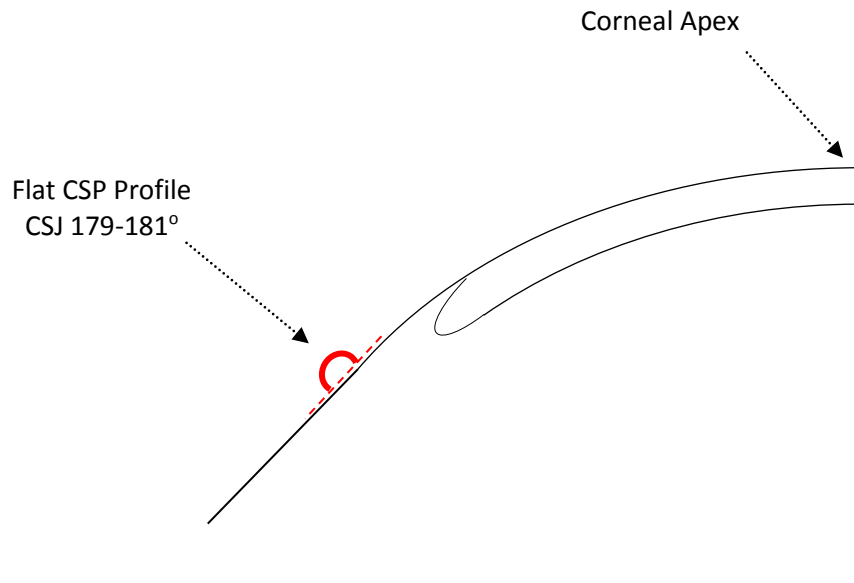


**Figure 3.2 (b):** 'Flat' corneoscleral profile

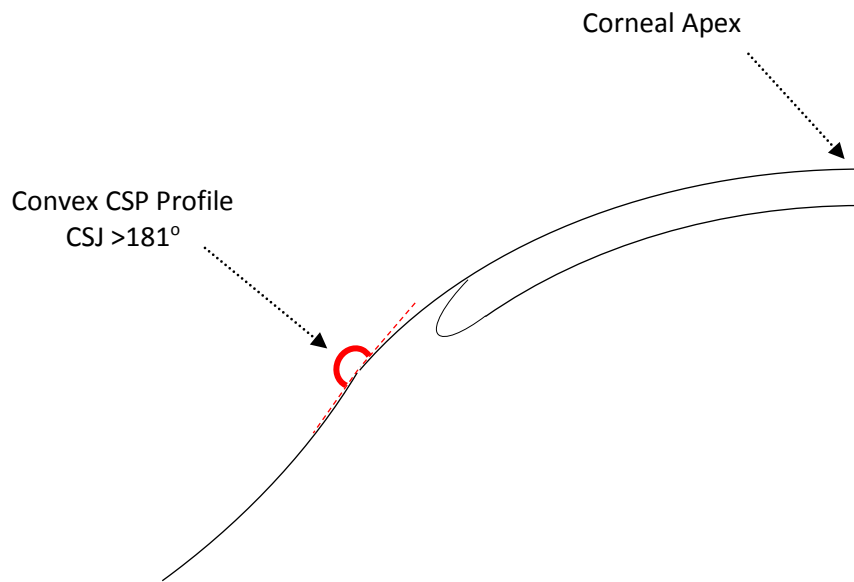


**Figure 3.2 (c):** 'Convex' corneoscleral profile

### 3.2.1 Statistical Analysis

Objective refraction data were converted into the power vector terms  $M$ ,  $J_0$  and  $J_{45}$  (Thibos et al., 1997). The Shapiro-Wilk's test was used to evaluate any deviations from normality, using a critical value of 0.05.

Pearson's and Spearman's correlation coefficients were used to examine similarities between right and left eyes. All variables showed strong positive correlations between right and left eyes ( $P \leq 0.0012$ ), indicating that the eyes were mirrored. Therefore, only data from the right eyes were analysed to alleviate any inter-ocular dependency issues and statistical bias due to enantiomorphism (Ray and O'Day, 1985), as well as to be consistent with previous studies.

Summary statistics (mean, median, standard deviation, and range) were calculated for the right eyes only for selected variables.

Data from the horizontal and vertical meridians were compared using either paired t-tests or the Wilcoxon signed-rank test, depending on the distribution of the variable. The Friedman test was used to compare CSJ angle and SR data between the four quadrants (nasal, temporal, superior, and inferior). The Wilcoxon signed-rank test was also used to compare horizontal CD with both HVID and ID, using a critical value of  $\leq 0.05$ . Spearman's rank correlation was used to examine the associations of age, sex, subject height, and power vectors with the ocular topography variables, and to examine associations between topography variables. In view of the conservative nature of multiple comparison corrections, such as Bonferroni (Hochberg and Benjamini, 1990), a critical value of  $P \leq 0.01$  was considered significant.

CS10 data measured with both videokeratoscopy and anterior segment OCT were compared using Bland-Altman plots (Bland and Altman, 2010). Also, for these plots, 95% confidence intervals of the mean differences were calculated as CS10 data measured with both videokeratoscopy and anterior segment OCT were compared using Bland-Altman plots (Bland and Altman, 2010). Also, for these plots, 95% confidence intervals of the mean differences were calculated as:

$$\bar{x} \pm \left[ t_{1-\alpha/2} \times SE(\bar{x}) \right] \quad (\text{where } \bar{x} = \text{Mean difference})$$

*Post-hoc* analysis (mixed model analysis) was undertaken to compare differences between sex and also ethnicity with respect to ocular topography variables. The models included subject age, sex, subject height, ethnicity (British Asian and Caucasian) and power vector terms as fixed factors. Since the majority (95%) of subjects were either British Asian or Caucasian, this analysis included only these

194 subjects and excluded the remaining 5% of subjects of other ethnicity due to their small sample size. Model estimates of mean and standard error were reported for the comparisons of ethnic group and sex. A  $P$ -value of  $\leq 0.01$  indicated a significant difference.

Data were analyzed using SPSS (PASW Version 18, IBM Inc., NY, US). Missing data were excluded from the analysis and not extrapolated from the collected data.

**Sample Size Calculation:**

A sample size calculation was not carried out as a primary aim of the study was to define normative corneoscleral topography enrolling in as large a cohort study as possible. However, taking a minimal critical correlation coefficient value of 0.35 to demonstrate moderate (or better) correlative strength and assuming a two-tailed test, the number of subjects required to achieve statistical significance to  $P \leq 0.01$  was determined to be 50 subjects, which was amply satisfied by the number of subjects who participated.

Similarly, as the analysis undertaken to compare differences in ocular topography between different ethnicities and sexes was undertaken *Post-hoc*, no sample size calculation was made for this element of the analysis. However, sample size calculation in this instance would have been complicated by subject age, sex, subject height, ethnicity (British Asian and Caucasian) and power vector terms taken as fixed factors in the mixed model analysis. Although an example sample size calculation assuming t-tests comparisons would require substantial subject numbers to elicit significant differences (Table 3.2), the mixed model approach showed significant differences for a relatively small number of subjects.

	Sample Size						
	CD	CSh	IDh	CS10h	OS15h	CSAn	SRn
Mean difference	0.09	0.05	0.06	0.00	0.03	0.37	-15.92
SD of each group (equal SD assumed)	0.4	0.21	0.40	0.08	0.18	3.63	42.24
Sample size per group	462	413	1039	NA	841	2249	165

**Table 3.2:** Sample size calculations, assuming a power of 80% and alpha value of 0.01

## **3.3 Results**

### **3.3.1 Biometric Data**

The mean age of subjects was 34.9 yrs (SD  $\pm$ 15.2, range 18 to 65) and 65% were female. The mean height of subjects was 169.0 cm (SD  $\pm$ 9.4, range 152 to 192).

Most of the variables (73%) showed significant variations from the normal distribution. All ocular variables showed significant correlations between right and left eyes ( $P < 0.0012$ ). Correlations between right and left eyes, and distributions, for ocular collected are shown in Table 3.3 and Table 3.4, respectively.

<b>Variables</b>	<b><i>n</i></b>	<b><i>r</i></b>	<b>P-value</b>	<b>Test</b>
M	203	0.95	<0.0001	Spearman's
J0	203	0.72	<0.0001	Spearman's
J45	203	0.42	<0.0001	Spearman's
HVID	198	0.90	<0.0001	Spearman's
PA	195	0.88	<0.0001	Spearman's
Kh	202	0.96	<0.0001	Spearman's
Kv	202	0.96	<0.0001	Pearson
SFh	202	0.85	<0.0001	Spearman's
SFv	195	0.57	<0.0001	Spearman's
CS10h-VK	202	0.80	<0.0001	Spearman's
CS10v-VK	202	0.88	<0.0001	Spearman's
CDh	203	0.68	<0.0001	Spearman's
CDv	171	0.71	<0.0001	Spearman's
ΔCD	170	0.45	<0.0001	Spearman's
CSH	203	0.79	<0.0001	Pearson
CSv	171	0.81	<0.0001	Pearson
CS10h-OCT	204	0.87	<0.0001	Spearman's
CS10v-OCT	200	0.82	<0.0001	Spearman's
OS15h	200	0.91	<0.0001	Pearson
OS15v	160	0.87	<0.0001	Pearson
IDh	203	0.83	<0.0001	Pearson
IDv	194	0.75	<0.0001	Pearson
LZh	202	0.58	<0.0001	Spearman's
LZv	171	0.57	<0.0001	Spearman's
CSJn	204	0.31	<0.0001	Spearman's
CSJt	203	0.38	<0.0001	Spearman's
ΔCSJh	203	0.07	0.30	Spearman's
CSJs	199	0.24	0.0006	Spearman's
CSJi	200	0.23	0.0012	Spearman's
ΔCSJv	198	-0.01	0.88	Spearman's
SRn	204	0.41	<0.0001	Spearman's
SRT	202	0.44	<0.0001	Spearman's
SRs	199	0.52	<0.0001	Spearman's
SRI	199	0.57	<0.0001	Spearman's

**Table 3.3:** Summary of correlations between right and left eyes for all ocular variables

Ocular Variable	Eye	Horizontal					Vertical				
		N	Mean (SD)	Range	Skewness	Kurtosis	N	Mean (SD)	Range	Skewness	Kurtosis
M (D)	Right	203	-1.95 (2.43)	-10.19 to +3.50	-0.71	+0.45	-				
	Left	203	-1.97 (2.53)	-9.75 to +2.88	-0.71	+0.22					
J <sub>0</sub> (D)	Right	203	0.08 (0.36)	-0.99 to +2.93	+2.64	+19.59	-				
	Left	203	0.08 (0.32)	-1.02 to +1.12	+0.46	+1.08					
J <sub>45</sub> (D)	Right	203	0.01 (0.17)	-0.53 to +0.60	+0.33	+1.10	-				
	Left	203	-0.01 (0.17)	-0.56 to +0.55	+0.18	+1.44					
HVID (mm)	Right	199	11.66 (0.48)	10.50 to 13.22	+0.23	+0.50	-				
	Left	199	11.57 (0.51)	9.26 to 13.13	-0.32	+2.25					
PA (mm)	Right						196	10.24 (1.41)	6.60 to 13.43	-0.25	-0.44
	Left						196	10.18 (1.44)	6.30 to 13.41	-0.09	-0.31
Sim. K (mm)	Right	202	7.84 (0.30)	7.09 to 8.75	+0.36	+0.60	202	7.68 (0.28)	6.96 to 8.51	+0.19	-0.09
	Left	203	7.82 (0.28)	6.96 to 8.73	+0.12	+0.69	203	7.67 (0.28)	6.84 to 8.45	+0.06	-0.22
CA (D)	Right	202	-1.04 (0.64)	-0.06 to -5.56	-2.39	+12.16					
	Left	203	-1.06 (0.56)	-0.11 to -3.01	-0.86	+0.48					
SF	Right	202	0.46 (0.15)	0.09 to 0.93	+0.36	-0.04	196	0.18 (0.11)	-0.44 to +0.53	-0.41	+3.79
	Left	203	0.46 (0.14)	0.18 to 0.94	+0.37	-0.19	201	0.19 (0.14)	-0.13 to +0.81	+1.13	+3.67
CS10m (mm)	Right	202	1.77 (0.08)	1.53 to 2.03	+0.17	+0.82	202	1.81 (0.10)	1.57 to 2.14	+0.38	+0.31
	Left	203	1.70 (0.08)	1.50 to 1.90	+0.12	-0.36	203	1.80 (0.10)	1.57 to 2.26	+0.50	+1.34
CD (mm)	Right	204	13.44 (0.41)	12.10 to 14.41	-0.47	+0.72	186	13.21 (0.62)	11.18 to 14.41	-0.83	+0.51
	Left	203	13.44 (0.44)	12.08 to 14.55	-0.58	+0.66	180	13.22 (0.57)	11.00 to 14.96	-0.55	+0.97
ΔCD (mm)	Right	186	0.23 (0.54)	-1.00 to +2.03	+0.64	+0.55	-				
	Left	179	0.22 (0.49)	-1.16 to +1.72	+0.09	+0.37					
CS (mm)	Right	204	3.17 (0.20)	2.57 to 3.71	+0.20	-0.02	186	3.09 (0.27)	2.26 to 3.73	-0.40	-0.07
	Left	203	3.18 (0.20)	2.57 to 3.75	-0.13	+0.07	180	3.10 (0.26)	2.18 to 3.80	-0.28	+0.60
CS10 (mm)	Right	204	1.75 (0.08)	1.53 to 1.98	+0.06	+0.47	202	1.78 (0.08)	1.43 to 2.02	-0.40	+1.56
	Left	204	1.74 (0.08)	1.51 to 1.92	-0.21	+0.15	200	1.79 (0.08)	1.61 to 2.02	+0.34	-0.11
OS15 (mm)	Right	202	3.70 (0.17)	3.23 to 4.08	-0.26	-0.10	178	3.75 (0.18)	3.20 to 4.24	-0.27	+0.20
	Left	202	3.72 (0.17)	3.25 to 4.10	-0.28	-0.09	172	3.75 (0.17)	3.31 to 4.14	-0.16	-0.16
ID (mm)	Right	203	11.58 (0.41)	10.63 to 12.81	+0.21	+0.01	199	11.16 (0.46)	9.69 to 12.17	-0.27	-0.05
	Left	204	11.56 (0.44)	10.47 to 12.67	+0.15	-0.30	194	11.17 (0.44)	9.77 to 12.22	-0.26	+0.30
LZ (mm)	Right	203	0.93 (0.18)	+0.43 to +1.38	-0.23	-0.13	186	1.03 (0.27)	-0.09 to +1.61	-0.73	+0.90
	Left	203	0.94 (0.19)	-0.04 to +1.47	-0.54	+3.29	180	1.02 (0.25)	+0.33 to +1.75	-0.41	+0.07
CSA (°)	Right	204	173.9 (3.4) n	149.1 to 179.9	-2.15	+12.82	200	178.1 (1.9) s	167.2 to 184.4	-1.45	+6.16
	Left	204	173.3 (3.1) n	160.3 to 179.8	-0.71	+1.70	200	178.2 (1.8) s	168.6 to 183.8	-1.45	+5.33
	Right	203	177.0 (2.4) t	169.5 to 183.8	-0.66	+0.67	201	177.7 (1.6) i	172.6 to 180.0	-0.68	-0.06
	Left	204	177.2 (2.5) t	168.0 to 184.7	-1.09	+1.68	201	177.5 (1.8) i	171.1 to 182.2	-0.71	+0.65
ΔCSA (°)	Right	203	3.6 (2.9)	0.0 to 24.9	+2.54	+14.83	199	1.6 (1.5)	0.0 to 12.2	+2.54	+12.47
	Left	204	4.3 (2.9)	0.0 to 19.0	+1.23	+3.33	199	1.9 (1.6)	0.0 to 9.7	+1.38	+2.94
SR (mm)	Right	204	35.5 (39.4) n	-57.4 to +312.5	+4.26	+24.58	199	29.3 (17.4) s	-19.7 to +142.0	+2.75	+11.95
	Left	204	32.0 (42.7) n	-99.5 to +312.5	+4.49	+27.08	201	33.5 (28.0) s	+3.0 to +157.5	+2.99	+9.57
	Right	202	22.4 (12.7) t	+3.1 to +100.0	+3.20	+12.90	201	33.5 (29.6) i	+9.4 to +313.8	+5.52	+42.87
	Left	204	20.1 (16.1) t	-155.6 to +78.8	-5.49	+72.55	200	35.6 (37.0) i	-40.1 to +313.8	+5.16	+33.30

Key: K = Simulated Keratometry; PA = Palpebral Aperture; VID = Visible Iris Diameter; SF = Shape Factor; CS10-VK = Corneal Sagittal Height of a Chord at 10mm (by Videokeratoscopy); CD = Corneal Diameter; CS = Corneal Sagittal Height; CS10-OCT = Corneal Sagittal Height of a Chord at 10mm (by OCT); OS15 = Ocular Sagittal Height of a Chord at 15mm; ID = Iris Diameter (by OCT); LZ = Limbal Zone Width; CSJ = Corneoscleral Junction Angle; SR = Scleral Radius; h = horizontal, v = vertical, s = superior, i = inferior, n = nasal, t = temporal.

**Table 3.4:** Summary of Shapiro-Wilk Tests for deviations from normality

The mean spherical equivalent, (M), was -1.96 D (SD  $\pm 2.47$ , range -10.20 to +3.50),  $J_0$  +0.08 D (SD  $\pm 0.34$ , range -1.00 to +2.90 D and  $J_{45}$  0.00 D (SD  $\pm 0.17$ , range -0.60 to +0.60), (Table 3.5, Figure 3.3).

	(eyes)	> -6.00D	-6.00 to -3.01D	-3.00to -0.01D	Plano to +3.00D	+3.01 to +6.00D
<b>18-39 yrs</b>	127 (62%)	8 (6.3%)	24 (18.9%)	76 (59.8%)	19 (15%)	0 (0%)
<b>40-65 yrs</b>	77 (38%)	7 (9.1%)	20 (26.0%)	33 (42.9%)	16 (20.8%)	1 (1.3%)
<b>Male</b>	72 (35%)	3 (4.2%)	15 (20.8%)	48 (66.7%)	5 (6.9%)	1 (1.4%)
<b>Female</b>	132 (65%)	12 (9.1%)	29 (22.0%)	61 (46.2%)	30 (22.7%)	0 (0%)
<b>Total</b>	204 (100%)	15 (7.4%)	44 (21.6%)	109 (53.4%)	35 (17.2%)	1 (0.5%)

**Table 3.5:** Mean spherical equivalent refractive error by age and sex (right eyes only)

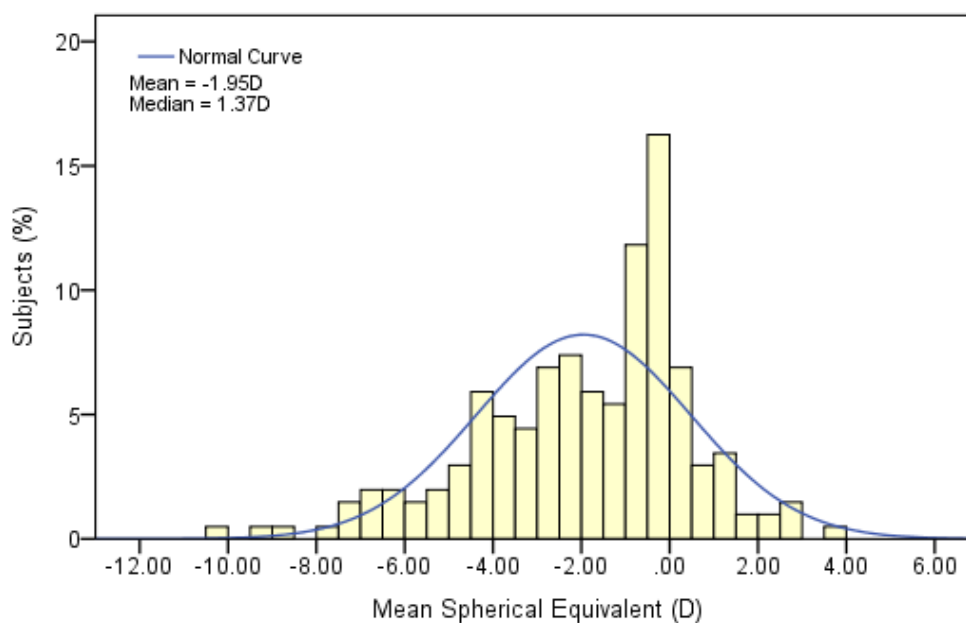


**Figure 3.3:** Frequency distribution of mean spherical equivalent (right eyes only)

### 3.3.2 Ocular Dimensions

There was a wide variation in corneal shape amongst the study sample, with horizontal K readings ranging from 7.09 to 8.75 mm (mean 7.81, SD  $\pm$  0.30 mm). As expected, the mean horizontal CD was larger than HVID (13.4 vs. 11.7 mm,  $P < 0.0001$ ) measured by slit-lamp, but also larger than horizontal ID measured by OCT (13.4 vs. 11.6 mm,  $P < 0.0001$ ). There was also a wide variation amongst the study population in LZ width, the transition zone between ID and outer corneal border (-0.09 to 1.61 mm); the mean horizontal LZ width was 0.94 mm (SD  $\pm$  0.18). The ocular topography results are summarised in Table 3.6. Frequency distributions of key ocular variables are shown in Figure 3.4 to Figure 3.6.

Ocular Variable	Horizontal					Vertical				
	Subjects <sup>‡</sup>	Mean	SD	Median	Range	Subjects <sup>‡</sup>	Mean	SD	Median	Range
K <sub>sim</sub> (mm)	202	7.84	0.30	7.81	7.09 to 8.75	202	7.68	0.28	7.64	6.96 to 8.51
PA (mm)	-	-	-	-	-	196	10.2	1.4	10.3	6.6 to 13.4
HVID (mm)	199	11.7	0.5	11.7	10.5 to 13.2	-	-	-	-	-
SF	202	0.46	0.15	0.44	0.09 to 0.93	196	0.18	0.11	0.17	-0.44 to 0.53
CS10-VK (mm)	202	1.77	0.08	1.77	1.53 to 2.03	202	1.81	0.10	1.80	1.57 to 2.14
CD (mm)	204	13.4	0.4	13.5	12.1 to 14.4	186	13.2	0.6	13.3	11.2 to 14.4
CS (mm)	204	3.17	0.20	3.15	2.57 to 3.71	186	3.09	0.27	3.12	2.26 to 3.73
CS10-OCT (mm)	204	1.75	0.08	1.75	1.53 to 1.98	202	1.78	0.08	1.78	1.43 to 2.02
OS15-OCT (mm)	202	3.70	0.17	3.71	3.23 to 4.08	178	3.75	0.18	3.75	3.20 to 4.24
ID (mm)	203	11.58	0.41	11.57	10.63 to 12.81	199	11.16	0.46	11.16	9.69 to 12.17
LZ (mm)	203	0.93	0.18	0.94	0.43 to 1.38	186	1.03	0.27	1.06	-0.09 <sup>†</sup> to 1.61
CSJ (°)	204	173.9 n	3.4	174.0	149.1 to 179.9	200	178.1 s	1.9	178.6	167.2 to 184.4*
	203	177.0 t	2.4	177.3	169.5 to 183.8*	201	177.7i	1.6	177.9	172.6 to 180.0
SR (mm)	204	35.5 n	39.4	22.5	-57.4 to 312.5	199	29.3 s	17.4	25.6	-19.7 to 142.0
	202	22.4 t	12.7	18.9	3.1 to 100.0	201	33.5i	29.6	26.1	9.4 to 313.8

\* Angle of >180° signifies a convex corneoscleral junction profile. <sup>†</sup> A minus value signifies where limbal transparency extended beyond the anterior corneal sulcus. <sup>‡</sup> Data could not be extracted from <2.5% of horizontal image scans, increasing to 4.5% on average for vertical scans due to the obstruction of the upper lid. See Table 3.1 for Ocular Variable abbreviations

**Table 3.6:** Ocular topography variables (right eyes only)

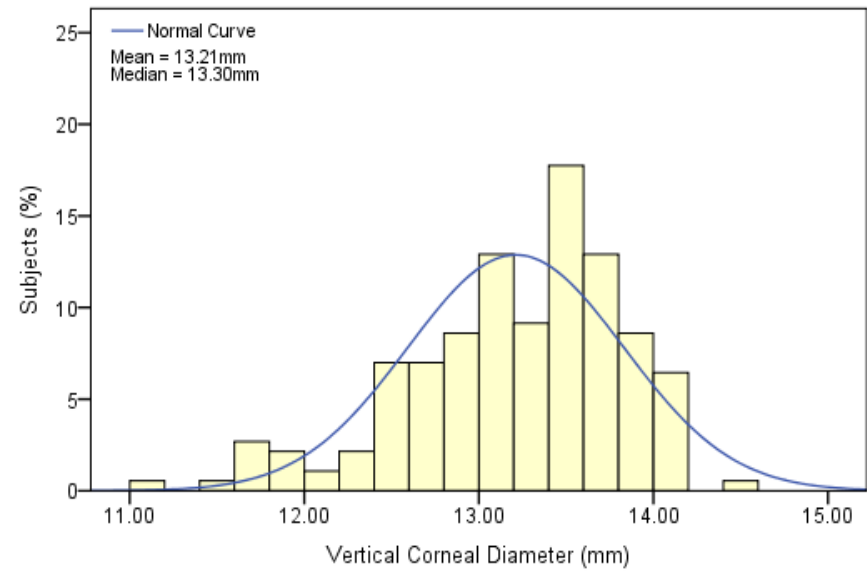
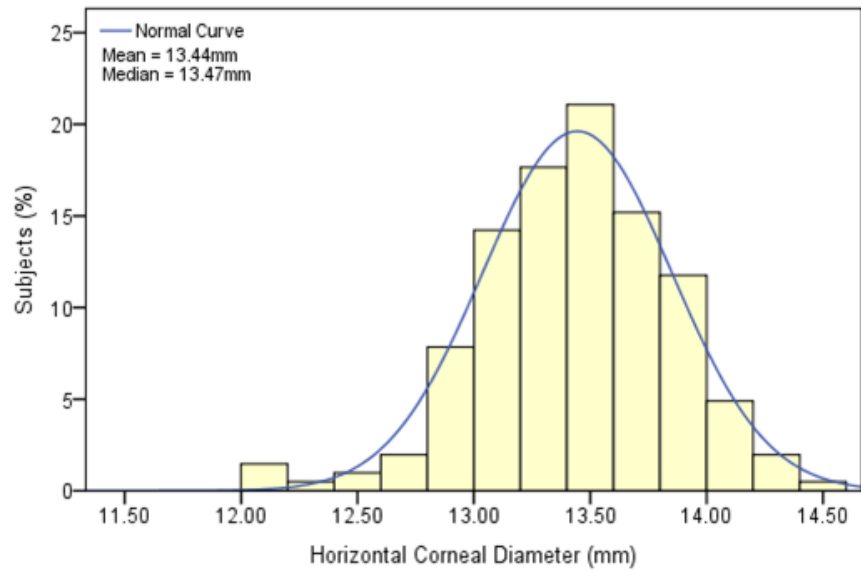


**Figure 3.4:** Frequency distribution of **(a)** horizontal and **(b)** vertical corneal diameter (right eyes only)

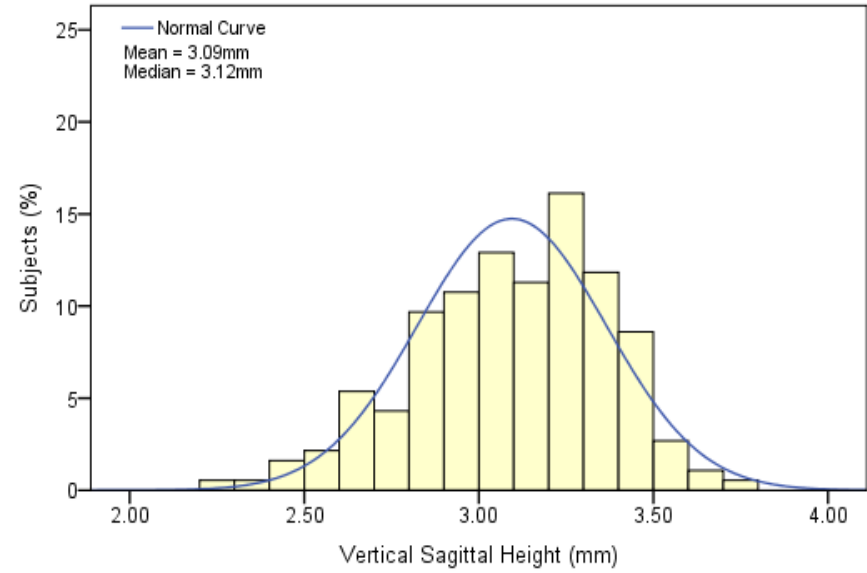
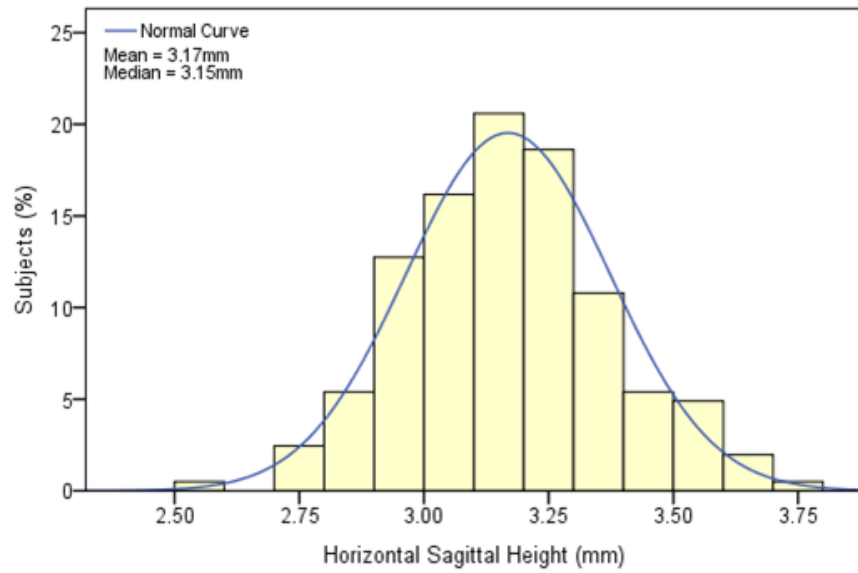


**Figure 3.5:** Frequency distribution of **(a)** horizontal and **(b)** vertical corneal sagittal height (right eyes only)

The mean CSJ angle tended to be sharpest at the nasal CSJ and became progressively (and significantly) flatter at the temporal, inferior and superior junctions (Friedman Test,  $\chi^2=220.1$ ,  $P<0.0001$ , Table 3.6, Figure 3.6).

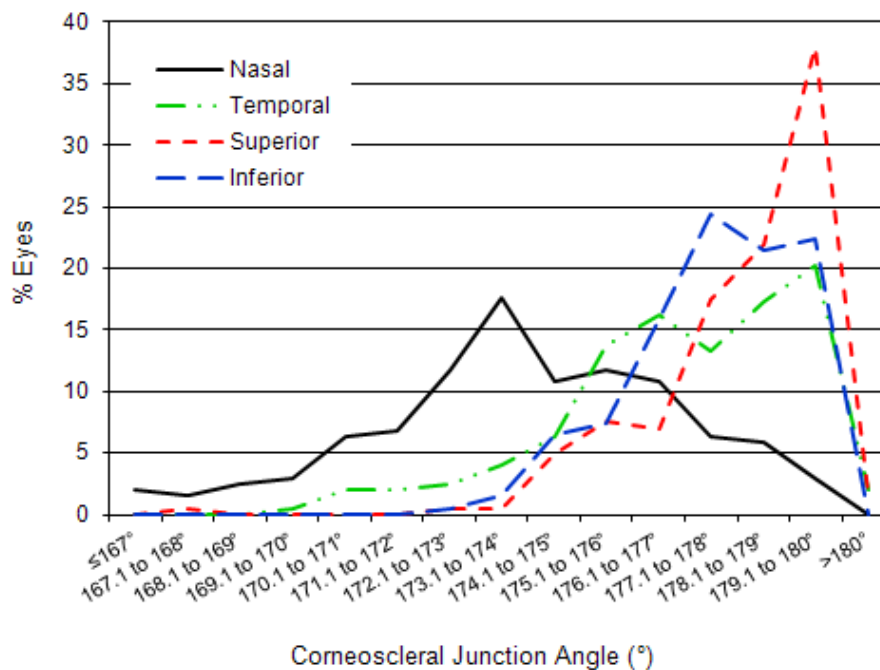


**Figure 3.6:** Frequency distribution of corneoscleral junction angles (right eyes only)

In many cases, CSJ angles lay within the 179-181<sup>0</sup> range, indicating almost tangential extensions of the peripheral cornea to form the sclera i.e. ‘flat’ corneoscleral profiles (Figure 3.2 b). This was evident in 40%, 24%, 21% and 3% of eyes at the superior, inferior, temporal and nasal corneoscleral junctions, respectively. In less than 1% of cases, CSJ angles were found to be greater than 181<sup>0</sup>, indicating a ‘convex’ corneoscleral profile (Figure 3.2 c). These profiles, although classified as ‘convex’, agree with the Gaggioni and Meier’s ‘concave’ (Profile 5) of CSP classification (Figure 1.5, Page 27) in that they share a concave scleral profile of a similar prevalence. A breakdown of the CSP types according to CSJ angle seen is summarised in Table 3.7.

		Superior	Inferior	Nasal	Temporal	All
	<i>n</i> (eyes)	200	201	204	203	808
CSJ Angle	<179° (Concave)	58.5% (117)	75.6% (152)	97.1% (198)	77.3% (157)	77.2% (624)
	180° ±1° (Flat)	40% (80)	24.4% (49)	2.9% (6)	21.2% (43)	22% (178)
	>181° (Convex)	1.5% (3)	0% (0)	0% (0)	1.5% (3)	0.7% (6)
	180° ±5°	94.0% (188)	93.0% (187)	38.7% (79)	84.2% (171)	77.4% (625)
	180° ±10°	99.5% (199)	100.0% (201)	91.2% (186)	99.5% (202)	97.5% (788)

**Table 3.7** Classifications of corneoscleral profile according to corneoscleral junction angle (*right eyes only*)

Scleral radius of curvature ranged from -57 to 313 mm. The mean scleral radius was steepest in the temporal sclera, but was similar in each of the nasal, superior and inferior scleral planes (Friedman Test,  $\chi^2=85.1$ ,  $P < 0.0001$ ).

Significant differences were found between horizontal and vertical planes with respect to all variables ( $P < 0.01$ ). The mean difference between opposing corneoscleral junctions ( $\Delta$ CSJ), e.g. nasal and temporal, was significantly greater for the horizontal meridian than for the vertical meridian (3.61 vs. 1.64°,  $P < 0.0001$ ).

### 3.3.3 Correlations between Ocular Topography Variables

Significant correlations were found between ocular variables are summarised in Table 3.8. OCT measurements of iris diameter (ID) correlated strongly with those of HVID measured with slit-lamp graticule ( $r= +0.68$ ,  $P <0.0001$ ). Corneal astigmatism was not significantly correlated with the difference in vertical and horizontal corneal diameter (i.e.  $\Delta CD$ )  $r= +0.12$ ,  $P =0.12$ .

Variable	<i>n</i> (eyes)	Ocular Variable	Correlation Coefficient (R)	<i>P</i> Value
ID	198	HVID	+0.68	<0.001
CDh	199	HVID	+0.43	<0.001
	203	IDh	+0.55	<0.001
CDv	186	CSv	+0.80	<0.001
	181	HVID	+0.37	<0.001
CSh	204	CDh	+0.63	<0.001
	202	SFh	-0.46	<0.001
CSv	186	CDv	+0.80	<0.001
LZh	203	CDh	+0.43	<0.001
	203	CSh	+0.34	<0.001
	203	IDh	-0.45	<0.001
	185	LZv	+0.39	<0.001
LZv	186	CDv	+0.61	<0.001
	186	CSv	+0.47	<0.001
	185	LZh	+0.39	<0.001
CSJn	199	SRn	+0.29	<0.001
CSJt	181	SRt	+0.29	<0.001

**Table 3.8:** Significant correlations between ocular variables

The only measurement derived from both videokeratometry and OCT was corneal sagittal height at 10 mm (CS10) which showed a significant correlation between the two measurement techniques ( $r = +0.87$ ,  $P < 0.0001$ ; mean difference  $+0.02 \pm 0.01$  mm [95% CI] and  $r = +0.78$ ,  $P < 0.0001$ ; mean difference  $+0.02 \pm 0.01$  mm [95% CI], for the horizontal and vertical meridians, respectively) (Figure 3.7).

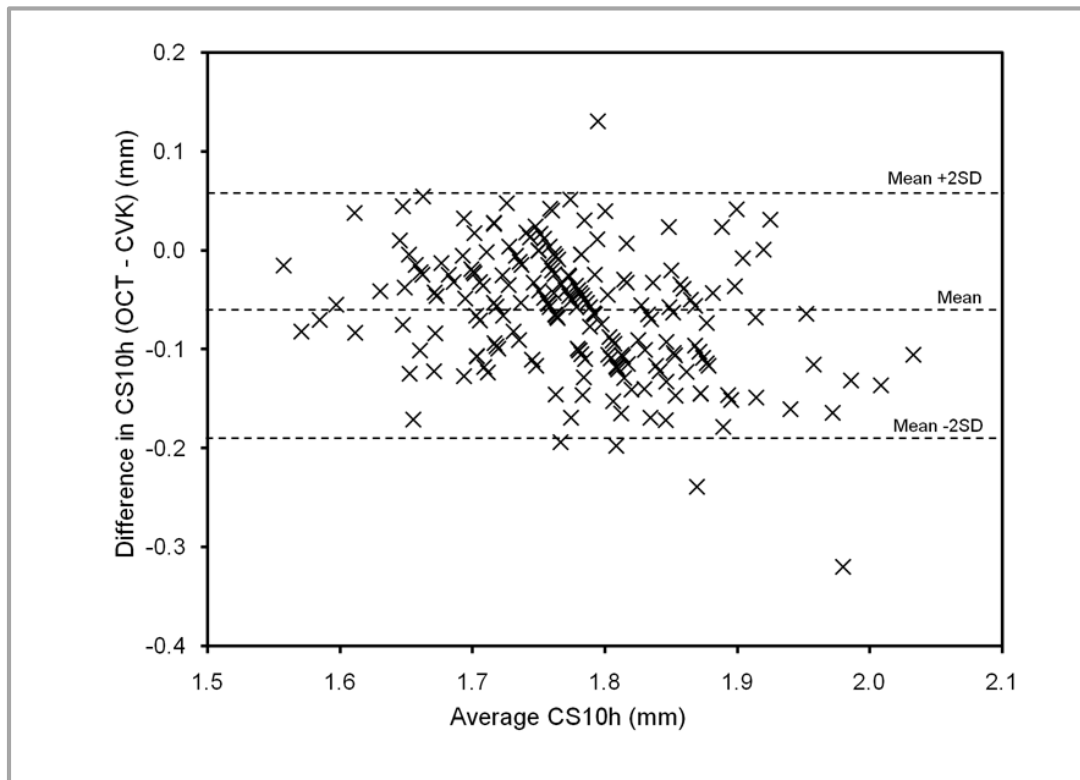


**Figure 3.7:** Comparison of the horizontal corneal sagittal height measurements of a chord at 10 mm by computerized videokeratometry and OCT and the average measurement (right eyes only), showing the 95% limits after Bland-Altman

### **3.3.4 Factors Affecting Ocular Topography Variables**

Significant correlations were found between various ocular variables and age, height, mean spherical equivalent and cylindrical power vector terms. However, age correlated with the greatest number of variables and had stronger associations than the other continuous variables (Table 3.9).

Subject age contributed to variance in the greatest number of ocular topography variables, while subject height did not influence variance (Table 3.10). Age alone accounted for up to 36%, 33%, 24%, 23%, and 13% of the variance in CSJ, SR, ID, CD and SF, respectively.

Significant differences were found between Caucasian and British Asian topographies with respect to horizontal CD ( $P=0.0046$ ), both horizontal and vertical CS ( $P=0.0068$  and  $P=0.0095$ ) and horizontal ID ( $P=0.0010$ ). The same ocular topography variables, with the exception of vertical CS, were also found to vary with sex; horizontal CD ( $P=0.0018$ ), horizontal CS ( $P=0.0018$ ), and ID ( $P=0.0012$ ) (Table 3.11).

Variable	Age			Height			Mean Equivalent Sphere			$J_0$			$J_{45}$		
	P	R	N	P	R	N	P	R	N	P	R	N	P	R	N
HVID	<b>&lt;0.0001</b>	<b>-0.40</b>	<b>199</b>	<b>0.0016</b>	0.23	189	0.85	-0.01	198	<b>0.0013</b>	<b>0.23</b>	<b>198</b>	0.61	-0.04	198
PA	<b>&lt;0.0001</b>	<b>-0.34</b>	<b>196</b>	0.11	0.12	186	0.046	-0.14	195	0.015	0.17	195	0.46	0.05	195
Kh	0.25	-0.08	202	0.076	0.13	192	0.033	0.15	201	0.24	0.08	201	0.65	-0.03	201
Kv	0.37	-0.06	202	0.011	0.18	192	<b>0.0030</b>	0.21	201	0.018	-0.17	201	0.71	-0.03	201
SFh	0.092	0.12	202	0.73	-0.02	192	0.12	0.11	201	0.018	0.17	201	0.37	-0.06	201
SFv	0.096	0.12	196	0.19	-0.10	186	0.46	-0.05	195	0.97	0.00	195	0.92	0.01	195
CS10h-VK	0.078	0.12	202	0.034	-0.15	192	0.16	-0.10	201	0.30	-0.07	201	0.56	0.04	201
CS10v-VK	0.69	-0.03	202	0.15	-0.11	192	0.041	-0.14	201	0.16	0.10	201	0.53	0.04	201
CDh	0.14	-0.10	204	0.026	0.16	194	<b>0.0097</b>	-0.18	203	0.20	0.09	203	0.018	0.17	203
CDv	0.064	-0.14	186	<b>0.0073</b>	0.20	177	0.66	-0.03	185	0.67	-0.03	185	0.86	-0.01	185
$\Delta$ CD	0.29	0.08	186	0.25	-0.09	177	0.13	-0.11	185	0.48	0.05	185	0.068	0.13	185
CSh	0.15	-0.10	204	0.093	0.12	194	<b>0.0001</b>	<b>-0.27</b>	<b>203</b>	0.70	0.03	203	<b>0.0054</b>	0.19	203
CSv	0.022	-0.17	186	0.019	0.18	177	0.20	-0.09	185	0.81	-0.02	185	0.34	0.07	185
CS10h-OCT	0.87	0.01	204	0.21	-0.09	194	0.12	-0.11	203	0.39	-0.06	203	0.63	0.03	203
CS10v-OCT	0.34	-0.07	202	0.18	-0.10	192	<b>0.0035</b>	-0.20	201	<b>0.0031</b>	0.21	201	0.21	0.09	201
OS15h	0.63	-0.03	202	0.83	0.02	192	0.050	-0.14	201	0.34	-0.07	201	0.25	0.08	201
OS15v	0.062	-0.14	178	0.26	0.09	171	0.099	-0.12	177	0.34	0.07	177	0.042	0.15	177
IDh	0.013	-0.17	203	0.012	0.18	193	0.97	0.00	202	0.46	0.05	202	0.21	0.09	202
IDv	<b>&lt;0.0001</b>	<b>-0.29</b>	<b>199</b>	<b>0.0069</b>	0.20	189	0.75	-0.02	198	0.99	0.00	198	0.88	-0.01	198
LZh	0.20	0.09	203	0.62	-0.04	193	<b>0.0065</b>	-0.19	202	0.68	0.03	202	0.31	0.07	202
LZv	0.25	0.08	186	0.90	0.01	177	0.88	-0.01	185	0.51	-0.05	185	0.59	-0.04	185
CSJn	0.011	-0.18	204	0.23	0.09	194	0.078	0.12	203	0.77	0.02	203	0.20	-0.09	203
CSJt	<b>&lt;0.0001</b>	<b>-0.35</b>	<b>203</b>	0.26	0.08	193	0.045	0.14	202	0.39	-0.06	202	0.58	-0.04	202
$\Delta$ CSJh	0.76	-0.02	203	0.80	-0.02	193	0.51	0.05	202	0.24	-0.08	202	0.32	0.07	202
CSJs	0.70	-0.03	200	0.57	-0.04	190	0.15	0.10	199	0.77	-0.02	199	0.66	0.03	199
CSJi	0.40	0.06	201	0.49	-0.05	191	0.38	0.06	200	0.16	0.10	200	0.26	0.08	200
$\Delta$ CSJv	0.77	-0.02	199	0.70	-0.03	189	0.40	-0.06	198	0.16	-0.10	198	0.43	-0.06	198
SRn	<b>&lt;0.0001</b>	<b>-0.41</b>	<b>204</b>	0.22	0.09	194	0.15	-0.10	203	0.016	0.17	203	0.44	-0.05	203
SRt	<b>&lt;0.0001</b>	<b>-0.32</b>	<b>202</b>	0.12	0.11	192	0.28	-0.08	201	0.20	0.09	201	0.51	0.05	201
SRs	<b>&lt;0.0001</b>	<b>-0.51</b>	<b>199</b>	0.34	0.07	189	0.40	-0.06	198	0.042	0.14	198	0.42	0.06	198
SRi	<b>&lt;0.0001</b>	<b>-0.36</b>	<b>201</b>	0.72	0.03	191	0.022	-0.16	200	0.15	0.10	200	0.80	-0.02	200

Spearman's rank correlation was used as all variable pairs included at least one non-normally distributed variable. P-values of  $\leq 0.01$  were considered significant.

**Table 3.9:** Significant correlations with subject age, height and refractive error (right eyes only)

Variable	Total Variance of Model	Ethnicity		Subject Age		Sex		Height		M		J <sub>0</sub>		J <sub>45</sub>	
	r <sup>2</sup>	P-value	F Stat.	P-value	F Stat.	P-value	F Stat.	P-value	F Stat.	P-value	F Stat.	P-value	F Stat.	P-value	F Stat.
HVID	0.38	0.30	1.07	<b>0.0036</b>	<b>8.71</b>	0.22	1.52	0.026	5.04	0.38	0.79	<b>&lt;0.0001</b>	<b>21.39</b>	0.76	0.10
PA	0.28	0.54	0.38	<b>0.0005</b>	<b>12.58</b>	0.12	2.50	0.74	0.11	0.092	2.87	0.20	1.69	0.081	3.09
Kh	0.22	0.58	0.30	0.51	0.44	0.59	0.29	0.22	1.51	<b>0.0006</b>	<b>12.19</b>	<b>0.0001</b>	<b>15.69</b>	0.21	1.60
Kv	0.18	0.95	0.00	0.24	1.38	0.28	1.16	0.38	0.78	<b>0.0012</b>	<b>10.90</b>	0.34	0.91	0.24	1.40
SFh	0.17	0.68	0.17	0.024	5.20	0.98	0.00	1.00	0.00	<b>0.0062</b>	<b>7.68</b>	<b>0.0001</b>	<b>16.71</b>	0.45	0.58
SFv	0.13	0.12	2.45	<b>0.0085</b>	<b>7.09</b>	0.76	0.09	0.86	0.03	0.81	0.06	0.45	0.58	0.57	0.33
CS10h-VK	0.19	0.73	0.12	0.050	3.90	0.61	0.26	0.30	1.08	0.017	5.82	<b>0.0007</b>	<b>11.81</b>	0.48	0.51
CS10v-VK	0.11	0.77	0.08	0.94	0.01	0.58	0.31	0.53	0.40	<b>0.0051</b>	<b>8.04</b>	0.60	0.28	0.62	0.25
CDh	0.21	<b>0.0046</b>	<b>8.25</b>	<b>0.0050</b>	<b>8.06</b>	<b>0.0018</b>	<b>10.01</b>	0.17	1.87	0.049	3.93	0.11	2.52	0.13	2.36
CDv	0.23	0.046	4.03	<b>0.0068</b>	<b>7.52</b>	0.16	2.02	0.74	0.11	0.92	0.01	0.22	1.52	0.47	0.53
CSh	0.23	<b>0.0068</b>	<b>7.71</b>	0.054	3.76	<b>0.0018</b>	<b>10.09</b>	0.12	2.38	<b>0.0003</b>	<b>13.34</b>	0.33	0.94	0.32	1.00
CSv	0.26	<b>0.0095</b>	<b>6.89</b>	<b>0.0003</b>	<b>13.42</b>	0.085	2.99	0.97	0.00	0.18	1.84	0.16	1.95	0.18	1.83
CS10h-OCT	0.15	0.51	0.43	0.38	0.78	0.77	0.09	0.50	0.45	<b>0.0096</b>	<b>6.86</b>	<b>0.0028</b>	<b>9.21</b>	0.33	0.95
CS10v-OCT	0.14	0.71	0.14	0.49	0.48	0.74	0.11	0.46	0.55	<b>0.0040</b>	<b>8.49</b>	0.24	1.41	0.89	0.02
OS15h	0.18	0.066	3.46	0.93	0.01	0.086	2.98	0.35	0.90	<b>0.0070</b>	<b>7.44</b>	<b>0.0034</b>	<b>8.82</b>	0.87	0.03
OS15v	0.10	0.30	1.10	0.022	5.36	0.14	2.25	0.62	0.24	0.24	1.37	0.65	0.21	0.053	3.79
IDh	0.21	<b>0.0010</b>	<b>11.73</b>	<b>0.0055</b>	<b>7.90</b>	<b>0.0012</b>	<b>10.76</b>	0.54	0.37	0.47	0.53	0.12	2.49	0.14	2.25
IDv	0.24	0.48	0.49	<b>0.0001</b>	<b>16.43</b>	0.030	4.80	0.88	0.02	0.85	0.03	0.57	0.32	0.16	1.97
LZh	0.11	0.88	0.02	0.47	0.53	0.98	0.00	0.50	0.45	0.018	5.67	0.97	0.00	0.87	0.03
LZv	0.26	0.82	0.05	0.48	0.50	0.72	0.13	0.73	0.12	0.94	0.01	0.38	0.77	0.81	0.06
CSAn	0.36	0.044	4.12	<b>0.0009</b>	<b>11.34</b>	0.47	0.52	0.55	0.35	0.042	4.19	0.84	0.04	0.69	0.16
CSAt	0.18	0.20	1.67	<b>&lt;0.0001</b>	<b>25.44</b>	0.91	0.01	0.87	0.03	0.057	3.65	0.93	0.01	0.60	0.28
CSAs	0.22	0.82	0.05	0.71	0.14	0.99	0.00	0.97	0.00	0.091	2.88	0.52	0.41	0.11	2.65
CSAi	0.11	0.84	0.04	0.87	0.03	0.38	0.76	0.49	0.48	0.20	1.67	0.16	2.03	0.12	2.49
SRn	0.17	0.62	0.25	<b>0.0024</b>	<b>9.46</b>	0.13	2.37	0.69	0.16	0.26	1.27	0.60	0.27	0.60	0.28
SRt	0.22	0.30	1.08	<b>0.031</b>	<b>4.74</b>	0.34	0.92	0.26	1.27	0.56	0.35	0.96	0.00	0.30	1.09
SRs	0.33	0.57	0.32	<b>&lt;0.0001</b>	<b>17.58</b>	0.59	0.29	0.42	0.65	0.80	0.07	0.78	0.08	0.13	2.26
SRI	0.17	0.16	2.00	0.21	1.60	0.082	3.06	0.75	0.10	0.092	2.86	0.48	0.50	0.092	2.86

Mixed model analysis with ethnicity, age, sex, height, M, J<sub>0</sub>, and J<sub>45</sub> as fixed effects. P-values of  $\leq 0.01$  were considered significant.

**Table 3.10:** Summary of multivariate analysis

Ocular Variable	Ethnicity						Sex					
	Horizontal			Vertical			Horizontal			Vertical		
	Caucasian	British Asian	P-value	Caucasian	British Asian	P-value	Male	Female	P-value	Male	Female	P-value
	Mean (SE)	Mean (SE)		Mean (SE)	Mean (SE)		Mean (SE)	Mean (SE)		Mean (SE)		
Ksim	7.83 (0.03)	7.86 (0.05)	0.58	7.67 (0.03)	7.67 (0.04)	0.95	7.86 (0.04)	7.83 (0.03)	0.59	7.70 (0.04)	7.64 (0.03)	0.28
SF	0.45 (0.01)	0.46 (0.02)	0.68	0.17 (0.01)	0.20 (0.02)	0.12	0.46 (0.02)	0.46 (0.02)	0.98	0.18 (0.02)	0.19 (0.01)	0.76
CS10-VK (mm)	1.77 (0.01)	1.77 (0.01)	0.73	1.81 (0.01)	1.81 (0.02)	0.77	1.77 (0.01)	1.78 (0.01)	0.61	1.81 (0.02)	1.82 (0.01)	0.58
PA (mm)	-	-	-	10.55 (0.26)	10.35 (0.29)	0.54	-	-	-	10.67 (0.29)	10.23 (0.25)	0.12
HVID (mm)	11.82 (0.12)	11.71 (0.12)	0.30	-	-	-	11.82 (0.12)	11.71 (0.12)	0.22	-	-	-
CD (mm)	13.55 (0.04)	13.33 (0.06)	<b>0.0046</b>	13.34 (0.06)	13.09 (0.10)	0.046	13.57 (0.06)	13.31 (0.05)	<b>0.0018</b>	13.30 (0.10)	13.12 (0.07)	0.16
CS (mm)	3.24 (0.04)	3.12 (0.04)	<b>0.0068</b>	3.16 (0.03)	3.01 (0.04)	<b>0.0095</b>	3.24 (0.04)	3.11 (0.04)	<b>0.0018</b>	3.13 (0.04)	3.04 (0.03)	0.085
ID (mm)	11.74 (0.07)	11.44 (0.08)	<b>0.0010</b>	11.19 (0.04)	11.12 (0.07)	0.48	11.73 (0.08)	11.45 (0.07)	<b>0.0012</b>	11.26 (0.07)	11.05 (0.05)	0.030
LZ (mm)	0.93 (0.02)	0.94 (0.03)	0.88	0.91 (0.11)	0.92 (0.11)	0.82	0.94 (0.03)	0.94 (0.02)	0.98	0.91 (0.11)	0.93 (0.11)	0.72
CS10-OCT (mm)	1.74 (0.01)	1.75 (0.01)	0.51	1.79 (0.01)	1.78 (0.01)	0.71	1.75 (0.01)	1.75 (0.01)	0.77	1.78 (0.01)	1.79 (0.01)	0.74
OS15 (mm)	3.75 (0.03)	3.68 (0.04)	0.066	3.77 (0.02)	3.73 (0.03)	0.30	3.75 (0.04)	3.69 (0.03)	0.086	3.78 (0.03)	3.72 (0.02)	0.14
CSJ (°)	174.3 (0.3) n	173.1 (0.5) n	0.044	178.2 (0.2) s	178.1 (0.3) s	0.82	173.9 (0.5) n	173.5 (0.3) n	0.47	178.2 (0.3) s	178.2 (0.2) s	0.99
	177.2 (0.2) t	176.6 (0.4) t	0.20	177.6 (0.2) i	177.6 (0.3) i	0.84	176.9 (0.4) t	176.8 (0.3) t	0.91	177.5 (0.3) i	177.8 (0.2) i	0.38
SR (mm)	36.3 (3.7) n	40.2 (6.4) n	0.62	34.1 (4.1) s	31.9 (4.2) s	0.57	44.6 (6.2) n	31.8 (4.6) n	0.13	33.9 (4.2) s	32.1 (3.8) s	0.59
	23.7 (2.2) t	20.9 (2.5) t	0.30	33.1 (2.9) i	41.8 (5.1) i	0.16	21.0 (2.5) t	23.6 (2.1) t	0.34	43.1 (4.9) i	31.8 (3.6) i	0.082

P-values of  $\leq 0.01$  were considered significant.

**Table 3.11:** Ocular Topography Variables by Ethnicity and Sex

### 3.4 Discussion

Advances in technology have allowed a more extensive assessment of ocular topography. Subjective evaluation of corneal reflection (Placido Disc) was superseded by the quantification of the separation of keratometry mires. The advent of photokeratoscopy, and more latterly digital imaging and advances in computing power (videokeratoscopy), have allowed further quantification of the separation of multiple mires extending over a wider area of the cornea to determine more peripheral corneal shape. Recent technologies, such as Scheimpflug imaging, have allowed the profiling of the anterior eye surface onto the less reflective sclera, but the development of OCT has enabled detailed imaging of the peripheral corneoscleral topography. The characterisation of the CSP using OCT has been shown to both repeatable and reliable (Chapter 2) (Hall et al., 2011).

An understanding of this ocular topography has application in scleral contact lens practice, has been shown to influence soft contact lens fitting characteristics, and also has implications for refining the positioning of corneal incisions and the determination of optimum intra-ocular lens (IOL) parameters. The factors likely to affect corneoscleral topography include subject height, refractive error size, sex, ethnicity and aging. The purpose of this study was to evaluate these factors, in a healthy population, and to determine their effect on the peripheral corneoscleral topography.

Although biological variables are usually normally distributed, many of the variables in this study did not show a normal distribution. While this could be thought to be linked to refractive error, since refractive error is typically skewed due to incomplete emmetropisation, the correlations with ocular topography did not support this rationale as few ocular variables were significantly correlated with refractive error. Most of the ocular variables were correlated with age and, as the age of our sample was not normally distributed, this would seem the most likely explanation for this observation.

Several smaller-scale studies have utilised OCT to define anterior segment metrics (Sorbara et al., 2010, Qin et al., 2012). This study supports the findings of the previous chapter and also provides normative data for a larger, wider population.

Two important clinically relevant findings were drawn from this study. First, 'true' corneal diameter, as assessed by OCT, was greater than that previously found using more conventional techniques. In defining the CSP an appreciation of the corneoscleral junction at the corneal sulcus, and therefore corneal diameter, is required. Various other methods have been used to determine corneal diameter (Martin and Holden, 1982, Pop et al., 2001, Baumeister et al., 2004, Potgieter et al., 2005, Rufer et al., 2005, Srivannaboon and Chotikavanich, 2005, Pinero et al., 2008, Buckhurst et al., 2009, Nemeth et

al., 2010), amongst which, automated methods of WTW corneal diameter measurement have previously been shown to provide more precise results than manual methods of measurement (Baumeister et al., 2004). In this study the mean horizontal corneal diameter was consistent with that of the study undertaken in Chapter 2 (13.4mm in both), but was greater than that reported by Martin and Holden (1982) using a photographic method (12.9mm), and also of other studies reporting WTW values. Of these, the three largest studies evaluating WTW data reported mean values ranging from 11.7 to 12.1mm. These utilised scanning-slit technology (Orbscan) (Rufer et al., 2005, Srivannaboon and Chotikavanich, 2005) and a photographic method (Lenstar/IOLMaster) (Buckhurst et al., 2009). Corneal diameter, however, as defined by the measurement of WTW (or HVID), is confounded by the three-dimensional transparency profile of the peripheral cornea. This, in turn, is further complicated by the fact that *en face* imaging is not normal to the peripheral cornea. The rate of change of transparency also differs widely, as highlighted by the variation in limbal zone width seen in this study. This is particularly noticeable vertically, as evidenced by the greater difference between HVID and ID seen in this meridian. In addition, the loss of transparency is not uniform across the depth of the cornea, and is not consistent between the quadrants.

WTW has been shown to be a poor predictor of capsular bag diameter in determining IOL size (Werner et al., 2004, Khng and Osher, 2008) which may, in part, be explained by the issues inherent with *en face* measurement. WTW is also used to determine IOL power; however, a better measure of corneal diameter such as that utilised in this study may enable better refractive outcomes.

Second, the junction between the cornea and the sclera is often portrayed as a sharp transition (Van Buskirk, 1989). However, in this study, 77% of CSJ angles were within  $5^\circ$  of  $180^\circ$  and approximately a fifth were within  $\pm 1^\circ$ , demonstrating an almost tangential extension of the cornea to form the para-limbal sclera in those cases.

The difference between opposing corneoscleral junction angles ( $\Delta$ CSJ) was significantly greater in the horizontal meridian compared with the vertical. The study undertaken in Chapter 2 showed previously a link between increasing differences in horizontal CSJ angles ( $\Delta$ CSJh) and lens tightness for soft contact lenses; it is likely that this difference limits horizontal contact lens movement in comparison with that in the vertical meridian. However, given the small differential between superior and inferior CSJ angles ( $\Delta$ CSJv), any restriction in contact lens movement in this meridian is unlikely to be due to the transitions at the corneoscleral junctions. Kikkawa (1979) proposed a model where a soft lens could be considered as a series of concentric elastic bands that stretch to accommodate changes in the ocular topography. Subsequently, any restriction in movement in the

vertical meridian is more likely to be due to raised squeeze pressure acting to re-centre the lens with increasing decentration, as it is forced to undergo greater stretching and flexing to align with the scleral topography.

It is likely that decreases in CSJ magnitude, resulting in sharper, more acute CSJ transitions, may also contribute to 3- and 9-o'clock corneal staining in rigid contact lens wear as a result of an increased gap between the ocular surface and inner eyelid due to lens thickness, so-called 'bridge effect' (van der Worp et al., 2003).

As independent variables, height and refractive error were both found to correlate with ocular topography. The correlation of height with ocular topography agrees with the findings of a previous study that found taller subjects had larger eyes with flatter corneas (Nangia et al., 2010), although this may have been influenced by general nutrition. However, height did not account for any of the *variance* in CSP within the multivariate model.

Age was the most important factor influencing CSP variables, resulting in decreases in variable magnitude with increasing age. This agrees with the findings of a previous OCT study investigating the effects of age on ocular variables (Qin et al., 2011). These are most likely to be due to the natural physiological changes associated with ageing. This is evidenced by the decreases in SR and CSJ angle, resulting in steepening of radius and CSJ angle, respectively. These are likely due to the accumulation of fatty deposits e.g. pingueculae, across the horizontal conjunctival face. The decreases in the non-CSP variables, PA fissure size and ID, due to a loss in muscle tone and as result of increasing peripheral corneal opacification with age, respectively, would also support this. Corneal diameter, however, was not found to be influenced by age. This finding would emphasize the unreliability of ID as a surrogate for CD, particularly given the significant decrease in ID with age seen in this study.

As with sex, ethnicity also influenced CD, CS and ID. These were independent of height and age, and hence must be related to some other genetic factor. In comparing ocular variables between ethnicities, though, this study was limited to Caucasians and British Asians and is, therefore, not necessarily representative of Asians throughout the Pacific Rim.

### **3.5 Conclusion**

This study has shown that age is the main factor influencing corneoscleral topography; hence age should be taken into consideration in contact lens design, in the optimisation of surgical procedures involving the cornea or sclera, and also in IOL lens selection.

In addition to assessing factors affecting corneoscleral topography, this chapter has provided substantive normative data for future modelling of soft contact lens fit, and also an alternative definition of corneal diameter to that of WTW. The use of AS-OCT imaging and videokeratoscopy in Chapter 2 allowed for the prediction of up to 24% of the variance in contact lens fit; however, it is likely that stronger associations and an increase in the modelled prediction of variance in fit may have occurred had an objective method of lens fit assessment been made. Consequently, a contact lens wearing study comparing subjective versus objective assessment of contact lens fit parameters was undertaken in Chapter 4, with the specific aim of assessing the repeatability of an objective technique.

# Chapter 4

## **Chapter 4: Subjective versus Objective Contact Lens Fit Assessment**

### **4.1 Introduction**

There is a growing body of evidence to support the long-held clinical view that the assessment of lens fit is critical to contact lens practice. Changes in lens fit cannot be predicted reliably by lens base-curve or material properties and vary between individuals (Tranoudis and Efron, 2004a, Wolffsohn et al., 2009). Poor fitting soft lenses negatively impact on ocular physiology, as assessed by bulbar and limbal hyperaemia and corneal staining, than well-fitting lenses (Young and Coleman, 2001). Lens mobility is presumed to be correlated with tear exchange (although only tear expulsion has been demonstrated and the effect of lens movement has not been examined (McNamara et al., 1999) and this is required for corneal oxygenation as well as to remove trapped debris, inflammatory cells and other tear components that would otherwise accumulate under the lens. The tear layer between the contact lens and cornea is also likely to reduce the friction between the surfaces, avoiding significant mechanical interaction, in the same way that the tear layer between the contact lens front surface and eye lid prevents tissue damage (Korb et al., 2010).

Studies attempting to assess the relative importance of contact lens fit metrics have generally been subjective in nature, assessing features such as centration, movement on blink, lag and push up (Young et al., 1993, Bruce, 1994, Young, 1996, Morgan and Efron, 2002), although the method of assessment is not always clearly articulated. A recent study assessing the impact of central and peripheral ocular surface shape on lens fit identified that the inherent variability of subjective lens fit was likely to have influenced the limited variability (24%) that could be explained (Chapter 2) (Hall et al., 2011). It has been clearly demonstrated that the grading ability of even experienced eye-care practitioners is more variable and less sensitive than objective assessment (Peterson and Wolffsohn, 2007), but this has not been evaluated with lens fit metrics.

Several studies have tried to overcome clinical bias and lack of precision by assessing lens movement on blink from video, but not all define the direction of gaze (primary or up-gaze), and other lens movements such as lag and push-up recovery speed have not been objectively evaluated. Pritchard and Fonn (1995) and Schwallie and Bauman (1998) video recorded lens movement through a slit lamp and assessed centration and blink movement with a ruler used to make measurements off a monitor. A similar technique was used by Maldonado-Codina and Efron (2004), but they superimposed a projected gauge over the videos. Tranoudis and Efron (2004a) used the same apparatus, but adjusted

the image to match an overlaid circle of known size to take measurements which additionally included up-gaze lag.

Wolffsohn and colleagues (2009) were the first to make a comprehensive objective evaluation of lens fit in primary and multiple other positions of gaze, showing that movement on blink in up-gaze, horizontal lag and push-up recovery speed were the key metrics to independently characterise soft contact lens mobility.

Despite the increasing availability of digital capture through slit-lamp biomicroscopes, the validity and repeatability of objective lens fit analysis has never been determined. The hypothesis of this study was therefore that objective assessment of contact lens fit can provide the same key parameters as subjective evaluation, but has the advantages of being more repeatable as well as having a higher resolution.

## **4.2 Method**

Thirty-one habitual contact wearing subjects (average  $22.0 \pm 3.0$  years: 61% female) gave informed consent to take part in the study. The study was approved by the University's Research Ethics Committee and conformed to the Declaration of Helsinki. Each subject was only included in the study if there was no evidence or history of binocular vision anomalies, or ocular disease including dry eye, or any pathology that would normally contraindicate contact lens wear. None of the subjects were on ocular medication.

The subjects, with a range of different corneal curvatures (horizontal meridian  $7.85 \pm 0.36$  mm; vertical meridian  $7.63 \pm 0.36$  mm; difference  $0.20 \pm 0.10$  mm), each wore soft contact lenses of power  $-2.50$  D; a conventional hydrogel design (Vistakon Acuvue® 2; etafilcon A material, modulus 0.30 MPa) in one randomly assigned eye and a silicone hydrogel design (Vistakon Acuvue® Advance®; galyfilcon A material, modulus 0.43 MPa) in the other (i.e. contralaterally). These lenses were chosen for their similar geometries and identical base curve (8.30 mm) and diameter (14.0 mm) parameters. The steepest available base curve (8.30 mm) was selected for dispensing in each case and lens blister packs were re-labelled by a clinical assistant so as to ensure both investigator and subject were masked to lens type. The study design with two lenses of different modulus allowed for a range of contact lens fit parameters that are commonly seen in clinical practice to be observed.

After insertion by the masked investigator, the contact lenses were allowed to settle for at least thirty minutes before assessment, a time representative of that a lens settled after several hours (Brennan

et al., 1994, Golding et al., 1995). The subject was asked to look straight ahead, then blink twice in primary gaze, look up and blink a further two times, look down while the upper lid was raised by the examiner to expose the superior lens edge and to look to the left and right. The lens was then pushed upwards digitally while the patient viewed in primary gaze so that the lower lens edge was raised to the middle of the cornea if this was possible, before being released. The assessment of lens fit was dynamically captured using a digital slit lamp (CSO digital camera; resolution 1392 x 1024 pixels, frame rate 11 Hz), providing 6x magnification, and the same resulting video footage was assessed for lens fit both subjectively and objectively to ensure a like-for-like evaluation of lens fit parameters.

#### **4.2.1 Subjective Lens Fit Analysis**

Two experienced investigator assessed four main lens fit variables; centration (mm), post-blink movement in upgaze (mm), horizontal version lag (average of displacement of the lens from the primary position with nasal and temporal gaze; mm) and push-up speed of recovery (slow/medium/fast) following digital displacement (Wolffsohn et al., 2009). Of the two observers, one repeated the analysis of all the subjects a week later.

#### **4.2.2 Objective Lens Fit Analysis**

The resulting video was objectively analysed by a separate masked observer using a purpose-developed image analysis program (LabVIEW, National Instruments, Austin, Texas). Lens centration was determined from the difference in millimetres between the centre of circles adjusted to circumscribe the visible limbus and contact lens edges (Figure 4.1). Movement on blink was determined from the number of pixels the lens moved from immediately after a blink until it stabilised. Lag was assessed as the difference in percentage of the lens overlap onto the sclera from the primary gaze position to nasal and temporal excursions and the values averaged. Push up recovery speed was determined from the number of pixels the lens moved from immediately after release until it stabilised divided by the time taken for this to occur. The analysis was repeated by the same masked researcher a week later.

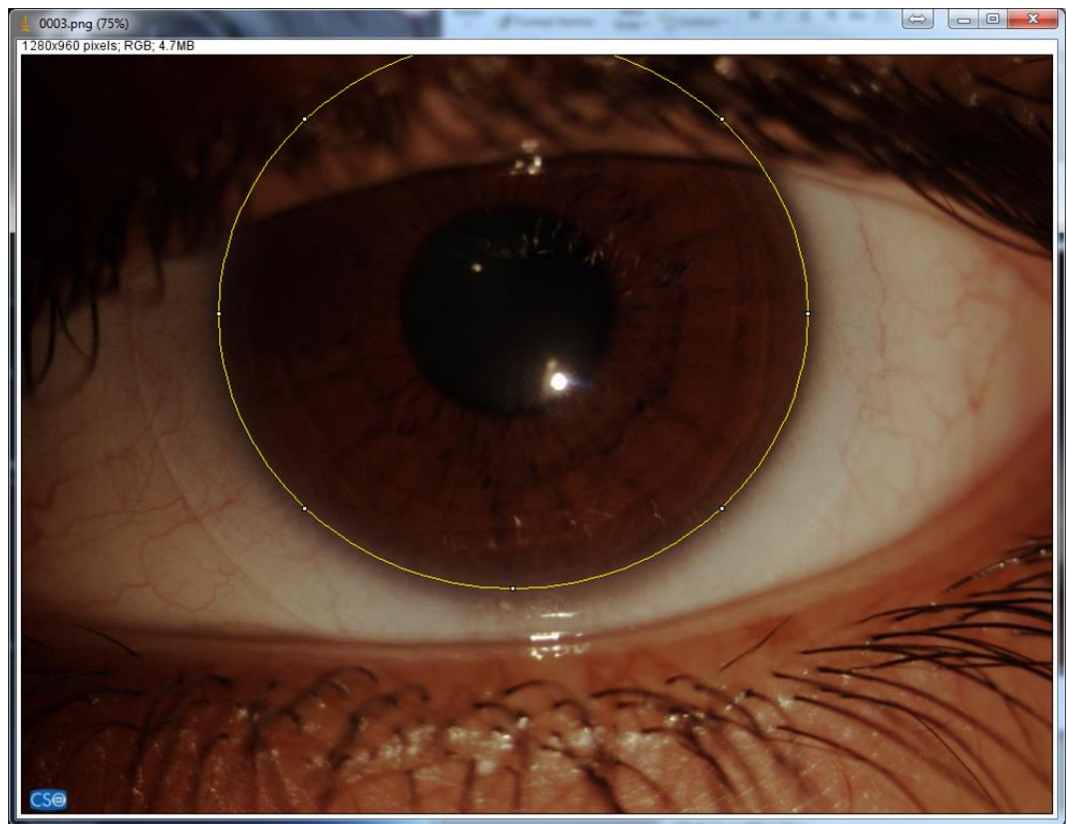
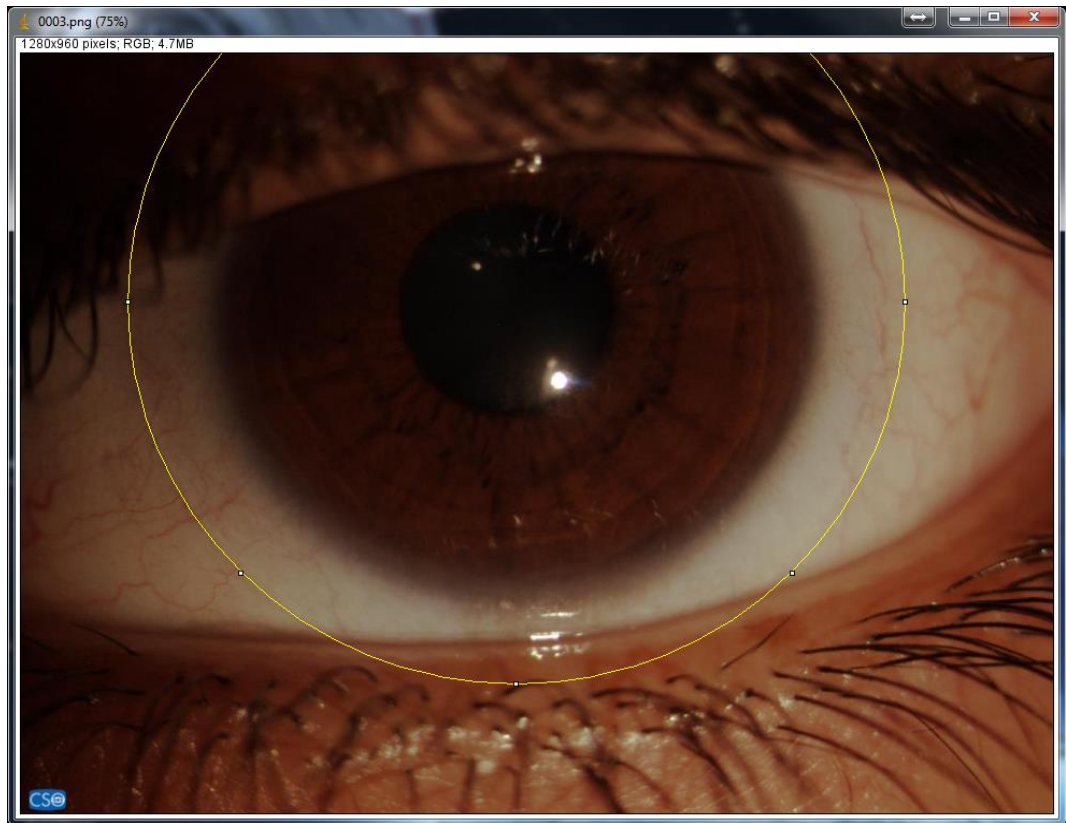


**Figure 4.1:** Determination of lens centration by objective means

Movement on blink in upgaze was assessed by the change in vertical lens position relative to the cornea from the first video frame following the blink (Figure 4.2).

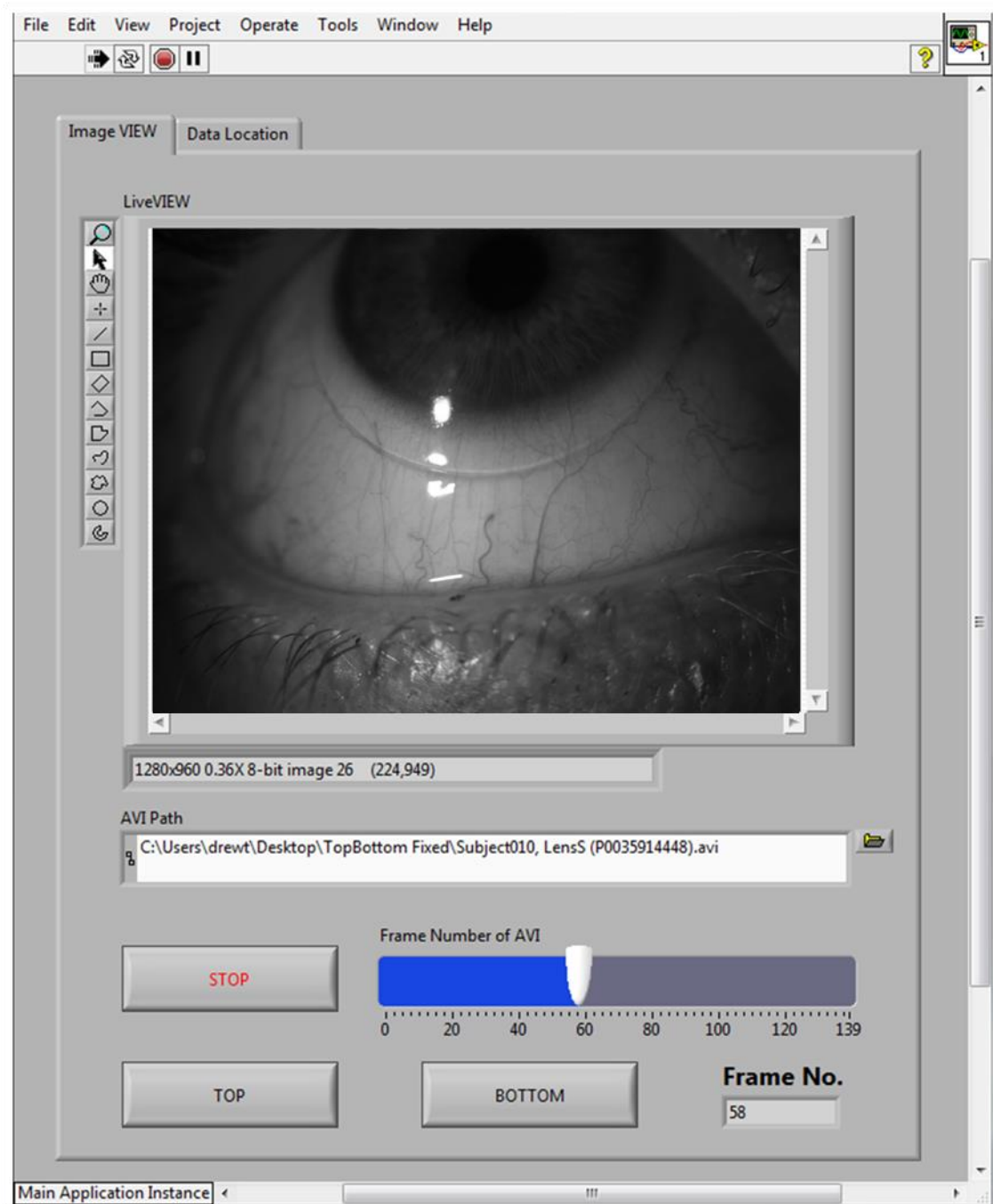


**Figure 4.2:** Determination of movement on blink using LabVIEW software

Lag was assessed as the difference in millimetres between the limbus to lens edge distance in each of the horizontal positions of gaze compared to the same distances when viewing in primary gaze

Finally, push-up recovery speed in millimetres per second was calculated from the change in vertical lens position relative to the cornea from the first video frame following the lens release, divided by the number of frames over which the movement occurred, times the frame rate (Figure 4.3). All measurements were taken by the same individual. Imaging a graticule through the same slit-lamp and camera system determined the calibration as 1 pixel being equivalent to 0.016 mm.

#### **4.2.3 Statistical Analysis**

The study design with two lenses of different modulus allowed for a range of contact lens fit parameters that are commonly seen in clinical practice to be observed. Hence as the study assessed lens movement assessment between techniques, rather than between eyes, both eyes data was considered within the analysis. The difference in values between the objective and subjective techniques of assessing horizontal and vertical centration, movement on blink in upgaze and horizontal lag were plotted versus the average and the Bland Altman comparison plotted for comparison. As push-up recovery speed could only feasibly assessed as slow, medium or fast subjectively, a Spearman's rank non-parametric correlation with the objectively assessed recovery speed was conducted.

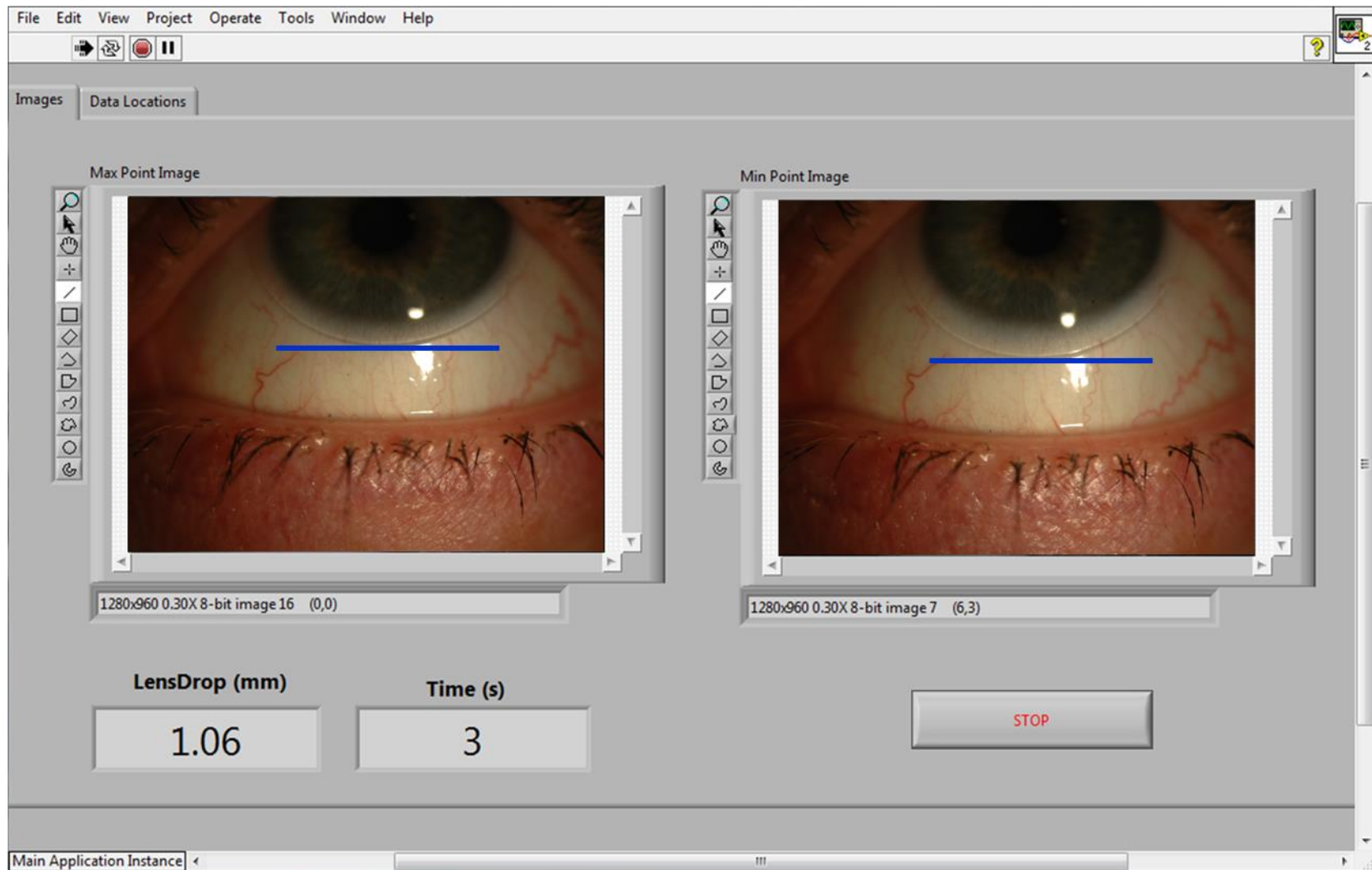


*Figure 4.3: Speed of Drop Calculator using purpose-developed LabVIEW software*

## 4.3 Results

### 4.3.1 Validity

#### 4.3.1.1 Centration

Objectively measured centration was  $-0.323 \pm 0.332$  mm vertically and  $0.119 \pm 0.202$  mm horizontally (average  $\pm 1$  standard deviation). Subjectively measured centration was significantly different at  $0.029 \pm 0.187$  mm vertically ( $p < 0.001$ ) and  $-0.045 \pm 0.123$  mm horizontally ( $p < 0.001$ ). The mean difference between objective and subjective centration was  $-0.395 \pm 0.239$  mm vertically (Figure 4.4) and  $0.147 \pm 0.244$  mm horizontally (average  $\pm 95\%$  confidence interval; Figure 4.5).

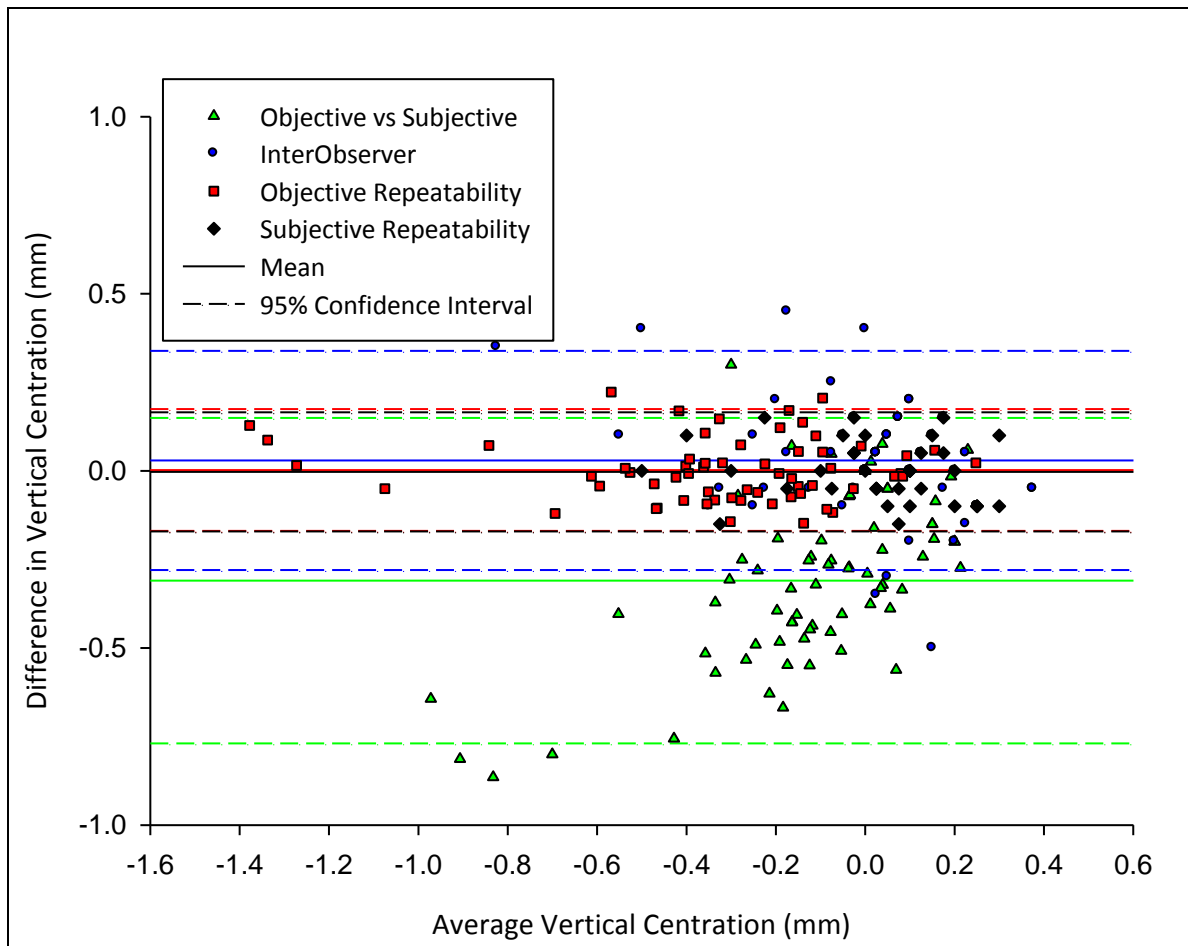


**Figure 4.4:** Bland-Altman plot of the difference in vertical centration compared to the mean for subjective versus objective measurement, interobserver assessment, objective repeatability and subjective repeatability.  $N = 62$  lenses.

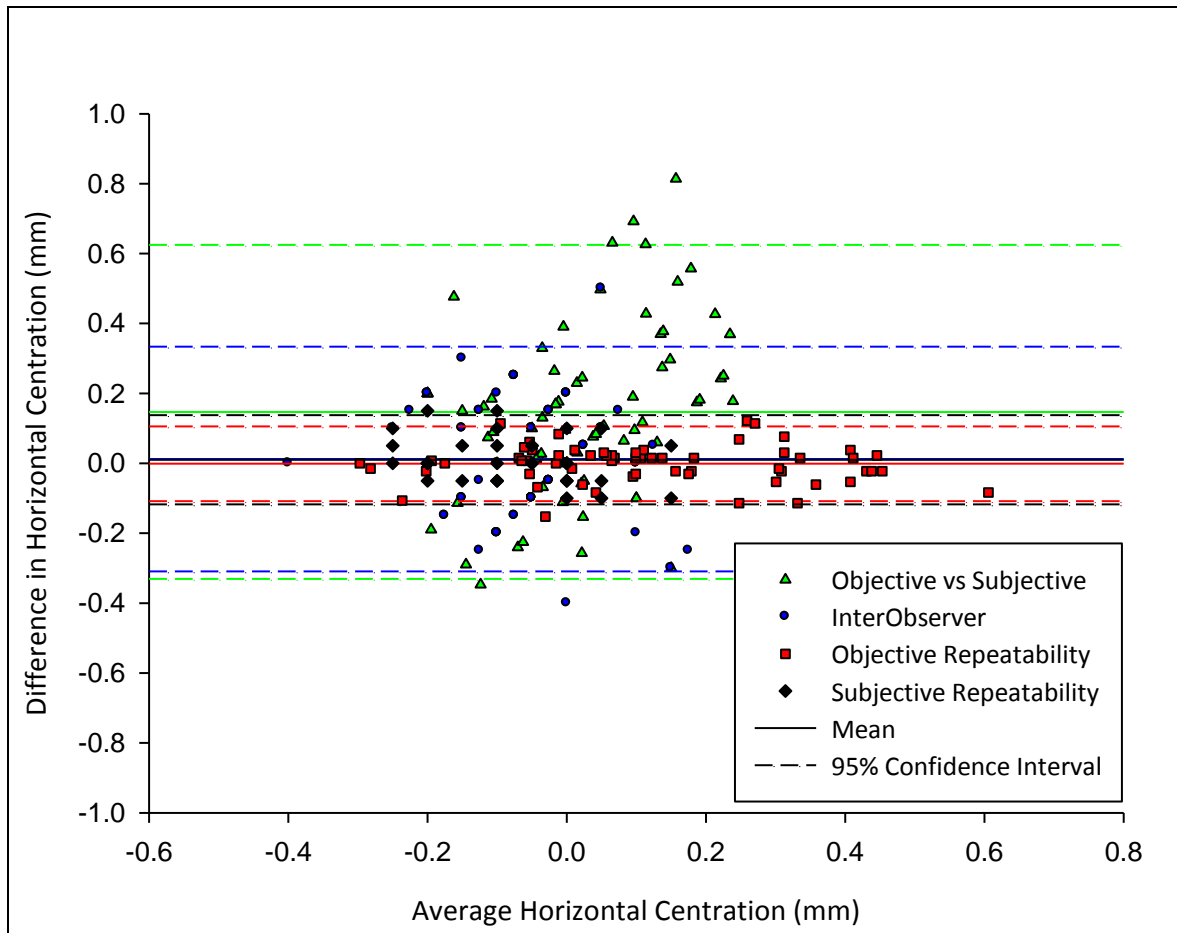


**Figure 4.5:** Bland-Altman plot of the difference in horizontal centration compared to the mean for subjective versus objective measurement, interobserver assessment, objective repeatability and subjective repeatability.  $N = 62$  lenses.

#### 4.3.1.2 Movement on Blink

Movement on blink in upgaze was  $0.319 \pm 0.231$  mm measured objectively and  $0.213 \pm 0.138$  mm assessed subjectively ( $p < 0.001$ ). The mean different between objective and subjective movement on blink was  $0.085 \pm 0.325$  mm (average  $\pm$  95% confidence interval; Figure 4.6).

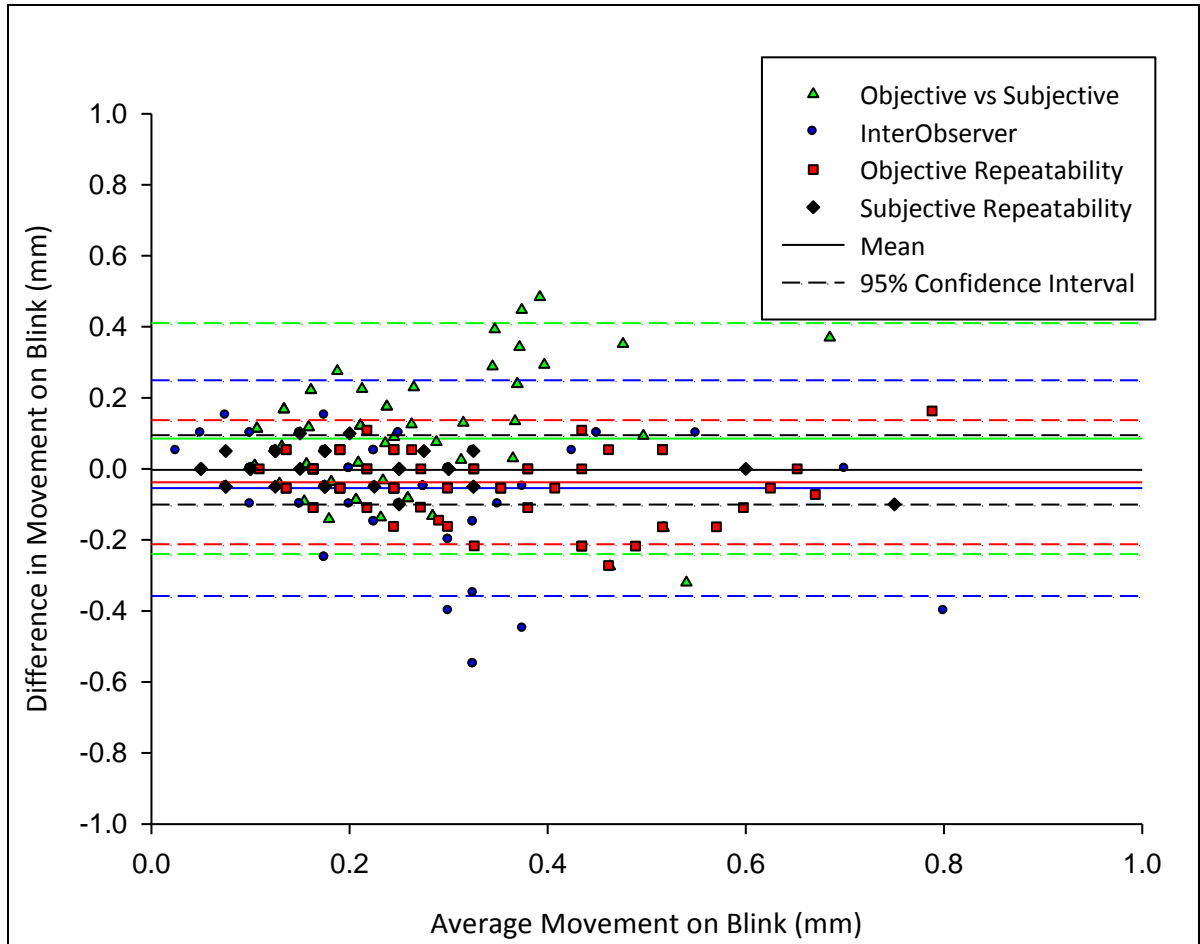


**Figure 4.6:** Bland-Altman plot of the difference in movement on blink compared to the mean for subjective versus objective measurement, interobserver assessment, objective repeatability and subjective repeatability.  $N = 62$  lenses.

#### 4.3.1.3 Lag

Horizontal lag was  $0.711 \pm 0.386$  mm measured objectively and  $0.193 \pm 0.077$  mm assessed subjectively ( $p < 0.001$ ). The mean different between objective and subjective lag was  $0.524 \pm 0.472$  mm (average  $\pm$  95% confidence interval; Figure 4.7).

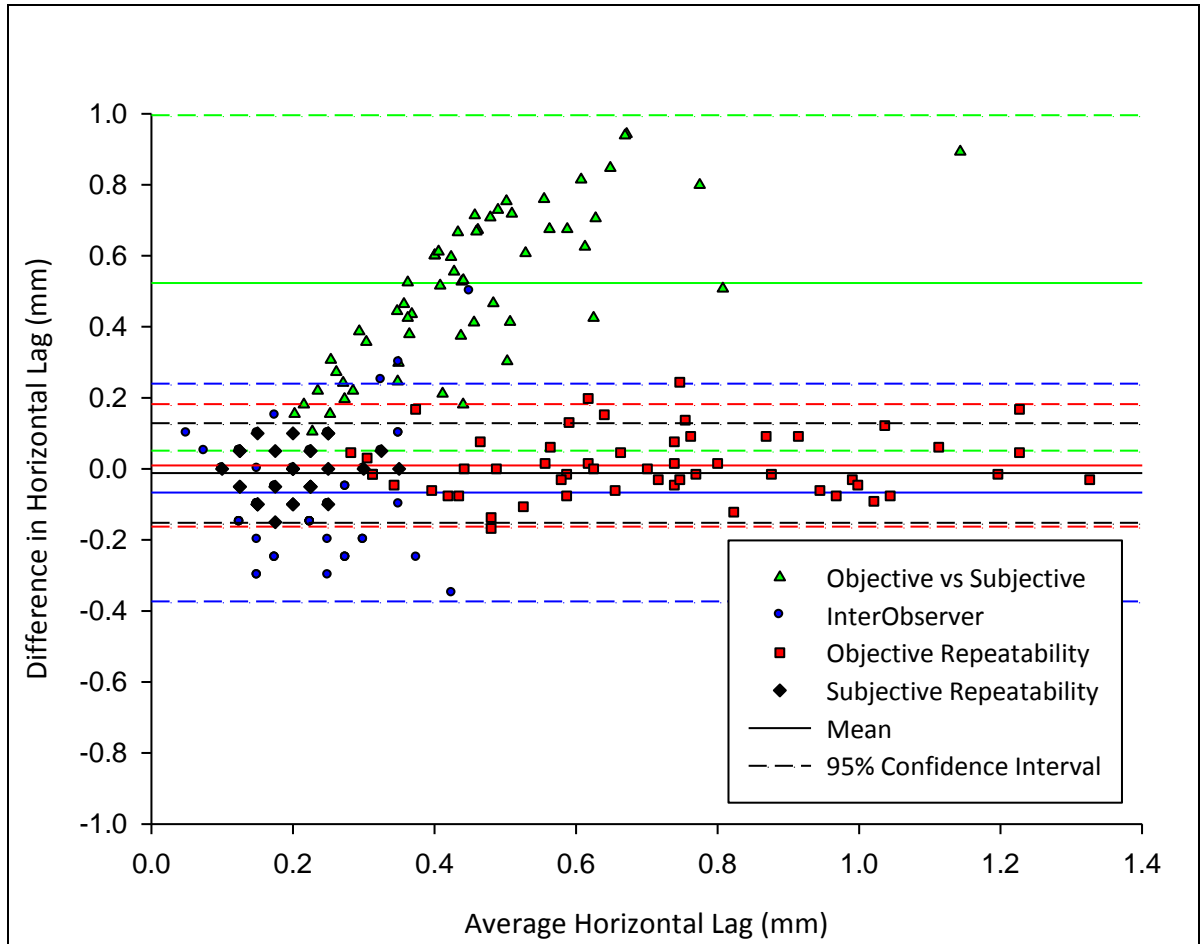


**Figure 4.7:** Bland-Altman plot of the difference in horizontal lag compared to the mean for subjective versus objective measurement, interobserver assessment, objective repeatability and subjective repeatability.  $N = 62$  lenses.

#### 4.3.1.3 Push-up Test

Push-up speed of recovery was  $0.330 \pm 0.214$  mm/s measured objectively. Subjectively 35% of push-up recoveries were rated as slow, 54% as medium and 10% as fast. The correlation between objective and subjective push-up speed was  $r = 0.237$ ,  $p = 0.057$  (Spearman's rank; Figure 4.8).

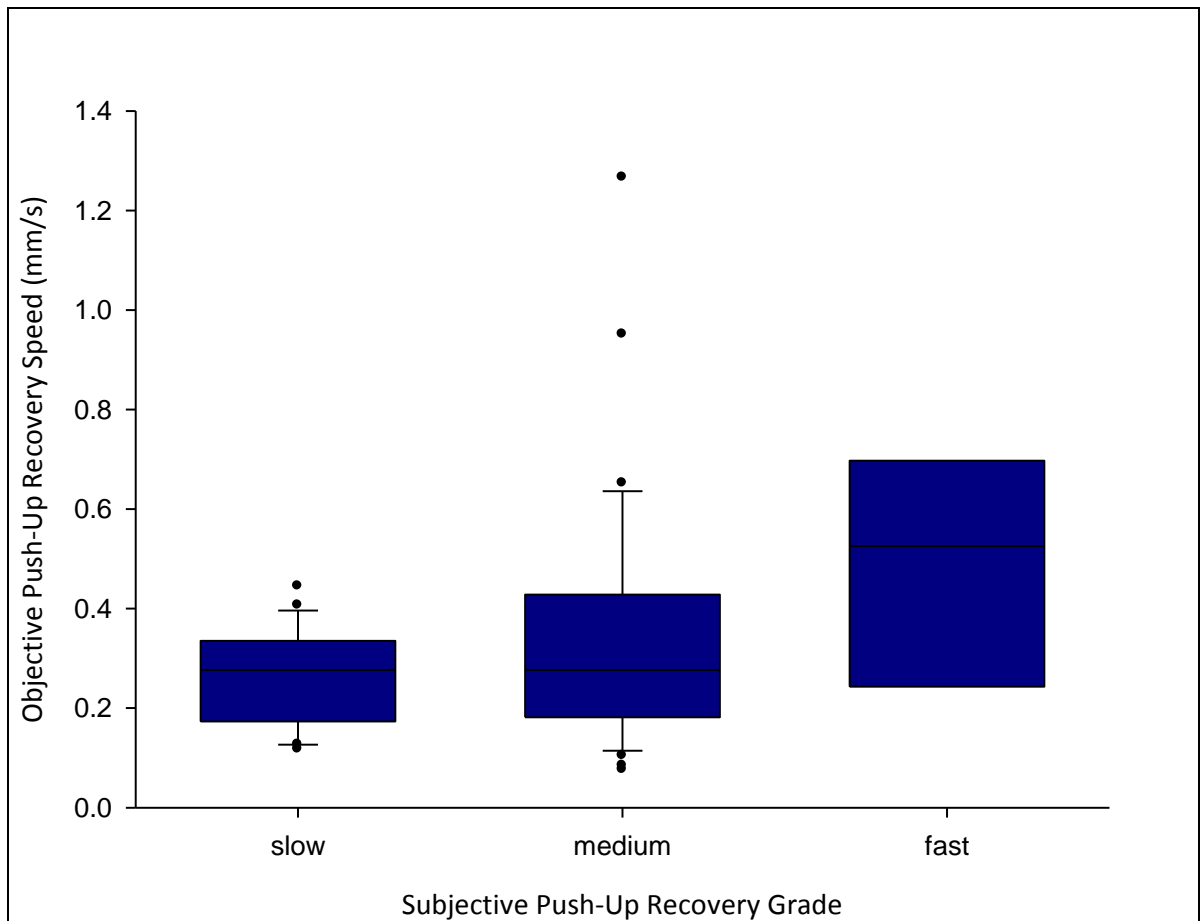


**Figure 4.8:** Box-plot of objective push-up recovery mean (line), standard deviation (box), 95% confidence interval (bars) and outliers (dots) for subjective push-up recovery grades.  $N = 62$  lenses.

### **4.3.2 Repeatability**

#### **4.3.2.1 Centration**

Objectively measured differences in centration between the first and second analysis was  $0.002 \pm 0.172$  mm vertically and  $-0.001 \pm 0.107$  mm horizontally (average  $\pm$  95% confidence interval). Subjectively measured differences in centration between the first and second analysis was  $-0.003 \pm 0.168$  mm vertically (Figure 4.4) and  $0.010 \pm 0.128$  mm horizontally (Figure 4.5). The range of centration deviations was  $-1.314$  to  $0.564$  mm with objective analysis, but only 53% of this range ( $-0.650$  to  $+0.350$ ) rated subjectively. The interobserver differences in subjectively assessed centration were  $0.029 \pm 0.309$  mm vertically (Figure 4.4) and  $0.012 \pm 0.322$  mm horizontally (Figure 4.5).

#### **4.3.2.2 Movement on Blink**

Objectively measured differences in movement on blink in upgaze between the first and second analysis was  $-0.037 \pm 0.176$  mm measured objectively and  $-0.003 \pm 0.098$  mm assessed subjectively (Figure 4.6). The range of horizontal lag was  $0.11$  to  $0.87$  mm with objective analysis and  $0.05$  to  $0.70$  mm rated subjectively. The interobserver differences in subjectively assessed movement on blink were  $-0.054 \pm 0.304$  mm (Figure 4.6).

#### **4.3.2.3 Lag**

Objectively measured differences in horizontal lag between the first and second analysis was  $0.010 \pm 0.172$  mm measured objectively and  $-0.012 \pm 0.140$  mm assessed subjectively (Figure 4.7). The range of horizontal lag was  $0.30$  to  $1.31$  mm with objective analysis, but only 69% of this range ( $0.0$  to  $0.7$  mm) rated subjectively. The interobserver differences in subjectively assessed horizontal lag were  $-0.066 \pm 0.306$  mm (Figure 4.7).

#### **4.3.2.4 Push-Up Test**

Objectively measured differences in push-up recovery speed between the first and second analysis was  $-0.039 \pm 0.206$  mm measured objectively. Assessed subjectively, 29% of second assessments differed by a grade from the first. The range of push-up recovery speed was  $0.07$  to  $1.27$  mm/s as measured with objective analysis. Interobserver differences in push-up speed graded subjectively differed by at least a grade in 53% of assessments.

## 4.4 Discussion

The aim of this study was to determine the validity and repeatability of objective lens fit analysis using images and video captured through a digital slit lamp as this has never previously been determined. It was hypothesised that the limited variance in soft lens fit accounted for by anterior eye biometry, even when the shape characteristics assessed by OCT was included, in Chapter 2 may have resulted from the generally poor repeatability of subjective evaluation. For example it has been demonstrated that the grading ability of even experienced eye-care practitioners is more variable and less sensitive than objective assessment (Peterson and Wolffsohn, 2007). The hypothesis of this study was therefore that objective assessment of contact lens fit can provide the same key parameters as subjective evaluation, but has the advantages of being more repeatable as well as having a higher resolution.

Subjectively quantified lens centration of the lenses assessed in this study were similar to the centration reported across a wide range of HEMA and silicone-hydrogel lenses measured objectively ( $0.06 \pm 0.42$  mm vertically and  $0.07 \pm 0.14$  horizontally) by Wolffsohn and colleagues (2009), with larger standard deviations vertically than horizontally. However, these values were significantly different compared to those assessed objectively in this study, mainly due to the much larger calibrated range measured objectively compared to that determined subjectively. Hence on the Bland Altman plots (Figures 4.4 and 4.5) it can be seen that the difference between objective and subjective has a positive slope, getting larger the further from zero the displacement is, with the mean shift away from zero on the vertical axis suggesting a subjective bias. This is greater and negative in the vertical centration assessment as lenses tend to centre low rather than high, whereas horizontal centration distribution is more even. The 95% confidence interval of subjective repeatability was equivalent to the objective assessment, although it would have been much larger if a similar range of values had been allocated. Despite both observers being very experienced, the 95% confidence interval of interobserver repeatability was larger ( $\pm 0.31$  vs.  $\pm 0.17$  vertically and  $\pm 0.32$  vs.  $\pm 0.11$ ) than from repeat objective assessment.

It has previously been shown that lens movement in up-gaze was more predictive of overall lens movement than that in primary gaze and hence this was assessed in this study (Wolffsohn et al., 2009). Lens movement as assessed subjectively in this study was similar to that reported across a wide range of HEMA and silicone-hydrogel lenses measured objectively ( $0.15 \pm 0.20$  mm) by Wolffsohn and colleagues (2009), but in both cases was lower than that measured objectively in this study. In this lens fit characteristic, the objective and subjective range was similar, although the

subjective values were lower. Hence on the Bland Altman plot (Figures 4.6) it can be seen that the difference between objective and subjective has a small mean shift away from zero on the vertical axis suggesting a subjective bias, and a low positive slope, getting larger the further from zero the displacement is. The 95% confidence interval of subjective repeatability was slightly less than objective repeat assessment, but interobserver repeatability was larger (subjective:  $\pm 0.10$ ; objective:  $\pm 0.18$ ; interobserver  $\pm 0.30$ ).

It has previously been shown that horizontal lag was more predictive of overall lens movement than vertical lag or a combination of the two and hence this was assessed in this study (Wolffsohn et al., 2009). Lag as assessed subjectively in this study ( $0.19 \pm 0.08$  mm) was lower than that reported across a wide range of HEMA and silicone-hydrogel lenses measured objectively ( $0.41 \pm 0.31$  mm) by Wolffsohn and colleagues (2009), but both was lower than that measured objectively with the study lenses ( $0.71 \pm 0.39$  mm). As with lens centration, this was mainly due to the much larger calibrated range measured objectively compared to that determined subjectively. Hence on the Bland Altman plot (Figures 4.7) it can be seen that the difference between objective and subjective has a positive slope, getting larger the further from zero the displacement is, with the mean shift away from zero on the vertical axis suggesting a subjective bias. The 95% confidence interval of subjective repeatability was slightly less than objective repeat assessment, but interobserver repeatability was larger (subjective:  $\pm 0.14$ ; objective:  $\pm 0.17$ ; interobserver  $\pm 0.31$ ).

Push-up speed of recovery was less in this study ( $0.33 \pm 0.21$  mm/s) compared to that reported across a wide range of HEMA and silicone-hydrogel lenses measured objectively ( $1.32 \pm 0.73$  mm) by Wolffsohn and colleagues (2009), also measured objectively. This was probably due to the range (maximum 1.3 mm/s in this study compared to 6.0 mm/s in the previous study) being much smaller with the narrower range of lens designs and geometries. It is not feasible subjectively to simultaneously assess movement and time; hence push-up recoveries were rated as slow, medium or fast, with over half assessed as falling in the middle category. The correlation with objectively measured push-up speed was poor (accounting for only 5.6% of the variance) and nearly one-third (29%) of second assessments differed by a grade from the first in the same observer and over half differed by at least a grade (53%) between observers.

## **4.5 Conclusion**

Hence, the hypothesis that objective assessment of contact lens fit can provide the same key parameters as subjective evaluation, but has the advantages of being more repeatable as well as having a higher resolution, was not proven to be correct. However, the limited range of values attributed by clinicians compared to that measured objectively and the poor interobserver variability have the potential to partially mask the impact of anterior eye biometry on lens fit, as suggested as an explanation of the limited variance accounted for in Chapter 2. Consequently subsequent chapters will use objective analysis of lens fit to confirm the previous finding of the link between central and peripheral corneal curvature with lens fit, as well as the additional variance explained by the corneoscleral junction and surrounding tissue.

Although the corneal and corneoscleral topography have both been shown to influence lens fit variables in Chapter 2, it seems likely that the same lens fit parameters may also be influenced by wearing time, potentially driving clinical symptoms and in particular impacting upon comfort. Consequently a contact lens wearing study assessing the impact of time on lens ocular comfort, physiology and lens wettability was undertaken in Chapter 5.

# Chapter 5

## Chapter 5: The Influence of End of Day Fit

### 5.1 Introduction

The assessment of soft contact lens fit is a critical part of the prescribing process. Well fitting lenses are an essential requirement to ensure good comfort, stable vision and minimal effect on ocular integrity. However, the assessment of lens fit in clinical practice is typically made only after a few minutes on initial trial and at aftercare appointments, taking place, at most, after a working day. The average duration of contact lens wear, though, has been reported to be around 13-14 hours a day, (Begley et al., 2001, Riley et al., 2006, Long and McNally, 2006) with approximately 25% of wearers reporting wearing their contact lenses for 16 hours, and circa 6% wearing their lenses for 17 hours a day or more (Riley et al., 2006). Furthermore, patients generally report comfortable wearing times of about 1 to 1.5 hours less than their total wearing time and this appears to be a factor influencing overall wearing time in a proportion of contact lens wearers (Riley et al., 2006, Long and McNally, 2006). Consequently, there is a need to understand the changes occurring in the lens-eye relationship towards the end of the wearing day. Despite this, few published studies have examined contact lens wearers who had been wearing their lenses greater than 12 hours (Maruyama et al., 2004, Riley et al., 2005, Peterson et al., 2006, Wolffsohn et al., 2010), and none of these evaluated silicone hydrogel daily disposable contact lenses.

Discomfort, particularly towards the end of the day, is a major cause of contact lens discontinuation (Pritchard et al., 1999). Dry eye symptoms are the most common complaint (Maruyama et al., 2004, Riley et al., 2006), with over 70% of wearers reporting symptoms late in the day (Begley et al., 2001), and approximately one-third of these discontinuing lens wear as a result (Pritchard et al., 1999). However, the relationship of discomfort with respect to changes in lens fit towards the end of the day has not been documented.

Silicone hydrogel contact lenses afford greater oxygen transmissibility, which result in less compromise in anterior eye physiology. However, no marked benefit in ocular comfort has been reported with these compared to traditional hydrogel lenses (Fonn and Dumbleton, 2003, Santodomingo-Rubido et al., 2010). Since, it is known that some combinations of contact lenses and multipurpose lens care solutions result in solution-induced corneal staining, potentially having an impact on comfort (Sorbara et al., 2009, Willcox et al., 2010, Keir et al., 2010, Dumbleton et al., 2010), use of the daily disposable modality eliminates this confounding effect.

The primary purpose of this study, therefore, was to assess the influence of end of day fitting characteristics of silicone-hydrogel daily disposables on ocular comfort, physiology and lens wettability.

## 5.2 Method

Thirty-nine subjects (average age  $22.1 \pm 3.5$  years; 54% female) were enrolled in a randomised, three-week, bilateral crossover evaluation of three silicone hydrogel daily disposable contact lenses, such that each lens was assessed after one week of wear (Figure 5.1). None of the subjects were on ocular medication, had incurred ocular injury or surgery within twelve weeks prior to commencing the study, had pre-existing ocular irritation or displayed evidence of systemic or ocular abnormality, infection or disease likely to affect successful wear of contact lenses. The subjects were all existing adapted contact lens wearers and were fitted with the same power of contact lens for all three silicone hydrogels (average  $-2.80 \pm 1.90$  D, range  $-0.50$  to  $-7.00$  D). The investigators were masked throughout the study, but due to the loss of sterility that would result in re-packaging, the study was open label. Subjects were, however, masked to the sponsor of the study. Subjects gave written informed consent after explanation of study procedures. The study was approved by the Aston University Research Ethics Committee and conformed to the Declaration of Helsinki.



**Figure 5.1:** Summary of study design/wearing schedule

The three silicone hydrogel daily disposable lenses used in the study encompass those currently marketed in the UK: 1-DAY ACUVUE® TruEye® (Vistakon, Johnson and Johnson, Jacksonville, Florida, USA), Clariti™ 1 day (Sauflon Pharmaceuticals, London, UK) and DAILIES TOTAL 1® (Alcon, Fort Worth, Texas, USA) (Table 5.1).

Lens Type	1 Day Acuvue® TruEye®	DAILIES TOTAL 1®	Clariti™ 1 Day
Manufacturer	Johnson & Johnson Vision Care, Inc	Alcon Ciba	Sauflon Pharmaceuticals Ltd
Material	narafilcon A	delefilcon A	filcon II 3
Water Content (%)	46	~33 at core >80 at surface	56
Base curve (mm)	8.5	8.5	8.6
Diameter (mm)	14.2	14.1	14.1
Oxygen Transmissibility @-3D (DK/t)	118	156	86
Modulus (MPa)	0.7	0.7	0.5
Storage Solution	Buffered saline with HydraClear	Buffered saline with polymeric wetting agents	Buffered saline

**Table 5.1:** Study lens specifications

Measures were taken at three time points throughout the final day of wear for each lens type, at 8, 12 and 16 hours after lens insertion. The assessment of dynamic lens fit was captured using a digital slit lamp (CSO, Scandicci, Italy) with a digital camera of resolution 1392 x 1024 pixels, frame rate 11 Hz. The resulting video was analysed by a masked observer using a purpose-developed image analysis program (Labview, National Instruments, Austin, Texas, USA). Movement on blink in upgaze was assessed by the change in vertical lens position relative to the cornea from the first video frame following the blink. Lag was assessed as the difference between the limbus to lens edge distance in each of the horizontal positions of gaze compared to the same distances when viewing in primary gaze. Finally, push-up recovery speed was calculated from the change in vertical lens position relative to the cornea from the first video frame following the lens release, divided by the number of frames over which the movement occurred, times the frame rate. These objective measures have been previously shown to be most appropriate to define soft contact lens fit and highly repeatable.

Comfort was assessed subjectively on a scale from 1 to 10 (1=poor, 10=excellent). Subjective grading of bulbar and limbal hyperaemia was assessed by the same experienced investigator to one decimal place using the Efron grading scale due to its linearity (Wolffsohn and Purslow, 2003). At the 16 hour visit, immediately after lens removal, sodium fluorescein and lissamine green were instilled in fluoret form and any observed staining recorded as trace, mild, moderate or severe.

Non-invasive tear break-up time (NITBUT) was evaluated using a modified CA-1000 topographer (Topcon, Newbury, UK), which projected circular mires onto the corneal surface, with the tear film reflection observed on a 30 inch flat panel monitor and the NITBUT recorded at the first sign of mire distortion. An average of 3 measures was taken. Tear-meniscus height was captured with the digital slit lamp and LabVIEW programming was used to measure the average meniscus heights from the line of reflection along the top of the tear prism, to the very first visible edge of the eyelid. This technique has previously been shown to be highly repeatable.

### **5.2.1 Statistical Analysis**

As the data was normally distributed, repeated measures analysis of variance (ANOVA) was used to assess the differences in lens fit with the time of day and between the lens designs. Eyes were treated as repeated measures to prevent statistical bias. Comfort, hyperaemia grading, staining and tear film metrics for the right eye only were correlated against lens fit using Spearman's ranked correlation to determine whether lens performance was related to the lens design or individual characteristics. A *P*-value of 0.05 was taken to indicate significance throughout as the use of ANOVAs minimised the number of comparisons, except for correlations where a value of  $P \leq 0.01$  to reduce the risk of type I errors associated with multiple comparisons of association.

## 5.3 Results

The lenses were worn on average  $6.9 \pm 0.3$  days a week for  $10.8 \pm 2.0$  hours a day, and for 16 hours on the assessment days.

### 5.3.1 Lens Fit

Movement on blink ranged from 0.06 to 1.73 mm. On blink, there was no difference with time after insertion (8 hours:  $0.34 \pm 0.24$  mm; 12 hours:  $0.35 \pm 0.28$  mm; 16 hours:  $0.36 \pm 0.28$  mm  $F = 0.403$ ,  $P = 0.670$ ). The narafilcon A lenses moved further on blink than the other lens brands (delefilcon A:  $0.33 \pm 0.21$  mm; narafilcon A:  $0.41 \pm 0.34$  mm; filcon II 3:  $0.33 \pm 0.25$  mm;  $F = 3.217$ ,  $P = 0.046$ ). There was no interaction between lens brands and time after insertion ( $F = 0.423$ ,  $P = 0.792$ ). Movement on blink with the delefilcon A lenses was significantly correlated with the narafilcon A lenses, but only after 8 hours of wear ( $r = +0.527$ ,  $P < 0.01$ ). Movement on blink was not correlated between assessment times with any of the lens brands (Table 5.2).

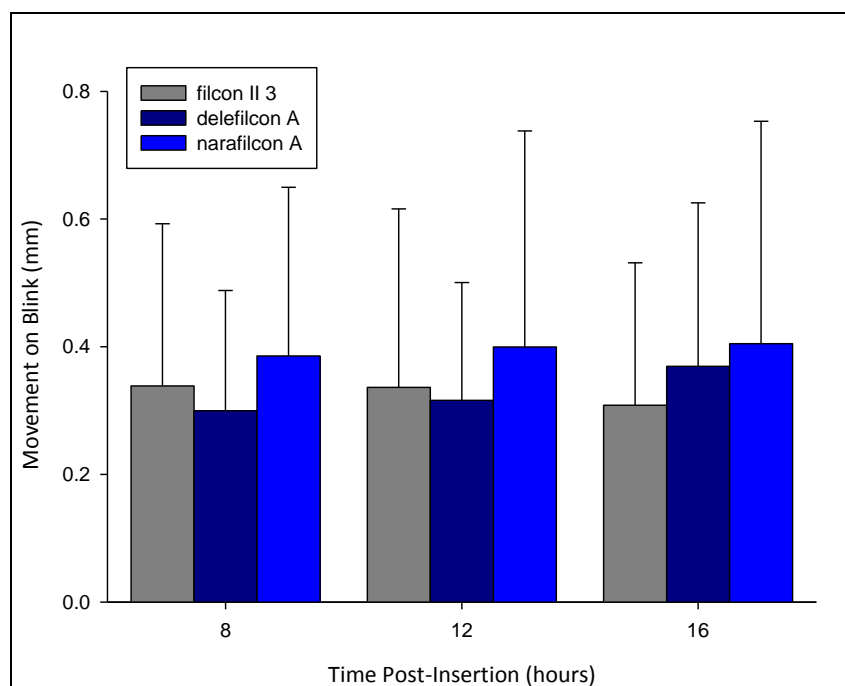


**Figure 5.2:** Movement on blink between study lenses with time after insertion.  $N=39$ . Error bars = 1 S.D.

	Blink			Lag			Push-Up		
Time	<i>delefilcon vs. narafilcon</i>	<i>narafilcon vs. filcon II 3</i>	<i>delefilcon vs. filcon II 3</i>	<i>delefilcon vs. narafilcon</i>	<i>narafilcon vs. filcon II 3</i>	<i>delefilcon vs. filcon II 3</i>	<i>delefilcon vs. narafilcon</i>	<i>narafilcon vs. filcon II 3</i>	<i>delefilcon vs. filcon II 3</i>
8 hours	<b>0.527*</b>	0.169	0.280	0.356	0.161	0.057	-0.116	0.175	-0.156
12 hours	0.151	0.214	-0.057	0.335	<b>0.626**</b>	0.416	0.201	-0.137	-0.073
16 hours	0.155	0.080	0.386	0.263	0.257	0.356	0.004	0.064	-0.0143
Brand	<b>8vs12</b>	<b>8vs16</b>	<b>12vs16</b>	<b>8vs12</b>	<b>8vs16</b>	<b>12vs16</b>	<b>8vs12</b>	<b>8vs16</b>	<b>12vs16</b>
narafilcon A	0.318	0.317	0.355	<b>0.525**</b>	<b>0.438*</b>	<b>0.633**</b>	0.372	-0.306	-0.122
delefilcon A	0.284	0.345	0.194	<b>0.494*</b>	<b>0.529**</b>	<b>0.660**</b>	0.038	0.219	-0.009
filcon II 3	-0.004	0.200	0.223	0.303	<b>0.499*</b>	<b>0.562**</b>	0.311	0.051	0.061

\*  $P < 0.01$ ; \*\*  $P < 0.001$  ( $n=39$ )

**Table 5.2:** Relationship in lens fit variables between lens brands with time

Lag in horizontal excursions ranged from -7% to 215%. Lag reduced towards the end of the day (8 hours:  $77.3 \pm 52.3$  %; 12 hours:  $69.2 \pm 31.1$  %; 16 hours:  $70.1 \pm 36.5$  %;  $F = 3.220$ ,  $P = 0.046$ ). The lens brands had a similar lag (delefilcon A:  $71.2 \pm 36.5$  %; narafilcon A:  $77.7 \pm 49.2$  %; filcon II 3:  $68.3 \pm 28.8$  %;  $F = 2.384$ ,  $P = 0.100$ ) and there was no interaction between lens brands and time after insertion ( $F = 1.421$ ,  $P = 0.230$ ). Lag was correlated for each brand between the assessment times ( $r=+0.527$ ,  $P<0.01$ ) but generally not significantly correlated between the lens brands (Table 5.2).

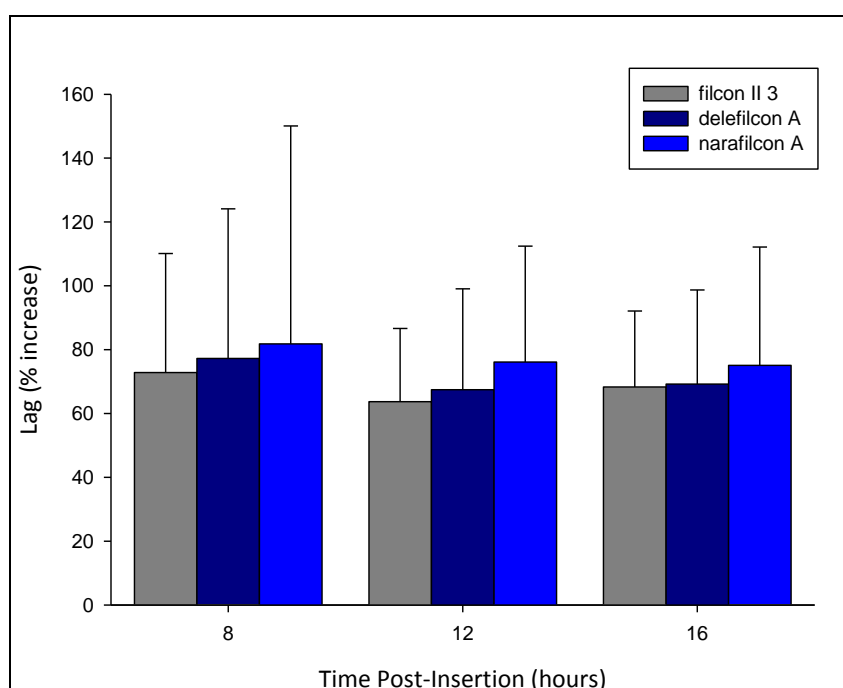


**Figure 5.3:** Increase in lag between study lenses with time after insertion.  $N=39$ . Error bars = 1 S.D.

Lens push-up recovery speed ranged from 0.0 to 3.4 mm/s. The lenses had a faster recovery speed after either 12 hours ( $0.76 \pm 0.44$  mm/s) or 16 hours ( $0.73 \pm 0.40$  mm/s) after insertion compared to at 8 hours ( $0.61 \pm 0.41$  mm/s;  $F = 3.345$ ,  $P = 0.041$ ). However, the recovery speed following push-up was similar between lens brand (delefilcon A:  $0.60 \pm 0.44$  mm/s; narafilcon A:  $0.71 \pm 0.38$  mm/s; filcon II 3:  $0.78 \pm 0.47$  mm/s;  $F = 2.903$ ,  $P = 0.062$ ), and there was no interaction between brand and time ( $F = 0.645$ ,  $P = 0.631$ ). Push-up recovery speed was not correlated between the lens brands or for each brand between assessment times (Table 5.2).

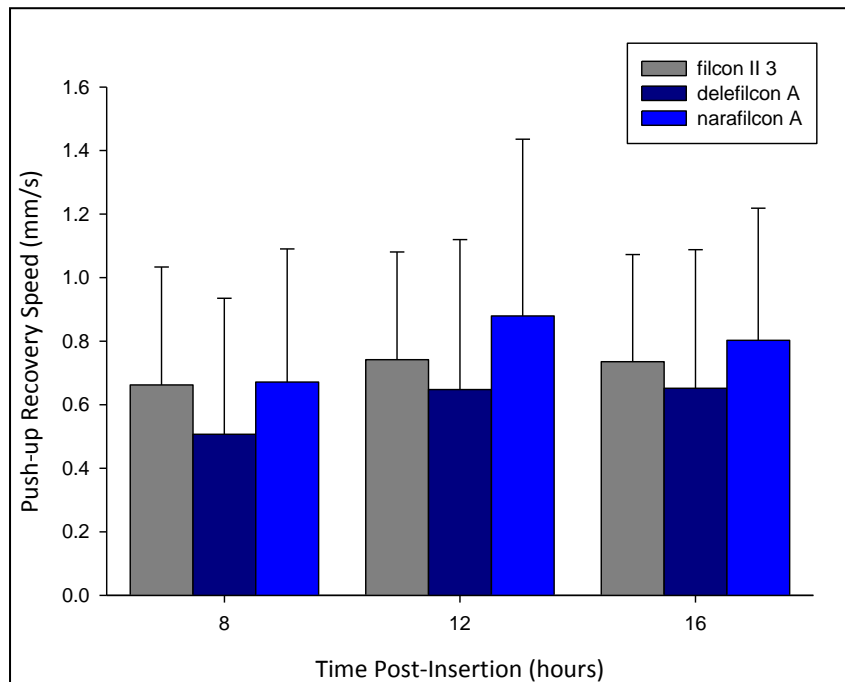


**Figure 5.4:** Push-up recovery speed between study lenses with time after insertion. N=39. Error bars = 1 S.D.

### 5.3.2 Ocular Comfort

Lens fit was generally not correlated with subjective comfort (Table 5.3). Having better comfort than other subjects with one lens brand did not result in having better comfort with other brands (Table 5.3). The change in lens fit (movement on blink, lag and push-up) between 8 and 12 hours of wear and between 8 and 16 hours of lens wear also did not correlate with the change in comfort over these times for any of the lenses tested (Spearman's Rank correlation  $P > 0.05$ ). When wearing each lens brand, the rating of comfort correlated between 8, 12 and 16 hour of wear assessments (Table 5.4).

### 5.3.3 Ocular Physiology

Lens fit was generally not correlated with bulbar or limbal hyperaemia (Table 5.5). However, having less pronounced bulbar hyperaemia than other subjects with one lens brand resulted in less bulbar hyperaemia with other brands, although this was not the case after 16 hours of wear (Table 5.5). There was an association between limbal hyperaemia when wearing delefilcon A lenses and other brands. When wearing each lens brand, the grading of bulbar and limbal hyperaemia

	narafilecon A			delefilecon A			filecon II 3			Comfort between Brands		
Time	<i>Blink</i>	<i>Lag</i>	<i>Push-up</i>	<i>Blink</i>	<i>Lag</i>	<i>Push-up</i>	<i>Blink</i>	<i>Lag</i>	<i>Push-up</i>	<i>delefilecon vs narafilecon</i>	<i>narafilecon vs filecon II 3</i>	<i>delefilecon vs filecon II 3</i>
<b>8 hours</b>	0.119	-0.346	0.106	-0.091	-0.11	0.148	0.244	-0.012	0.250	-0.047	0.048	0.029
<b>12 hours</b>	0.121	-0.104	0.066	-0.130	-0.11	-0.020	0.163	-0.095	0.232	0.014	0.089	0.094
<b>16 hours</b>	-0.060	0.127	0.217	-0.163	-0.14	0.253	0.032	0.051	0.027	0.262	0.390	-0.059

\*  $P < 0.01$ ; \*\*  $P < 0.001$  ( $n=39$ )

**Table 5.3:** Effect of lens fit (correlation coefficients) on comfort and relationship between lens brands

	Ocular Comfort			Bulbar Hyperaemia			Limbal Hyperaemia			NITBUT			TMH		
	<i>8vs12</i>	<i>8vs16</i>	<i>12vs16</i>	<i>8vs12</i>	<i>8vs16</i>	<i>12vs16</i>	<i>8vs12</i>	<i>8vs16</i>	<i>12vs16</i>	<i>8vs12</i>	<i>8vs16</i>	<i>12vs16</i>	<i>8vs12</i>	<i>8vs16</i>	<i>12vs16</i>
narafilcon A	<b>0.846**</b>	<b>0.650**</b>	<b>0.704**</b>	<b>0.501*</b>	0.092	0.292	<b>0.493*</b>	<b>0.611**</b>	<b>0.594**</b>	0.128	<b>0.498*</b>	<b>0.449*</b>	0.123	0.128	<b>0.498*</b>
delefilcon A	<b>0.515**</b>	<b>0.645**</b>	<b>0.657**</b>	<b>0.453*</b>	<b>0.577**</b>	<b>0.459*</b>	<b>0.621**</b>	<b>0.668**</b>	<b>0.554*</b>	0.347	0.283	<b>0.553**</b>	0.337	0.347	0.283
filcon II 3	<b>0.684**</b>	<b>0.484*</b>	<b>0.594**</b>	<b>0.587**</b>	<b>0.576**</b>	<b>0.559**</b>	<b>0.512*</b>	<b>0.532**</b>	<b>0.616**</b>	0.228	0.424	<b>0.756**</b>	0.387	0.228	0.424

\*  $P < 0.01$ ; \*\*  $P < 0.001$  ( $n=39$ )

**Table 5.4:** Relationship in ocular comfort, physiology and lens wettability between lens brands

	narafilecon A			delefilecon A			filecon II 3			Between Brands		
Time	<i>Blink</i>	<i>Lag</i>	<i>Push-up</i>	<i>Blink</i>	<i>Lag</i>	<i>Push-up</i>	<i>Blink</i>	<i>Lag</i>	<i>Push-up</i>	<i>delefilecon vs. narafilecon</i>	<i>narafilecon vs. filecon II 3</i>	<i>delefilecon vs. filecon II 3</i>
<b>Bulbar Hyperaemia</b>												
<b>8 hours</b>	-0.036	-0.093	-0.164	0.306	0.071	0.076	0.029	-0.276	-0.039	<b>0.663*</b>	<b>0.527**</b>	<b>0.496*</b>
<b>12 hours</b>	0.196	-0.092	0.146	0.128	-0.211	0.146	-0.149	-0.370	0.144	<b>0.504*</b>	0.297	<b>0.397*</b>
<b>16 hours</b>	0.234	-0.113	0.198	0.283	0.001	0.226	-0.006	-0.276	0.378	0.123	0.211	0.389
<b>Limbal Hyperaemia</b>												
<b>8 hours</b>	-0.024	-0.369	-0.131	0.249	0.356	-0.055	0.176	0.065	-0.100	0.377	0.266	0.440
<b>12 hours</b>	0.228	0.078	0.086	0.080	-0.084	0.124	0.001	-0.033	0.093	<b>0.589**</b>	0.285	<b>0.542**</b>
<b>16 hours</b>	0.199	0.081	0.072	0.259	-0.032	0.262	-0.206	-0.188	0.180	<b>0.482*</b>	0.275	0.230
<b>Corneal Staining</b>												
<b>16 hours</b>	0.216	-0.013	-0.178	-0.172	-0.198	-0.111	-0.123	-0.109	-0.105	0.057	0.196	0.303
<b>Conjunctival Staining</b>												
<b>16 hours</b>	0.358	-0.089	-0.216	0.152	0.037	0.134	-0.147	0.078	0.106	0.330	0.154	0.027

\*  $P < 0.01$ ; \*\*  $P < 0.001$  ( $n=39$ )

**Table 5.5:** Effect of lens fit (correlation coefficients) on ocular physiology and relationship between lens brands

	narafilecon A			delefilecon A			filecon II 3			Between Brands		
Time	<i>Blink</i>	<i>Lag</i>	<i>Push-up</i>	<i>Blink</i>	<i>Blink</i>	<i>Lag</i>	<i>Push-up</i>	<i>Blink</i>	<i>Blink</i>	<i>delefilecon vs narafilecon</i>	<i>narafilecon vs filecon II 3</i>	<i>delefilecon vs filecon II 3</i>
<b><i>Non-Invasive Lens Surface Tear Break-Up Time</i></b>												
<b>8 hours</b>	-0.135	0.164	0.098	0.217	0.022	0.077	0.041	0.182	0.369	-0.115	0.125	0.083
<b>12 hours</b>	-0.004	-0.279	-0.191	0.182	-0.174	0.016	-0.140	-0.359	0.108	0.035	0.235	0.098
<b>16 hours</b>	0.053	0.039	-0.048	0.086	0.012	0.297	0.195	-0.157	0.163	<b>0.524**</b>	0.405	0.109
<b><i>Lens Surface Tear Meniscus Height</i></b>												
<b>8 hours</b>	0.073	-0.053	-0.183	-0.169	0.038	0.117	-0.123	-0.062	-0.125	-0.234	0.295	0.025
<b>12 hours</b>	-0.084	0.260	0.095	-0.411	0.069	-0.082	-0.024	0.012	0.031	0.289	<b>0.458*</b>	-0.016
<b>16 hours</b>	-0.254	-0.011	-0.172	-0.090	-0.153	0.283	-0.146	-0.048	-0.103	<b>0.415*</b>	0.027	-0.028

\*  $P < 0.01$ ; \*\*  $P < 0.001$  ( $n=39$ )

**Table 5.6:** Effect of lens fit (correlation coefficients) on tear physiology and relationship between lens brands

generally correlated between 8, 12 and 16 hour of wear assessments (Table 5.4). Lens fit was not correlated with end of day (16 hour) corneal or conjunctival staining (Table 5.5). Having more corneal or conjunctival staining than other subjects with one lens brand did not result in having a high level of staining with other brands (Table 5.5).

#### **5.3.4 Lens Wettability**

Lens fit was generally not correlated with non-invasive lens surface break-up time or tear meniscus height (Table 5.6). Having a more wettable contact lens surface than other subjects with one lens brand was not generally associated with a higher surface wettability with the other brands (Table 5.6). When wearing each lens brand, the grading of non-invasive lens surface tear break-up time was correlated between 12 and 16 hour of wear and for the narafilcon additionally between 8 and 16 hours of lens wear and tear meniscus height between 12 and 16 hours (Table 5.4).

## 5.4 Discussion

This study shows lens fit changes between 8 hours, the longest duration of wear previously examined, and 16 hours, which encompasses the wearing day of the majority of contact lens wearers. While one might intuitively expect all lens mobility metric to change in the same direction, movement on blink remained relatively constant over this period, the lens lag on horizontal excursion decreased by approximately 10%, but conversely the push-up recovery speed increased by about 20%.

On excursion, the anatomical interaction between the eyelid and ocular surface displaces the lens, which results in lens lag. This interaction is unlikely to change during the day so it can be presumed the friction between the lens surfaces and the ocular anatomy which is associated with the tear film changes over the day results in the decrease seen between 8 and 16 hours of wear. However, lens fit including lag was generally not correlated with measures of lens surface wettability, in the form of non-invasive lens surface break-up time or tear meniscus height. These measures seem reasonably robust as for each lens brand investigated, with the measures being correlated between some of the time points. However, these tear film metrics only assess anterior surface lens wettability and hence the key frictional component that changes towards the end of the day may be between the rear surface of the lens and the ocular surface due to potential changes in tear composition (although this has not been researched in the peer reviewed literature) or the effect of tear composition on the lens curvature due to hydration (Tranoudis and Efron, 2004b). The lack of change in movement with blink over this period may result from this increase in back surface friction having a greater effect on the horizontal meridian (the direction that lag was assessed), than the steeper vertical meridian (the direction movement on blink was assessed) in this young population of principally with-the-rule low astigmats.

Some authors have investigated the ease of push-up rather than just recovery speed, which would be related to lens binding as well as friction between the ocular and posterior lens surfaces. However, push-up recovery speed has been shown to independently contribute to overall lens mobility, unlike ease of push-up, and can be assessed in-vivo objectively (Wolffsohn et al., 2009). The push-up recovery speed involves greater displacement of the lens than assessment of lag, as well as being influenced by the friction between the ocular and posterior lens surface, it is also moderated by the elastic properties of the lens. Lenses are known to dehydrate towards the end of the day (Tranoudis and Efron, 2004b), increasing its modulus, and hence it could be postulated that this results in the increase in push-up recovery speed with time.

Objective assessment of lens fit was not strongly correlated between lens brands despite their similar base curves and diameters. Previous studies have shown that changing the base curve of a soft lens does not generally have a significant effect on lens fit (Wolffsohn et al., 2009) and this is because the lens fit is influenced by peripheral corneal topography (Chapter 2) (Hall et al., 2011) and the corneoscleral anatomy (Chapter 3) (Hall et al., 2013). Currently marketed daily disposable silicone-hydrogel contact lenses differ in shape profile and material composition and the lack of correlation in lens fit between the brands indicates these features affect the lens fit differently for individual patients. Hence clinically, if a trialled lens does not fit adequately, it is appropriate to trial fit another brand of lens even if the stated base curve and diameter parameters are similar. It also proves beyond doubt that lens substitution, even of a lens with similar base curve and diameter parameters, without a clinical lens assessment, is inappropriate.

Lag was the fit characteristic that was best correlated between assessment times with each individual lens brand. Hence lens mobility in the vertical meridian as assessed by movement on blink or push-up recovery speed, may be a less reliable indicator of lens fit than lag when investigating differences between lens brands. Subjective assessment of ocular comfort was consistent between assessment times with each lens brand (i.e. subjects with the best comfort within the cohort at one time point were likely to have the best comfort at subsequent time points and vice versa, even if the overall comfort had reduced), suggesting it is a robust measure. Lens fit was generally not correlated with subjective comfort over the end of a day. It is possible that a population with less comfortable eyes may have been more sensitive to changes in lens fit. Having better comfort than other subjects with one lens brand did not result in having better comfort with other brands. Therefore it is the lens-patient interaction that drives lens comfort, rather than the lens design/material or patient in isolation. Hence clinically, if a patient is uncomfortable in their current lenses, it does not necessarily follow that they will be uncomfortable in another brand.

Grading of bulbar and limbal hyperaemia was consistent between assessment times with each lens brand, suggesting they are also robust measures. Lens fit was generally not correlated with bulbar or limbal hyperaemia. However, patients who exhibited greater redness with one lens brand often had a greater redness with the other brands and vice versa. Limbal hyperaemia is associated with ocular insult (Young and Coleman, 2001), however, in this study there was no difference between the investigated lenses in lens fit or ocular staining. Limbal hyperaemia is also associated with insufficient oxygen transmissibility (Papas, 1998), so the correlation between delefilcon A lenses and the other brands, but not between narafilcon A and filcon II 3, may result from the higher oxygen transmissibility difference inherent between the former, even in daily wear. The lack of relationship

in corneal or conjunctival staining between brands on lens removal suggests that staining is not related just to patient susceptibility, but an interaction between an individual and a particular lens design (Maissa et al., 2012).

*In-vivo* lens surface wettability was a less consistent measure across time for a particular brand than subjective comfort and ocular physiology. Clinical tear film techniques have previously been shown to be susceptible to wide variation between repeated measurement and this may contribute to this finding (Best et al., 2012). Non-invasive lens surface break-up time or tear meniscus height was not affected by lens fit as expected. However, having a more wettable contact lens surface with one brand was not associated with having a more wettable surface with another brand, suggesting that lens surface wetting is not related just to lens characteristics, but an interaction between an individual's ocular surface including their tear film and interaction with the lens.

## **5.5 Conclusion**

In conclusion, this chapter shows objectively that lens fit changes between 8 hours and the end of the typical contact lens wearing day, and consequently that wearing time is an additional factor driving lens fit dynamics. However, lens fit in initially acceptable fitting lenses was not associated with ocular comfort, ocular physiology or lens surface wettability. This chapter also showed that if a lens fitted adequately or was comfortable, it did not follow that another lens brand of similar base curve and diameter parameters would fit acceptably and/or be comfortable; consequently, lens substitution without a clinical lens assessment is inadvisable.

The use of AS-OCT technology in previous chapters allowed for the characterisation of the anterior ocular topography (Chapters 2&3) and prediction of the variance in lens fit (Chapter 2). The cost of dedicated AS-OCT systems capable of capturing full corneal width generally makes them accessible to research establishments, hospitals and specialist optical practices only. Chapter 6 assessed a new implementation of a more readily available technology for the determination of the ocular topography and further determination of the variance in lens fit.

# Chapter 6

## **Chapter 6: Prediction of Soft Contact Lens Fit Using Enhanced Corneal Topography**

### **6.1 Introduction**

Computerised videokeratometry (CVK) is considered the current standard in the measurement of corneal surface topography (Alonso-Caneiro et al., 2008). However, for Placido disc-based devices corneal coverage is limited since the instrument is based on specular reflection from the corneal surface, and further limited by the obscuration of the reflected images by the protrusion of the nose, brow, eyelids and eyelashes (Read et al., 2006). This may in part be overcome by the use of small Placido cone devices which facilitate much closer imaging of the corneal surface as a result of their smaller physical footprint, although many of these limitations remain.

Franklin et al. (2006) described a technique to extend the area of standard topography maps by combining a central topography map with six additional maps taken in peripheral positions of gaze. Since the point corresponding to the vertex normal of the central map could be found in each of the peripheral maps, the data from these peripheral maps was added to the edges of the central map to create a topography map that extended from limbus to limbus, both horizontally and vertically. They concluded the technique enabled an increase in measurable surface area of approximately 70%. In a later paper published the same year, Read et al. (2006) described the compositing of central and peripheral topography maps and found that the peripheral cornea becomes significantly flatter and less astigmatic than the central cornea. Despite these and other descriptions of compositing in the literature, the technique has not previously been made commercially available.

The Medmont E300 corneal topographer (Medmont, Camberwell, Australia) is an established and validated (Tang et al., 2000) small cone Placido disc-based device. Like all Placido disc devices though, and despite its small cone technology, it too is limited by the physical limitations of specular reflection and obscuration of the circular mire images as a result of the ocular adnexa of the eye. However, a recently introduced software upgrade to the Medmont system (Medmont Studio 5) now offers the ability to image and composite multiple image scans in a commercial implementation of Franklin's work in a bid to overcome of the limitations of Placido videokeratometry.

The aim of this study was to determine if significantly greater variance in lens fit could be accounted for using multiple topographical scans, if a better and wider area quantification of the peripheral cornea from the same, and also whether this would substitute for the additional information gained from OCT biometry of the corneoscleral topography. In addition, the study enabled confirmation of

the results of Chapter 4, leading from the findings of Chapter 2, that objective assessment of lens fit would overcome some of the variance lost in the noise of subjective fit analysis.

## 6.2 Method

This was a prospective study undertaken at a single site in the UK, Aston University (Birmingham, UK). The research followed the tenets of the Declaration of Helsinki and approval of the study was given by the University's Research Ethics Committee prior to commencing. Subjects gave written informed consent after an explanation of the nature of the study.

Thirty-five subjects' standard corneal topography was assessed with the Medmont E300 taking a single scan, with subjects looking straight ahead in primary gaze. Further Medmont scans were then acquired in the four main cardinal directions of gaze (Figure 6.1) and finally in the oblique positions (Figure 6.2) of gaze. The resulting scans were then composited using the Medmont Studio Five software's inbuilt compositing feature, and key videokeratometry data (Table 6.1) were extracted for the single scan taken in primary gaze, for a composited scan of five images (single scan plus the scans taken in the four cardinal directions of gaze), and finally for a composited scan of nine images (the single scan plus the all of the scans taken in the cardinal and oblique directions of gaze).

Additional ocular topography data (Table 6.2) were collected from OCT images captured with the eye in the primary-gaze position and also in the four cardinal directions of gaze to give both full sagittal cross-sections of the cornea and cross-sections of the corneoscleral junctions at the superior, inferior, nasal and temporal positions, as described in Chapter 3. External fixation targets were used to ensure consistency of subject's direction of gaze for images taken perpendicularly in the horizontal and vertical planes, as previously described in Chapter 2.

Two daily wear soft contact lens types, of power -2.50 D, were evaluated; a conventional hydrogel design (Acuvue® 2 [Vistakon]; etafilcon A material, modulus 0.30 MPa) and a silicone hydrogel design (Acuvue® Advance® [Vistakon]; galyfilcon A material, modulus 0.43 MPa). These lenses were chosen for their similar geometries and identical base curve (8.3 mm) and diameter (14.0 mm). Subjects were randomly assigned to wear one lens design in each eye, i.e. contralaterally. The steepest available base curve (8.30 mm) was selected for dispensing in each case and lens blister packs were re-labelled by a clinical assistant so as to ensure both investigator and subject were masked to lens type. Lenses were inserted by an investigator and allowed to settle for 30 minutes. Lens fit was then assessed both subjectively and objectively, as described in Chapter 4.

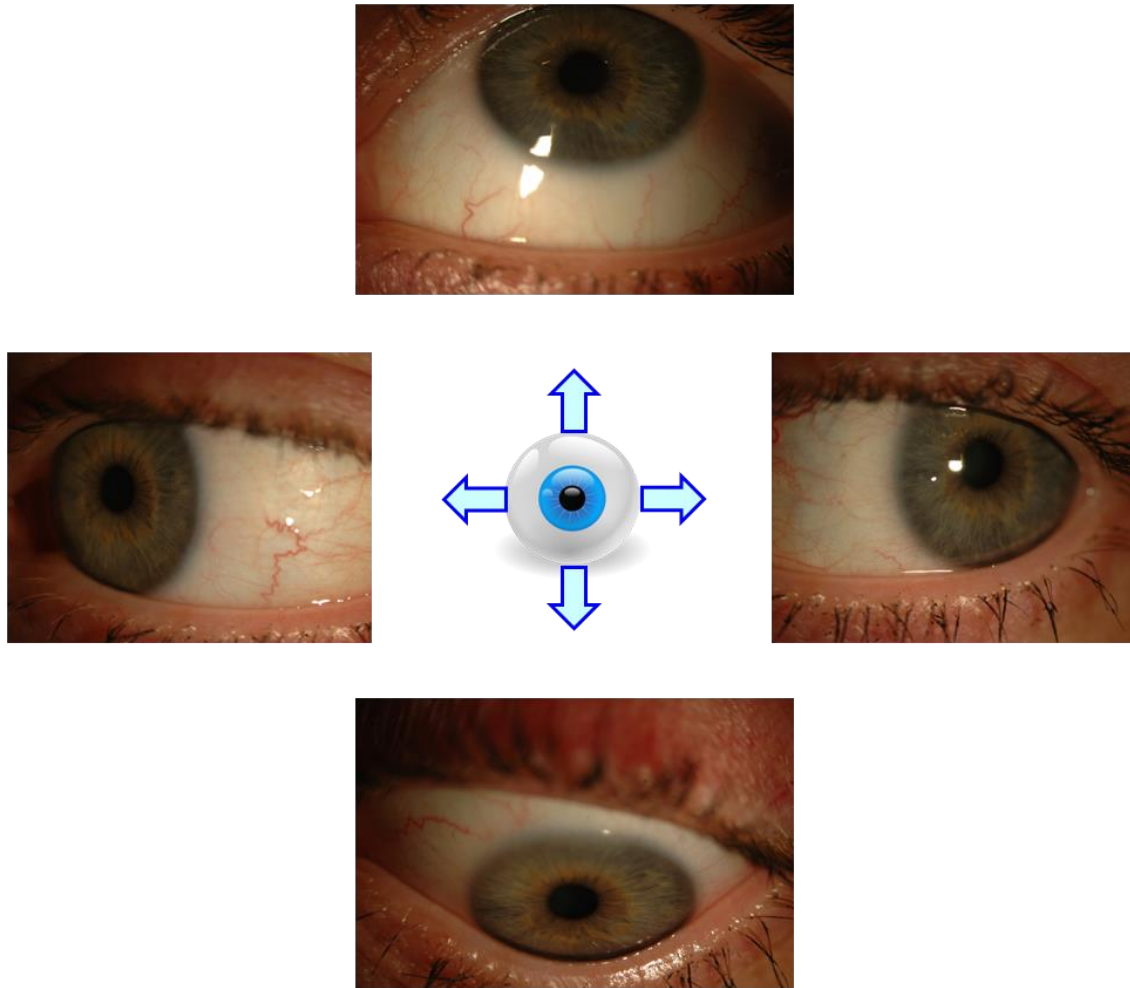


**Figure 6.1:** Medmont E300 corneal topography scans captured in the four main cardinal directions of gaze

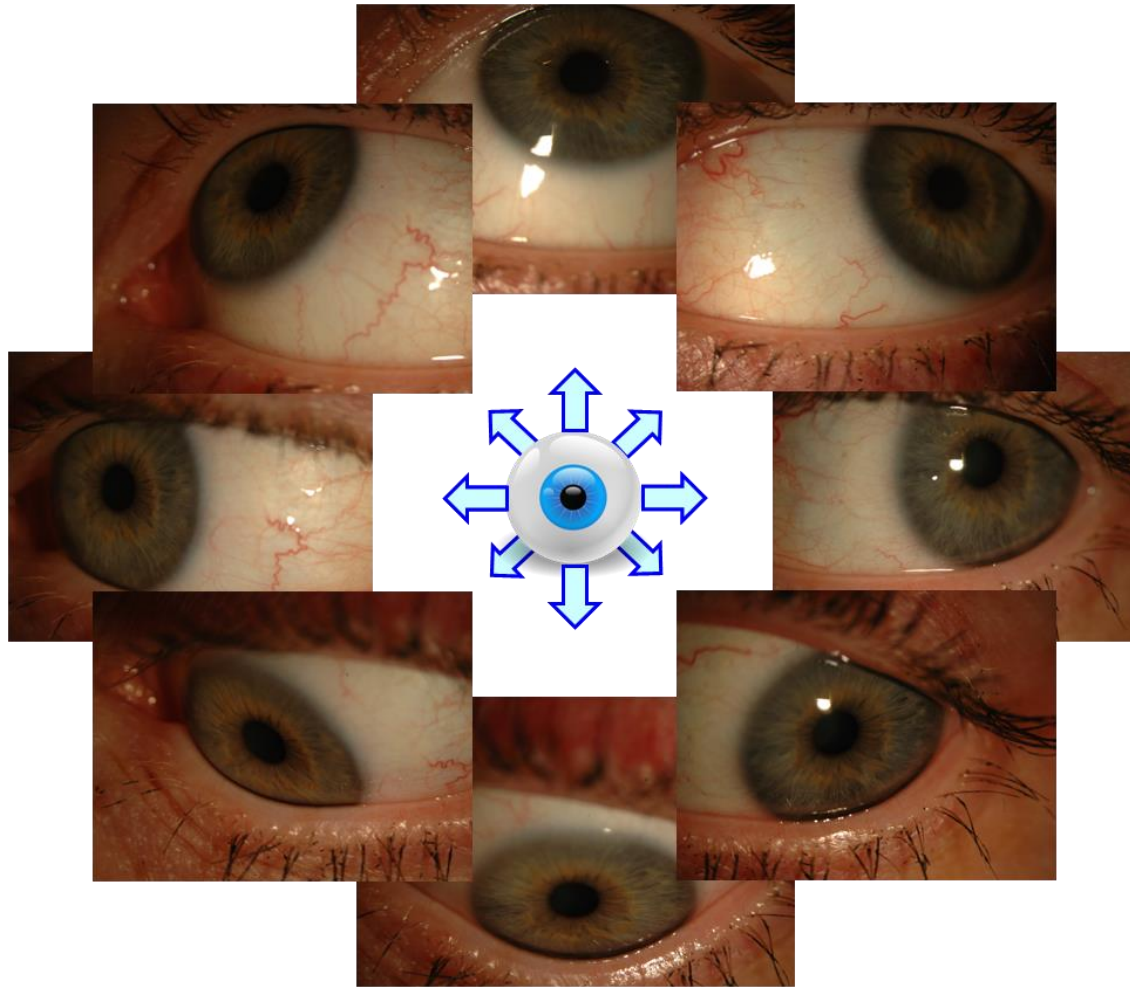


**Figure 6.2:** Medmont E300 corneal topography scans captured in the oblique directions of gaze

Abbreviation	Description	Instrument
K	Simulated keratometry reading	EVK
Q_SF	Corneal shape factor ( $SF=e^2$ )	EVK
CA	Corneal astigmatism	EVK
CS10-VK	Corneal sagittal height of a chord at 10 mm	EVK
	Maximum chord length obtainable at the maximum chord length obtainable with either the single, composite of five or composite of nine scans	EVK
CS_Max	Sagittal height at the maximum chord length obtainable with either the single, composite of five or composite of nine scans	EVK
e2_Max	Eccentricity at the maximum chord length obtainable with either the single, composite of five or composite of nine scans	EVK
Fl, St	Flat, step meridians	-
0, 90, 180, 270	0, 90, 270, and 270 meridians	-

**Table 6.1:** Medmont videokeratometry measurements

Abbreviation	Description	Instrument
CD	Corneal diameter	OCT
CS	Corneal sagittal height of a chord taken between the anterior corneal sulci	OCT
CS10_OCT	Corneal sagittal height of a chord at 10 mm	OCT
OS15_OCT	Ocular sagittal height of a chord at 15 mm	OCT
ID	Iris diameter	OCT
CSJ	Corneoscleral junction angle	OCT
SR	Scleral radius	OCT
$\Delta$ CD	Difference in corneal diameter between the horizontal and vertical meridians	-
$\Delta$ CSJ	Difference between the two corneoscleral junction angles in a given meridian	-
n, t, s, i	Nasal, temporal, superior, inferior	-
h, v	Horizontal, vertical	-

**Table 6.2:** AS-OCT ocular topography measurements

### **6.2.1 Statistical analysis**

Differences between the single image videokeratotomy scan, composite of five and composite of nine videokeratotomy scan results were compared using repeated measures ANOVA. Differences were also compared between meridians for the same A *P*-value of 0.050 or less was taken to indicate a statistically significant difference.

Multiple regression analysis (forward stepwise method; entry *P*=0.05, removal *P*=0.10) was undertaken to determine the predictive values for key fit variables when measured using keratometry alone, keratometry and videokeratotomy and, finally, keratometry, videokeratotomy and OCT in combination. Ocular topography variables were tested for entry into the model sequentially, based on the significance level of the score statistic. After each entry, variables that were already in the model were tested for possible removal, and variables not included thus far were tested for inclusion. This was repeated until no more variables met entry or removal criteria, or until the model remained unchanged.

The analysis was undertaken using SAS 9.4 (SAS Institute Inc., Cary, NC, USA). Missing data were excluded from the analysis and not extrapolated from the collected data.

## **6.3 Results**

### **6.3.1 Biometric Data**

Thirty-five subjects (63% female) were enrolled and completed the study. The mean age of subjects was 21.9 yrs (SD  $\pm$ 3.3, range 18 to 31). The mean spectacle sphere on auto-refraction was -1.44 D (SD  $\pm$ 2.15, range -7.50 to +3.12) and the mean spectacle cylinder -0.90 DC (SD  $\pm$ 0.61, range 0.00 to -3.12).

### **6.3.2 Maximum Chord Width Obtained Using Single versus Composite Scans**

Both the composite of five and composite of nine videokeratotomy scans yielded significantly greater maximum chord length data in each meridian than for a single scan (*P*<0.0001). A summary of the maximum chord lengths obtained using single versus composite scans for the 0°, 90°, 180° and 270° meridians and for right and left eyes are shown Table 6.3 and Table 6.4, and also in Figure 6.3 and Figure 6.4, respectively. A comparison of maximum chord length by meridian for the single, composite of five and composite of nine scans, respectively is shown in Table 6.5.

Orientation		Single	Composite of 5 Summary <i>P</i> -value*	Composite of 9 Summary <i>P</i> -value*
No. of Eyes		35	35	35
0°	Mean	10.44	11.49 <0.0001	11.98 <0.0001
	SD	0.44	1.14	0.67
	Min	8.8	7.8	10.8
	Max	10.8	13.4	13.4
90°	Mean	7.26	8.36 <0.0001	9.31 <0.0001
	SD	1.47	1.42	1.16
	Min	3.6	4.6	6.6
	Max	9.8	10.2	11.2
180°	Mean	10.13	12.06 <0.0001	12.28 <0.0001
	SD	0.42	0.90	1.19
	Min	9.4	10.8	8.8
	Max	10.8	13.8	13.8
270°	Mean	9.15	11.18 <0.0001	11.27 <0.0001
	SD	0.65	0.72	0.94
	Min	7.4	9.8	7.6
	Max	9.8	12.8	12.8

\* *P*-value from Repeated Measures Analysis comparing composites of multiple images to the single image.

**Table 6.3:** Summary of maximum chord lengths acquired with single vs. composite Medmont scans (right eye)

Orientation		Single	Composite of 5 Summary P-value*		Composite of 9 Summary P-value*	
No. of Eyes		34	35		35	
0°	Mean	10.13	12.50	<0.0001	12.87	<0.0001
	SD	0.42	1.41		0.80	
	Min	9.4	6.6		11.2	
	Max	10.8	14.4		14.4	
90°	Mean	7.07	9.05	<0.0001	9.34	<0.0001
	SD	1.30	1.21		1.16	
	Min	4.0	6.2		6.2	
	Max	9.4	10.8		11.8	
180°	Mean	10.29	11.86	<0.0001	12.10	<0.0001
	SD	0.39	0.71		0.72	
	Min	9.4	10.8		10.2	
	Max	10.8	13.8		13.8	
270°	Mean	9.10	11.21	<0.0001	11.34	<0.0001
	SD	0.66	0.77		0.60	
	Min	7.0	9.8		10.2	
	Max	9.8	12.8		12.2	

\* P-value from Repeated Measures Analysis comparing composites of multiple images to the single image.

**Table 6.4:** Summary of maximum chord lengths acquired with single vs. composite Medmont scans (left eye)

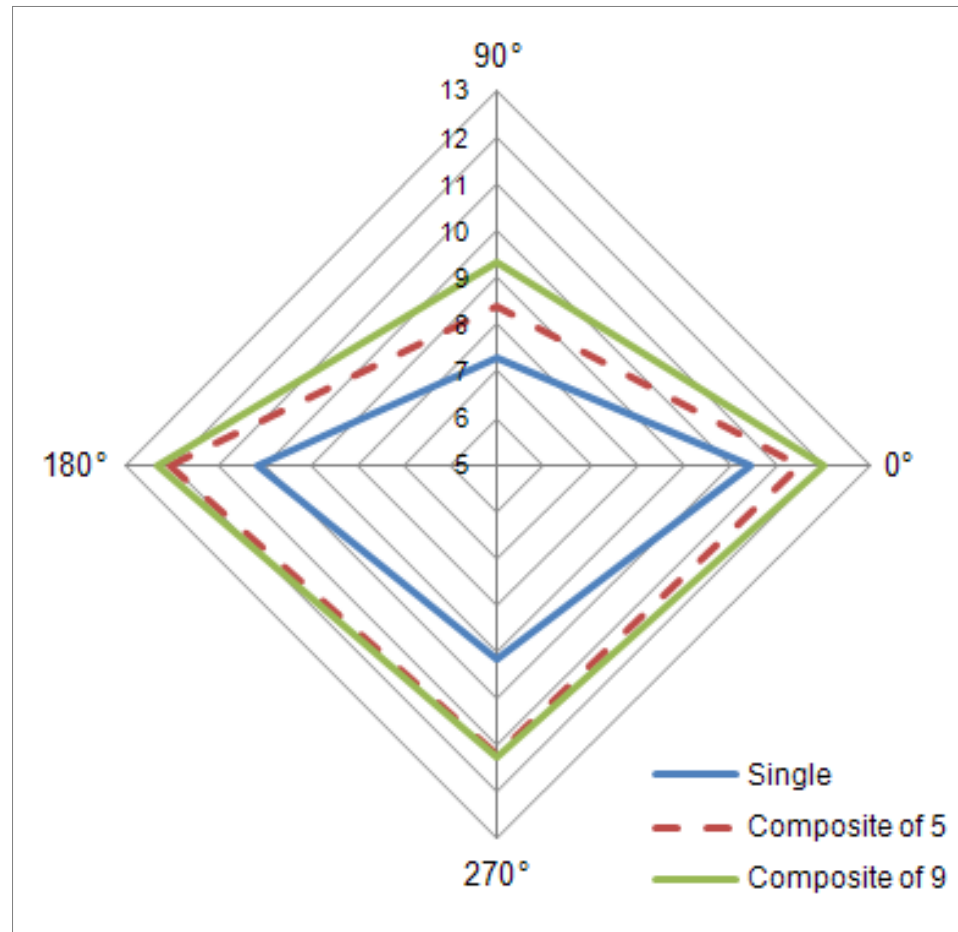


**Figure 6.3:** Plot showing the maximum measurable chord width using single versus composite Medmont scans. Right eye. N=35.

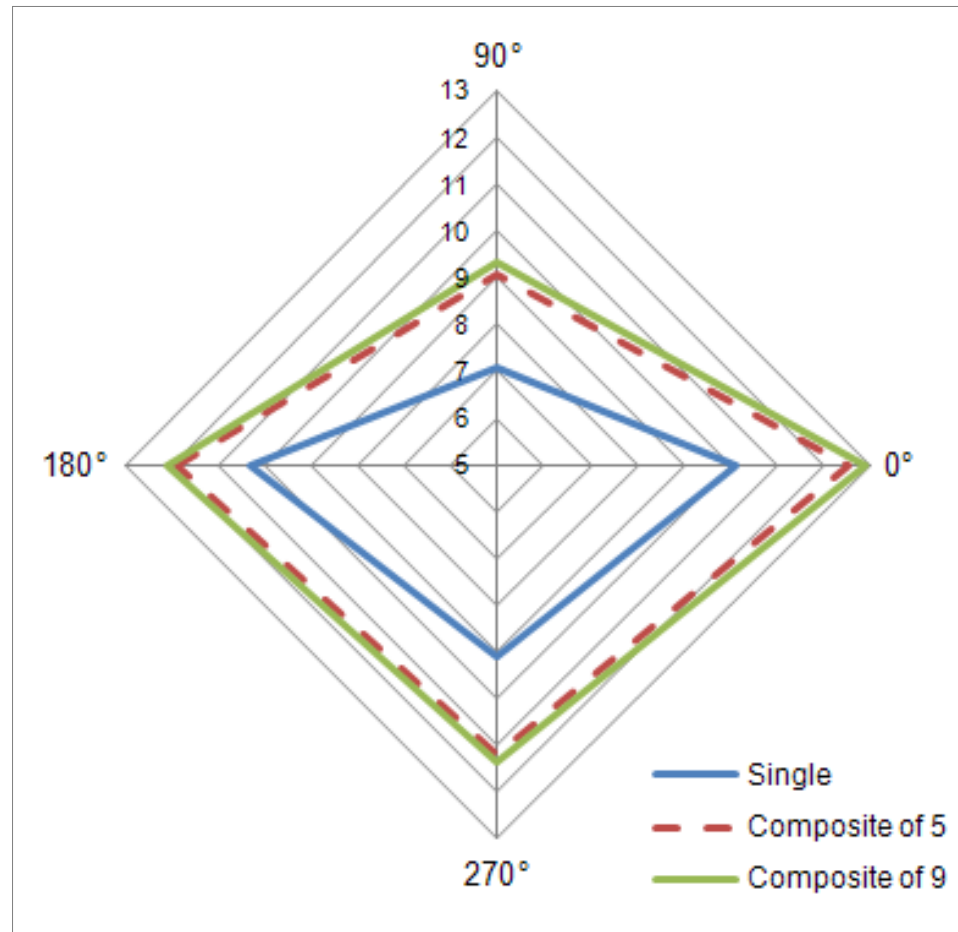


**Figure 6.4:** Plot showing the maximum measurable chord width using single versus composite Medmont scans. Left eye. N=35.

Orientation	Right Eye Summary <i>P</i> -value*	Left Eye Summary <i>P</i> -value*
<b>Single Scan</b>		
0 vs. 90	<0.0001	<0.0001
0 vs. 180	0.0005	0.060
0 vs. 240	<0.0001	<0.0001
90 vs. 180	<0.0001	<0.0001
90 vs. 240	<0.0001	<0.0001
180 vs. 240	<0.0001	<0.0001
<b>Composite of Five Scans</b>		
0 vs. 90	<0.0001	<0.0001
0 vs. 180	0.031	0.011
0 vs. 240	0.17	<0.0001
90 vs. 180	0.0001	<0.0001
90 vs. 240	0.0001	<0.0001
180 vs. 240	<0.0001	0.0007
<b>Composite of Nine Scans</b>		
0 vs. 90	<0.0001	0.0001
0 vs. 180	0.20	<0.0001
0 vs. 240	0.0009	<0.0001
90 vs. 180	<0.0001	<0.0001
90 vs. 240	<0.0001	<0.0001
180 vs. 240	<0.0001	<0.0001

\* *P*-value from Repeated Measures Analysis comparing meridians.

**Table 6.5:** Comparison of maximum chord length by meridian for the single, composite of five and composite of nine scans, respectively

### 6.3.2 Lens Fit

Modelling of the principal factors of lens fit with topography measurements showed that central keratometry was a poor predictor of contact lens fit, while the addition of single scan videokeratometry data allowed for up to 22% of the lens fit variance to be accounted for. The use of composite of five videokeratometry scan data increased the predictive power of the model up to a maximum of 77%, compared to only 22% with composite of nine videokeratometry scan data. Combining AS-OCT and composite of five scan data, and AS-OCT and composite of nine scan data accounted for 83% and 89% of the variance of post-blink movement for the silicone hydrogel lens, respectively (Table 6.6).

Type	Measurement Method	Dependent	Keratometry				Single Image VK				Composite of 5 Image VK				Composite of 9 Image VK				OCT				Composite of 5 Image VK and OCT				Composite of 9 Image VK and OCT					
			Predictor Variables	Regression Mode	P-values	Adjusted R <sup>2</sup>	P-value	Variable	P-values	Adjusted R <sup>2</sup>	P-value	Variable	P-values	Adjusted R <sup>2</sup>	P-value	Variable	P-values	Adjusted R <sup>2</sup>	P-value	Variable	P-values	Adjusted R <sup>2</sup>	P-value	Variable	P-values	Adjusted R <sup>2</sup>	P-value	Variable	P-values	Adjusted R <sup>2</sup>	P-value	
Acuvue Advance	Objective	Tightness on push-up	No significant predictor variables				Intercept Q_SF_st	<b>0.0000</b> <b>0.0058</b>	0.22	<b>0.0058</b>	Intercept CS_Max_0	<b>0.0000</b> <b>0.0018</b>	0.26	<b>0.0018</b>	Intercept Q_SF_st	<b>0.0000</b> <b>0.031</b>	0.12	<b>0.031</b>	Intercept CDSH CSAn SRt	<b>0.0002</b> <b>0.0024</b> <b>0.0006</b> <b>0.034</b>	0.44	<b>0.0012</b>	Intercept CS_Max_0	<b>0.0000</b> <b>0.0034</b>	0.28	<b>0.0034</b>	Intercept Q_SF_st CDSH CSAn SRt	<b>0.0001</b> <b>0.040</b> <b>0.0040</b> <b>0.0005</b> <b>0.036</b>	0.52	<b>0.0005</b>		
		Post-blink Movement	No significant predictor variables				Intercept e2_Max_0	<b>0.066</b> <b>0.025</b>	0.14	<b>0.025</b>	Intercept e2_Max_0 CS_Max_0	<b>0.0006</b> <b>0.0000</b> <b>0.026</b>	0.77	<b>0.0000</b>	Intercept e2_Max_180	<b>0.89</b> <b>0.031</b>	0.12	<b>0.031</b>	No significant predictor variables				Intercept e2_Max_0 CS_Max_0 OS15_OCTv	<b>0.13</b> <b>0.0000</b> <b>0.014</b> <b>0.013</b>	0.83	<b>0.0000</b>	Intercept Q_SF_fl Q_SF_st e2_Max_180 CS_Max_270 CDh CS10_OCTh SRs	<b>0.073</b> <b>0.0000</b> <b>0.0000</b> <b>0.0000</b> <b>0.0000</b> <b>0.0000</b> <b>0.0000</b>	0.89	<b>0.0000</b>		
		Version Lag	No significant predictor variables				Intercept e2_Max_270	<b>0.0000</b> <b>0.033</b>	0.13	<b>0.033</b>	Intercept e2_Max_90	<b>0.0000</b> <b>0.021</b>	0.15	<b>0.021</b>	Intercept Q_SF_st	<b>0.0000</b> <b>0.019</b>	0.15	<b>0.019</b>	Intercept IDh SRt	<b>0.0017</b> <b>0.0032</b> <b>0.039</b>	0.29	<b>0.0080</b>	Intercept IDh SRt	<b>0.0017</b> <b>0.0032</b> <b>0.039</b>	0.29	<b>0.0080</b>	Intercept CS_Max_270 IDh	<b>0.0017</b> <b>0.0087</b> <b>0.0078</b>	0.36	<b>0.0021</b>		
		Horizontal Decentration	No significant predictor variables				No significant predictor variables				Intercept CS_Max_270	<b>0.14</b> <b>0.049</b>	0.10	<b>0.049</b>	No significant predictor variables				No significant predictor variables				No significant predictor variables				No significant predictor variables					
		Vertical Decentration	No significant predictor variables				No significant predictor variables				Intercept e2_Max_0	<b>0.0021</b> <b>0.0013</b>	0.29	<b>0.0013</b>	No significant predictor variables				No significant predictor variables				Intercept e2_Max_0	<b>0.0018</b> <b>0.0021</b>	0.30	<b>0.0021</b>	No significant predictor variables					
		Tightness on push-up	No significant predictor variables				No significant predictor variables				Intercept e2_Max_180	<b>0.0000</b> <b>0.037</b>	0.11	<b>0.037</b>	Intercept e2_Max_180	<b>0.0000</b> <b>0.016</b>	0.15	<b>0.016</b>	No significant predictor variables				Intercept Q_SF_st	<b>0.0000</b> <b>0.050</b>	0.11	<b>0.050</b>	Intercept Q_SF_st	<b>0.0000</b> <b>0.018</b>	0.16	<b>0.018</b>		
		Post-blink Movement	No significant predictor variables				Intercept CS_Max_90	<b>0.32</b> <b>0.047</b>	0.10	<b>0.047</b>	Intercept Q_SF_st e2_Max_0	<b>0.0000</b> <b>0.036</b> <b>0.0082</b>	0.22	<b>0.0095</b>	No significant predictor variables				Intercept OS15_OCTv SRs	<b>0.16</b> <b>0.032</b> <b>0.0077</b>	0.31	<b>0.0038</b>	Intercept Q_SF_st SRs CDv OS15_OCTv SRs	<b>0.024</b> <b>0.0062</b> <b>0.016</b> <b>0.049</b> <b>0.0055</b> <b>0.0051</b>	0.57	<b>0.0002</b>	Intercept Q_SF_st SRs	<b>0.0000</b> <b>0.029</b> <b>0.0037</b>	0.31	<b>0.0034</b>		
	Version Lag	No significant predictor variables				Intercept CS_Max_90	<b>0.0026</b> <b>0.032</b>	0.13	<b>0.032</b>	Intercept CS_Max_90	<b>0.0016</b> <b>0.036</b>	0.12	<b>0.036</b>	Intercept CS_Max_180	<b>0.37</b> <b>0.042</b>	0.11	<b>0.042</b>	Intercept CSAt Sri	<b>0.0098</b> <b>0.014</b> <b>0.021</b>	0.38	<b>0.0021</b>	Intercept CSAt Sri	<b>0.0098</b> <b>0.014</b> <b>0.021</b>	0.38	<b>0.0021</b>	Intercept CSAt Sri	<b>0.0098</b> <b>0.014</b> <b>0.021</b>	0.38	<b>0.0021</b>			
	Horizontal Decentration	No significant predictor variables				No significant predictor variables				Intercept e2_Max_0 e2_Max_90	<b>0.0001</b> <b>0.0012</b> <b>0.012</b>	0.41	<b>0.0000</b>	No significant predictor variables				Intercept SRs	<b>0.10</b> <b>0.035</b>	0.12	<b>0.035</b>	Intercept e2_Max_0 CDh	<b>0.015</b> <b>0.0001</b> <b>0.018</b>	0.41	<b>0.0003</b>	Intercept e2_Max_270	<b>0.019</b> <b>0.029</b>	0.13	<b>0.029</b>			
	Vertical Decentration	No significant predictor variables				No significant predictor variables				Intercept e2_Max_0 e2_Max_180	<b>0.0000</b> <b>0.0005</b> <b>0.0090</b>	0.29	<b>0.0016</b>	No significant predictor variables				Intercept CDSv	<b>0.0063</b> <b>0.029</b>	0.13	<b>0.029</b>	Intercept e2_Max_0 e2_Max_180 CS_Max_180 CDSv	<b>0.0005</b> <b>0.0000</b> <b>0.0078</b> <b>0.011</b> <b>0.0004</b>	0.58	<b>0.0000</b>	Intercept CDSv	<b>0.0063</b> <b>0.029</b>	0.13	<b>0.029</b>			
	Acuvue 2	Objective	Tightness on push-up	No significant predictor variables				Intercept e2_Max_0 e2_Max_180	<b>0.0000</b> <b>0.0005</b> <b>0.0090</b>	0.29	<b>0.0016</b>	No significant predictor variables				Intercept Q_SF_st CS_Max_90	<b>0.46</b> <b>0.025</b> <b>0.0082</b>	0.22	<b>0.0068</b>	Intercept LZv	<b>0.0000</b> <b>0.027</b>	0.13	<b>0.027</b>	Intercept LZv	<b>0.0000</b> <b>0.027</b>	0.13	<b>0.027</b>	Intercept LZv	<b>0.0000</b> <b>0.027</b>	0.13	<b>0.027</b>	
			Post-blink Movement	No significant predictor variables				No significant predictor variables				Intercept e2_Max_0 CS_Max_90	<b>0.0000</b> <b>0.041</b> <b>0.018</b>	0.22	<b>0.013</b>	No significant predictor variables				No significant predictor variables				No significant predictor variables				Intercept Q_SF_st	<b>0.0000</b> <b>0.042</b>	0.13	<b>0.042</b>	
			Version Lag	No significant predictor variables				Intercept CS_Max_270	<b>0.051</b> <b>0.020</b>	0.15	<b>0.020</b>	Intercept CS_Max_0	<b>0.047</b> <b>0.0079</b>	0.20	<b>0.0079</b>	Intercept CS_Max_0	<b>0.098</b> <b>0.029</b>	0.13	<b>0.029</b>	Intercept CSAn OS15_OCTv	<b>0.0009</b> <b>0.0059</b> <b>0.015</b>	0.35	<b>0.0026</b>	Intercept CS_Max_90 CSAn OS15_OCTv	<b>0.0004</b> <b>0.037</b> <b>0.0043</b> <b>0.0024</b>	0.45	<b>0.0011</b>	Intercept CSAn OS15_OCTv	<b>0.0009</b> <b>0.0059</b> <b>0.015</b>	0.35	<b>0.0026</b>	
			Horizontal Decentration	No significant predictor variables				Intercept CS_Max_0	<b>0.038</b> <b>0.018</b>	0.15	<b>0.018</b>	Intercept Q_SF_st	<b>0.17</b> <b>0.048</b>	0.10	<b>0.048</b>	No significant predictor variables				No significant predictor variables				Intercept Q_SF_st	<b>0.12</b> <b>0.049</b>	0.12	<b>0.049</b>	No significant predictor variables				
Vertical Decentration			No significant predictor variables				Intercept CS_Max_270	<b>0.0001</b> <b>0.016</b>	0.14	<b>0.016</b>	No significant predictor variables				Intercept CS_Max_270	<b>0.0000</b> <b>0.013</b>	0.15	<b>0.013</b>	Intercept IDSh dCSAv	<b>0.0000</b> <b>0.0023</b> <b>0.0024</b>	0.38	<b>0.0006</b>	Intercept IDSh dCSAv	<b>0.0000</b> <b>0.0023</b> <b>0.0024</b>	0.38	<b>0.0006</b>	Intercept CS_Max_270 IDSh dCSAv	<b>0.0000</b> <b>0.025</b> <b>0.0039</b> <b>0.0021</b>	0.47	<b>0.0002</b>		
Subjective		Post-blink Movement	No significant predictor variables				Intercept CS_Max_270	<b>0.34</b> <b>0.049</b>	0.09	<b>0.049</b>	Intercept Q_SF_fl	<b>0.073</b> <b>0.032</b>	0.11	<b>0.032</b>	No significant predictor variables				No significant predictor variables				No significant predictor variables				No significant predictor variables					
		Version Lag	No significant predictor variables				No significant predictor variables				No significant predictor variables				No significant predictor variables				No significant predictor variables				Intercept	<b>0.0000</b>	0.00		No significant predictor variables					
		Horizontal Decentration	No significant predictor variables				No significant predictor variables				No significant predictor variables				No significant predictor variables				Intercept OS15_OCTv	<b>0.024</b> <b>0.031</b>	0.13	<b>0.031</b>	Intercept e2_Max_90 dCSAv OS15_OCTv	<b>0.0024</b> <b>0.017</b> <b>0.043</b> <b>0.0048</b>	0.31	<b>0.0055</b>	Intercept OS15_OCTv	<b>0.024</b> <b>0.031</b>	0.13	<b>0.031</b>		
		Vertical Decentration	No significant predictor variables				No significant predictor variables				No significant predictor variables				No significant predictor variables				No significant predictor variables				No significant predictor variables				No significant predictor variables					
		Horizontal Decentration	No significant predictor variables				No significant predictor variables				No significant predictor variables				No significant predictor variables				No significant predictor variables				No significant predictor variables				No significant predictor variables					

**Table 6.6:** Stepwise multiple regression analysis with keratometry; keratometry and single scan videokeratometry (VK); composite of five videokeratometry; composite of nine videokeratometry; composite of five videokeratometry and anterior segment OCT (AS-OCT); composite of nine videokeratometry and anterior segment OCT variables

## 6.4 Discussion

This study examined whether compositing of corneal topographies from different versions of gaze would overcome the physical limitations of traditional Placido disc-based video keratoscopy resulting from the cone size and the protrusion of the nose, brows, eyelid and lashes. It then considered if significantly greater variance in lens fit could be accounted for using multiple topographical scans to enable better and a wider area quantification of the peripheral cornea and whether this would substitute for the additional information gained from OCT biometry of the corneoscleral topography. As both subjective and objective lens fit was analysed, in addition, the study could be used to confirm the results of Chapter 4 leading from the findings of Chapter 2, that objective assessment of lens fit would overcome some of the variance lost in the noise of subjective fit analysis.

As can be seen in Table 6.6 and as with the previous study in Chapter 2, central keratometry alone provided no predictive information as to variance in lens fit for either the HEMA or silicone hydrogel lenses. The addition of central video-keratoscopy, again as previously shown in Chapter 2 and by other studies (Young et al., 2010) started to explain some of the variance in lens fit for both the HEMA and the silicone hydrogel lens, but only in the order of 9-22%. The use of video compositing, as first described by Franklin et al (2006), but not previously implemented in a commercially available instrument, increased the maximum chord length of corneal topography that could be extracted in all meridians. It should be noted that the topographical assessment in the vertical meridian still remained significantly narrower than horizontally (Table 6.5), due mainly to the eyelids and lashes intervening with the Placido disc reflection. The fact that this difference still remains for the composite stitched images suggests that the limitation is related also to the difference in corneal diameter between the principal meridians, assuming typical values of 11.46 and 10.63 mm for the horizontal and vertical corneal diameters, respectively (Khng and Osher, 2008). Hence with compositing an increase of up to 16.8 to 18% of the horizontal corneal diameter can be topographically mapped and 19 to 20% of the vertical corneal diameter can be topographically mapped. This additional topographical area contributed to the amount of lens fit variance that could be explained in both the HEMA and the silicone hydrogel lenses, increasing this to between 10 and 77%. Interestingly, the compositing of nine topographical Placido images did not significantly impact on the area that could be extracted topographically, but in general decreased the amount of variance in lens fit that could be accounted for. This would suggest that the compositing algorithm was affected by the additional data, perhaps leading to erroneous artefacts. This was further confirmed the modelling of lens fit variance of composite topographies with OCT, which in Chapter 2

significantly improved the variance accounted for. As can be seen in Table 6.6, the modelling of both five and nine composited topographical images in combination with OCT further increased the variance of lens fit accounted for, but the impact was not as great proportionally as the variance accounted for using the composited map of five images alone.

Stiffer soft contact lenses, as has been shown previously in Chapter 2, were more influenced by anterior ocular topography than lower modulus lenses with up to approaching 90% of some lens fit variables being accounted for in the galyfilcon A silicone hydrogel material compared to approaching 60% in the etafilcon A HEMA material.

The amount of subjectively assessed lens fit variance that could be accounted for was generally less than that achieved for objective lens fit variables for both the HEMA and silicone hydrogel lenses. Consequently, the hypothesis derived from the lack of variance explained by the model including corneal and scleral ocular topography in Chapter 2, due to the variability of subjectively derived lens fit, has been shown to be the case once more.

## **6.5 Conclusion**

The compositing of images together from a conventional commercially available topographer provides significantly greater topography data over a wider corneal area leading to an improved ability to predict lens fit. There appears to be no significant benefit from conducting 9 compared to 5 scans, reducing the time required to achieve this advantage. Information regarding corneoscleral topography from OCT still has further benefit, advocating the need for instrumentation to rapidly assess these parameters in clinical practice; however data from a composited videokeratology map of five images yielded significantly greater data, and therefore predictive power, than that of single scan videokeratology alone.

# Chapter 7

## **Chapter 7: Thesis Discussion**

### **7.1 Introduction**

Contact lenses provide an affordable, convenient and cosmetically acceptable alternative to the correction of refractive error with spectacles. Soft contact lens fitting dominates the market and currently accounts for some 88% of new fits worldwide. Despite the high penetration of these remarkable medical devices, relatively little is still known to fully account for the variation in lens fit in, and between, different soft contact lens wearers. Various models have been proposed in an attempt to predict the lens, anterior eye parameters and physiological factors that influence soft lens fit dynamics, although these do not fully account for the total variation in lens fit observed and many basic questions remain unanswered.

Conventional biometry has proved inadequate in predicting soft contact lens fit. A number of workers (Gaggioni and Meier, 1987, Young et al., 2010, Young, 1992) have speculated that the corneoscleral profile will influence lens fit. Newer technologies have enabled the ocular surface to be characterised over a greater area and with greater precision than that previously possible.

The principal experimental theme of this thesis was to further identify factors affecting, and thus consequently better predict, variation in soft contact lens fit. A series of investigations were conducted in order to assess potential factors affecting lens fit using a variety of different imaging techniques.

### **7.2 Lens Fit and Variation**

AS-OCT has been used for the first time to both quantify and assess the influence of the corneoscleral topography on soft contact lens fit (Chapter 2). Ocular biometry data were measured using videokeratoscopy and AS-OCT, and associations were sought between ocular variables and soft lens fit. A number of significant correlations were noted between the peripheral ocular topography and fit, especially for the silicone hydrogel lens. The assessments of contact lens fit, however, were observational and this likely weakened the strength of the associations. Neither the use of keratometry or single scan videokeratoscopy added significantly to the prediction of lens fit. However, the incorporation of data gained from the AS-OCT characterisation of the peripheral topography allowed for increased prediction of that over of more conventional means.

The corneoscleral measurements acquired using AS-OCT were shown to be both accurate and repeatable. The least repeatable variable was that of scleral radius. Measurements were deliberately

taken over the anterior scleral (peri-limbal) face, since this area was considered of most interest and is the area where the edge of the soft contact lens skirt sits and is most likely required to flex to align to the corneoscleral profile. Determination of the scleral radius was achieved through the measurement of chords and sags using the Visante's built-in calipers and measurement tools; however, in assessing just the peri-limbal sclera, the chords measured were typically of small width and correspondingly small sagittal height, and therefore frequently difficult to measure. Retrospectively, the fitting of forced curves with bespoke software may have enabled a more accurate and repeatable determination of the peri-limbal scleral radius.

Given that the peripheral ocular topography was shown to influence lens fit, an understanding of the effect of any potential change in peripheral architecture variables as a result of body size (as dictated by height), and also eye size (as dictated by refractive error size, sex, ethnicity and ageing), might help clinically predict changes in lens fit. Consequently a large-cohort study was undertaken to assess the factors affecting the peripheral topography (Chapter 3). The use of AS-OCT in this study allowed for an objective quantification of the peripheral corneal profile as it transitions into the sclera, and substantive normative data was collected for a large sample size for future modeling of lens fit. The junction between the cornea and sclera is often portrayed as a sharp transition; however, the data presented in Chapter 3 showed that in many cases CSJ angles were within  $\pm 1^\circ$  of  $180^\circ$ , demonstrating an almost tangential extension of the cornea to form the peri-limbal sclera. The mean CSJ angle also tended to be sharpest at the nasal side and became progressively flatter at the inferior, temporal and superior junctions, demonstrating the asymmetric nature of the scleral face, as previously described by van der Worp et al. (2010).

Height and refractive error were both found to correlate with the ocular topography; however, height did not account for any of the variance in the CSP model. Of the factors examined, age was the most significant factor influencing ocular and CSP variables and consequently should be taken into consideration in contact lens design. Sex and ethnicity, were both found to influence ocular topography variables, although this study was limited to Caucasian and British Asians only. Future studies should address other ethnicities, particularly those with large and growing populations such as the Chinese and Hispanic ethnicities.

A sub aim of this thesis was to identify a more robust determination of corneal diameter. Automated assessment of corneal diameter is typically made based on the measurement of WTW, which itself is dependent on the highly variable nature of the transparency of the cornea. Any potential over- or underestimation of corneal diameter has implications in contact lens fitting since corneal sagittal height is so critically affected by changes in corneal diameter. The assessment of corneal diameter

using AS-OCT was significantly greater than that in the published literature, but also found to be repeatable. The use of the 'true' corneal diameter metric may be more applicable in certain circumstances and has application in the selection of IOLs.

Chapter 2 allowed for the prediction of up to 24% of the variance in contact lens fit; however, this still left approximately 75% of the variation in lens fit unaccounted for. It is likely that stronger associations and an increase in the modelled prediction of variance in fit may have occurred had an objective method of lens fit assessment been made. Consequently, a contact lens wearing study comparing subjective versus objective assessment of contact lens fit parameters was undertaken in Chapter 4, with the specific aim of assessing the repeatability of objective imaging, and for potential use in later experimental chapters.

The assessment of lens fit was dynamically captured using a digital video slit lamp system and the resulting video footage assessed both objectively and subjectively to ensure like-for-like comparison. Two experienced investigators then separately assessed the same footage for four main lens fit variables, so as to allow for a comparison of interobserver subjective fit assessment. The resulting video was objectively analysed by a separate masked observer by the same operator a week apart.

In general, the subjective assessment of lens fit showed a narrower range of readings and was not as repeatable as objective assessment. Consequently, the hypothesis that objective assessment of contact lens fit could provide the same key parameters as subjective evaluation, but have the advantages of being more repeatable as well as having higher resolution, was not proved to be correct. However, the limited range of values attributed by clinicians compared to that measured objectively, and the poor interobserver variability could still weaken associations between ocular topography and contact lens fit (Chapter 2). Consequently, objective assessment of lens fit was employed in subsequent chapters.

Although the corneoscleral topography had been shown to influence lens fit in Chapter 2, it seems likely that the same lens fit parameters may also be influenced by wearing time. The average duration of contact lens wear has been reported to be around 13-14 hours per day, although a sizeable minority of patients wear their lenses for 16 hours a day or more. However, comfortable wearing time is known to tail off in the last 1½ hours of wear. Previous studies have only assessed clinical lens performance after no more than 12 hours of wear. A novel study was undertaken in Chapter 5 to assess the influence of end of day fitting characteristics of silicone hydrogel lenses on ocular comfort, physiology and lens wettability, taking objective measures at 8, 12 and 16 hours after insertion. The

use of objective lens fit assessment showed that lens fit changes between 8 hours of wear and the end of the typical contact lens wearing day, and that consequently wearing time is an additional factor driving lens fit dynamics.

Multiple factors driving contact lens fit dynamics were identified in Chapters 2, 3 and 5. The use of AS-OCT in previous chapters had allowed for the characterisation of the anterior ocular topography (Chapters 2&3) and also prediction of up to 24% of the variance in lens fit. However, the cost of dedicated AS-OCT systems generally makes them available to research establishments, hospital environments and specialist optical practices.

An assessment of a new implementation of a more readily available and affordable technology for the determination of ocular topography and further determination of the variance in fit was carried out in Chapter 6. Placido disc videokeratoscopes are limited in the area of corneal coverage they can readily image, as described in Chapter 1. The implementation of compositing allows for the stitching of central and peripheral corneal topography maps for enhanced coverage of the cornea. The aim of the study was to determine if significantly greater variance in lens fit could be accounted for using multiple (composited) topographical scans and whether this would substitute for the additional information gained from OCT imaging of the cornea and corneoscleral profile. Additionally, the study sought to confirm the findings of Chapter 4, following on from Chapter 2, that objective assessment of lens fit would overcome some of the variance lost due to the noise inherent in subjective assessment. The use of compositing (using composites of both five and nine scans) provided for significantly greater corneal coverage in all meridians than that of single scan videokeratoscopy. The modelling of both five and nine composite scans in combination with OCT further increased the variance in lens fit that could be accounted for, at 83% and 89% of the variance post-blink movement for the silicone hydrogel, for the two composite scan types respectively. However, the modelling of lens fit using composite of five maps allowed for up to 77% of the variance, close to that in combination with OCT. An additional finding was that the modelling of composite of nine maps accounted for less of the variance in lens fit than with the composite of five, speeding up the acquisition and analysis process. Consequently, it was concluded that the use of composite videokeratoscopy might offer an affordable and viable alternative to OCT in busy, everyday working practice.

### **7.3 Instrumentation and Technology**

A sub-aim aim of this thesis was to assess those technologies used in this body of work and their suitability in context of both the research and practice-based environments.

The use of AS-OCT in Chapter 2 allowed for both a more complete characterisation of the cornea and corneoscleral profile than with conventional keratometry or videokeratoscopy alone, and allowed for prediction of some of the variance (up to 24%) in soft lens fit. The use of AS-OCT in combination with composited videokeratoscopy in Chapter 6 further allowed for the prediction of up to an extra 12% of the variance seen in lens fit over that using composited videokeratoscopy alone (83% vs. 77%). However, the acquisition and subsequent analysis of the OCT images in each case was time and labour intensive and not suited to everyday practice. The high cost of dedicated AS-OCT systems capable of capturing full corneal width, and also limited application compared to a hybrid OCT device capable of capturing both (limited) anterior segment width but also posterior segment, generally makes the ownership of such devices impractical for the average eye care practitioner. The use of enhanced videokeratoscopy, as implemented in the Medmont Studio 5, allowed for rapid assessment and for a similarly high prediction of lens fit variance than with dedicated AS-OCT but at substantially reduced cost. Consequently, it can be argued that the use of enhanced videokeratoscopy should be widely adopted in practice based settings. The market penetration of even single scan videokeratometers in the UK remains low, especially in comparison with other regions such as Europe and the United States. However, AS-OCT remains a powerful tool for the assessment of anterior ocular biometry and should not be discounted.

## **7.4 Clinical Implications**

The assessment of anterior ocular topography with AS-OCT devices such as the Zeiss Visante allows for the imaging of full corneal depth and width, to give 'true' corneal diameter and also sagittal height data. As long ago as 2001, André and co-workers (André et al., 2001) espoused the fitting of soft contact lenses based on corneal sagittal height. However, the trend in soft contact lens manufacturing in the last couple of decades has been to move almost exclusively away from offering multiple lens diameters (i.e. fitting by sagittal height) and offer one-lens-fits-all solutions instead. It seems likely that the lack of readily available measuring technologies, coupled with commercial expediency, may have accelerated this trend. In a case of evolution, rather than revolution, the availability of high speed, high resolution imaging instrumentation may facilitate a reversal in this trend. While the use of technologies such as AS-OCT and enhanced videokeratoscopy may provide empirical data for the fitting of all types of lenses (including soft, rigid and scleral lenses) in the present, it is envisaged that automated systems of topography measurement, coupled with an automated version of the objective lens fit system described in Chapter 4, may in future enhance the fitting of both more routine and specialised bespoke lenses in the future.

## 7.5 Conclusion

Various models have been put forward in an attempt to predict the lens and anterior eye parameters that influence soft contact lens fit dynamics; however, the factors that influence variation in soft lens fit are still not fully understood, as discussed in Chapter 1. The stated primary aim of this thesis was to identify further factors affecting, and thus better predict, such variation in lens fit. Using a variety of imaging techniques, this body of work has identified a number of different factors affecting lens fit, and has demonstrated an increased ability to predict variation (up to 90%) for some lens fit variables in comparison with standard techniques such as keratometry. However, it remains the case that a substantial amount of the variation in some lens fit variables remains unaccounted for. Consequently, it is hoped that this body will lead to further studies examining factors that influence soft contact lens dynamics, especially as new imaging technologies become available to researchers and eye care practitioners alike.

A sub-aim of this thesis was to identify a more robust measurement technique of corneal diameter using the imaging technologies utilised in this body of work. The assessment of corneal diameter using AS-OCT provided a robust method of determining corneal diameter which was not dependent upon the highly variable transparency of the peripheral cornea, as measured by WTW. The measure of 'true' corneal diameter has great potential application in both the contact lens and IOL fields.

Another sub-aim of this thesis was assess the use of differing imaging technologies employed in the body of the work. This thesis has successfully demonstrated the use of a range of imaging technologies to fulfil the primary aim of identifying factors driving variation in lens fit, and has further assessed the use of an affordable implementation of an existing technology in comparison with that of OCT.

## Bibliography

- ABAD, J. C., RUBINFELD, R. S., DEL VALLE, M., BELIN, M. W. & KURSTIN, J. M. 2007. Vertical D: a novel topographic pattern in some keratoconus suspects. *Ophthalmology*, 114, 1020-1026.
- AL-LATAYFEH, M. M., SUN, J. K. & AIELLO, L. P. 2010. Ocular coherence tomography and diabetic eye disease. *Semin Ophthalmol*, 25, 192-197.
- ALONSO-CANEIRO, D., ISKANDER, R. & COLLINS, M. 2008. Computationally efficient interference detection in videokeratotomy images. *Multimedia Signal Processing*, 486-490.
- AMIN, A. 2013. *Visante OCT Evaluation* [Online]. Available: <http://www.askdrash.com/visante-oct/> [Accessed 29<sup>th</sup> September 2013].
- ANDRÉ, M., DAVIS, J. & CAROLINE, P. 2001. A New Approach to Fitting Soft Contact Lenses. *Eyewitness*, Second Quarter 12-16.
- BAIKOFF, G. 2006. Anterior segment OCT and phakic intraocular lenses: A perspective. *J Cataract Refract Surg.*, 32, 1827–1835.
- BARR, J. 2000. The Contact Lens Spectrum Millennium Report. *Cont Lens Spect*, 15, 24-30.
- BAUMEISTER, M., TERZI, E., EKICI, Y. & KOHNEN, T. 2004. Comparison of manual and automated methods to determine horizontal corneal diameter. *J Cataract Refract Surg*, 30, 374-380.
- BEGLEY, C. G., CHALMERS, R. L., MITCHELL, G. L., NICHOLS, K. K., CAFFERY, B., SIMPSON, T., DUTOIT, R., PORTELLO, J. & DAVIS, L. 2001. Characterization of ocular surface symptoms from optometric practices in North America. *Cornea*, 20, 610-618.
- BEST, N., DRURY, L. & WOLFFSOHN, J. S. 2012. Clinical evaluation of the Oculus Keratograph. *Cont Lens Ant Eye*, 35, 171-174.
- BIBBY, M. 1979a. A model for lens flexure - validation and predictions. *Int Cont Lens Clin* 7, 124-138.
- BIBBY, M. M. 1979b. Sagittal depth considerations in the selection of the base curve radius of a soft contact lens. *Am J Optom Physiol Opt*, 56, 407-413.
- BIBBY, M. M. & TOMLINSON, A. 1983. A model to explain the effect of soft lens design specifications on movement. *Am J Optom Physiol Opt*, 60, 287-291.
- BIGELOW, C. E., IFTIMIA, N. V., FERGUSON, R. D., USTUN, T. E., BLOOM, B. & HAMMER, D. X. 2007. Compact multimodal adaptive-optics spectral-domain optical coherence tomography instrument for retinal imaging. *J Opt Soc Am A Opt Image Sci*, 24, 1327-1336.
- BLAND, J. M. & ALTMAN, D. G. 2010. Statistical methods for assessing agreement between two methods of clinical measurement. *Int J of Nurs Stud*, 47, 931–936.

- BOKERN, S., HOPPE, M. & BANDLITZ, S. 2007. [Accuracy and repeatability in the classification of the corneo-scleral profile]. *Die Kontaklinse*, 7, 26-28.
- BRENNAN, N. A., LINDSAY, R. G., MCCRAW, K., YOUNG, L., BRUCE, A. S. & GOLDING, T. R. 1994. Soft lens movement: temporal characteristics. *Optom Vis Sci*, 71, 359-363.
- BRUCE, A. 1994. Influence of corneal topography on centration and movement of low water content soft contact lenses. *Int Cont Lens Clin*, 21, 45-49.
- BUCKHURST, P. J., WOLFFSOHN, J. S., SHAH, S., NAROO, S. A., DAVIES, L. N. & BERROW, E. J. 2009. A new optical low coherence reflectometry device for ocular biometry in cataract patients. *Br J Ophthalmol*, 93, 949-953.
- BUEHL, W., STOJANAC, D., SACU, S., DREXLER, W. & FINDL, O. 2006. Comparison of three methods of measuring corneal thickness and anterior chamber depth. *Am J Ophthalmol*, 141, 7-12.
- BUSIN, M., WILMANN, I. & SPITZNAS, M. 1989. Automated corneal topography: computerized analysis of photokeratoscope images. *Graefe's Arch Clin Exp Ophthalmol* 27, 230-236.
- CARL ZEISS MEDITECH, I. 2009. Visante omni - A new dimension in anterior segment evaluation. *Manufacturer's literature*.
- CAROLINE, P. & ANDRÉ, M. 2010. Effects of Corneal Eccentricity. *Cont Lens Spect*, 25, 56.
- CAROLINE, P., ANDRÉ, M. & NORMAN, C. 1994. Corneal topography and computerised lens-fitting modules. *Int Cont Lens Clin*, 21, 185-195.
- CAROLINE, P. J. & ANDRÉ, M. P. 2002. The Effect of Corneal Diameter on Soft Lens Fitting, Part 1. *Cont Lens Spect*, 17, 62.
- CEDARSTAFF, T. H., TOMLINSON, A. & BIBBY, M. M. 1983. Validation of a model describing soft lens movement as a function of lens specification. *Am J Optom Physiol Opt*, 60, 292-296.
- CHO, P., LAM, A. K., MOUNTFORD, J. & NG, L. 2002. The performance of four different corneal topographers on normal human corneas and its impact on orthokeratology lens fitting. *Optom Vis Sci*, 79, 175-183.
- CLAUSEN, T. 1841. Beschreibung eines neuen Micrometers. *Astronomische Nachrichten*, 18, 95-96.
- CORBETT, M. C. 2000. Corneal topography – Basic principles and applications to refractive surgery (Part 2). *Optometry Today*, 50, 33-41.

- DAVIS, R. & BARRY EIDEN, S. 2011. Advanced Technology in Contact Lens Practice. *Cont Lens Spect*, 26, 24-29.
- DE CASTRO, A., ROSALES, P. & MARCOS, S. 2007. Tilt and decentration of intraocular lenses in vivo from Purkinje and Scheimpflug imaging. Validation study. *J Cataract Refract Surg*, 33, 418-429.
- DOUGHTY, M. J. & ZAMAN, M. L. 2000. Human corneal thickness and its impact on intraocular pressure measures: a review and meta-analysis approach. *Surv Ophthalmol*, 44, 367-408.
- DOUTHWAITE, W. A. 2002. Initial selection of soft contact lenses based on corneal characteristics. *CLAO J*, 28, 202-205.
- DUBBELMAN, M. & VAN DER HEIJDE, G. L. 2001. The shape of the aging human lens: curvature, equivalent refractive index and the lens paradox. *Vision Res*, 41, 1867-1877.
- DUMBLETON, K., WOODS, C., JONES, L., RICHTER, D. & FONN, D. 2010. Comfort and vision with silicone hydrogel lenses: effect of compliance. *Optom Vis Sci*, 87, 421-425.
- DUNNE, M., DAVIES, L. & WOLFFSOHN, J. 2007. Accuracy of cornea and lens biometry using Anterior Segment Optical Coherence Tomography. *J Biomed Opt*, 12, 064023.
- EFRON, N. 2010. Obituary--rigid contact lenses. *Cont Lens Ant Eye*, 33, 245-252.
- FENG, M. T., BELIN, M. W., AMBROSIO, R., JR., GREWAL, S. P., YAN, W., SHAHEEN, M. S., MCGHEE, C., MAEDA, N., NEUHANN, T. H., BURKHARD DICK, H., ALAGEEL, S. A. & STEINMUELLER, A. 2011. Anterior chamber depth in normal subjects by rotating scheimpflug imaging. *Saudi J Ophthalmol*, 25, 255-259.
- FENG, Y. & SIMPSON, T. L. 2005. Comparison of human central cornea and limbus in vivo using optical coherence tomography. *Optom Vis Sci*, 82, 416-419.
- FINK, W. 2005. Refractive correction method for digital charge-coupled device-recorded Scheimpflug photographs by means of ray tracing. *J Biomed Opt*, 10, 024003.
- FONN, D. & DUMBLETON, K. 2003. Dryness and discomfort with silicone hydrogel contact lenses. *Eye Cont Lens*, 29, S101-4; discussion S115-8, S192-194.
- FRANKLIN, R. J., MORELANDE, M. R., ISKANDER, D. R., COLLINS, M. J. & DAVIS, B. A. 2006. Combining central and peripheral videokeratoscope maps to investigate total corneal topography. *Eye Cont Lens*, 32, 27-32.
- FUKUDA, S., KAWANA, K., YASUNO, Y. & OSHIKA, T. 2010. Repeatability and reproducibility of anterior ocular biometric measurements with 2-dimensional and 3-dimensional optical coherence tomography. *J Cataract Refract Surg*, 36, 1867-1873.

- GAGGIONI, M. & MEIER, D. 1987. [The Corneo Scleral Profile]. *Neues Optiker*, 1, 66-71.
- GARNER, L. F. 1982. Sagittal height of the anterior eye and contact lens fitting. *Am J Optom Physiol Opt*, 59, 301-305.
- GATINEL, D., RACINE, L. & HOANG-XUAN, T. 2007. Contribution of the corneal epithelium to anterior corneal topography in patients having myopic photorefractive keratectomy. *J Cataract Refract Surg*, 33, 1860-1865.
- GEMOULES, G. 2008. A novel method of fitting scleral lenses using high resolution optical coherence tomography. *Eye Cont Lens*, 34, 80-83.
- GOLDING, T. R., BRUCE, A. S., GATERELL, L. L., LITTLE, S. A. & MACNAMARA, J. 1995. Soft lens movement: effect of blink rate on lens settling. *Acta Ophthalmol Scand*, 73, 506-511.
- GOLDSMITH, J. A., LI, Y., CHALITA, M. R., WESTPHAL, V., PATIL, C. A., ROLLINS, A. M., IZATT, J. A. & HUANG, D. 2005. Anterior chamber width measurement by high-speed optical coherence tomography. *Ophthalmology*, 112, 238-244.
- GOSS, D. & GERSTMAN, D. 2000. The optical science underlying the quantification of corneal contour. *Indiana J Optom*, 3, 13-16.
- GOTO, T., KLYCE, S. D., ZHENG, X., MAEDA, N., KURODA, T. & IDE, C. 2001. Gender- and age-related differences in corneal topography. *Cornea*, 20, 270-276.
- GUNDAL, R., COHEN, H. & DIVERGILLIO, D. 1986. Peripheral keratometry and soft contact lens fitting. *Int Eyecare*, 2, 611-613.
- GUTMARK, R. & GUYTON, D. L. 2010. Origins of the keratometer and its evolving role in ophthalmology. *Surv Ophthalmol*, 55, 481-497.
- HALL, L. A., HUNT, C., YOUNG, G. & WOLFFSOHN, J. 2013. Factors affecting corneoscleral topography. *Invest Ophthalmol Vis Sci*, 54, 3691-3701.
- HALL, L. A., YOUNG, G., WOLFFSOHN, J. S. & RILEY, C. 2011. The influence of corneoscleral topography on soft contact lens fit. *Invest Ophthalmol Vis Sci*, 52, 6801-6806.
- HANSEN, D. 2003. Evaluating the eye with corneal topography. *Cont Lens Spect*, 18, 27-32.
- HASHEMI, H., YAZDANI, K., MEHRAVARAN, S. & FOTOUHI, A. 2005. Anterior chamber depth measurement with a-scan ultrasonography, Orbscan II, and IOLMaster. *Optom Vis Sci*, 82, 900-904.
- HIRJI, N., PATEL, S. & CALLANDER, M. 1989. Human tear film pre-rupture phase time (TP-RPT)--a non-invasive technique for evaluating the pre-corneal tear film using a novel keratometer mire. *Ophthalmic Physiol Opt*, 9, 139-142.

- HO, T., CHENG, A. C., RAO, S. K., LAU, S., LEUNG, C. K. & LAM, D. S. 2007. Central corneal thickness measurements using Orbscan II, Visante, ultrasound, and Pentacam pachymetry after laser in situ keratomileusis for myopia. *J Cataract Refract Surg*, 33, 1177-1182.
- HOCHBERG, Y. & BENJAMINI, Y. 1990. More powerful procedures for multiple significance testing. *Stat Med*, 9, 811-818.
- HUANG, D., SWANSON, E., LIN, C., SCHUMAN, J., STINSON, W., CHANG, W., HEE, M., FLOTTE, T., GREGORY, K., PULIAFITO, C. & FUJIMOTO, J. 1991. Optical coherence tomography. *Science*, 254, 1178-1181.
- IBRAHIM, O. M., DOGRU, M., TAKANO, Y., SATAKE, Y., WAKAMATSU, T. H., FUKAGAWA, K., TSUBOTA, K. & FUJISHIMA, H. 2010. Application of visante optical coherence tomography tear meniscus height measurement in the diagnosis of dry eye disease. *Ophthalmology*, 117, 1923-1929.
- ISHIBAZAWA, A., IGARASHI, S., HANADA, K., NAGAOKA, T., ISHIKO, S., ITO, H. & YOSHIDA, A. 2011. Central corneal thickness measurements with Fourier-domain optical coherence tomography versus ultrasonic pachymetry and rotating Scheimpflug camera. *Cornea*, 30, 615-619.
- ISKANDER, D. R. & COLLINS, M. J. 2005. Applications of high-speed videokeratoscopy. *Clin Exp Optom*, 88, 223-231.
- ISKANDER, D. R., COLLINS, M. J. & READ, S. A. 2007. Extrapolation of central corneal topography into the periphery. *Eye Cont Lens*, 33, 293-299.
- IZATT, J. A., HEE, M. R., SWANSON, E. A., LIN, C. P., HUANG, D., SCHUMAN, J. S., PULIAFITO, C. A. & FUJIMOTO, J. G. 1994. Micrometer-scale resolution imaging of the anterior eye in vivo with optical coherence tomography. *Arch Ophthalmol*, 112, 1584-1589.
- JENKINS, J. T. & SHIMBO, M. 1984. The distribution of pressure behind a soft contact lens. *J Biomech Eng*, 106, 62-65.
- JONGSMA, F. H., DE BRABANDER, J., HENDRIKSE, F. & STULTIENS, B. A. 1998. Development of a wide field height eye topographer: validation on models of the anterior eye surface. *Optom Vis Sci*, 75, 69-77.
- JONUSCHEIT, S. & DOUGHTY, M. J. 2007. Regional repeatability measures of corneal thickness: Orbscan II and ultrasound. *Optom Vis Sci*, 84, 52-58.
- KALUZNY, B. J., KALUZNY, J. J., SZKULMOWSKA, A., GORCZYNSKA, I., SZKULMOWSKI, M., BAJRASZEWSKI, T., TARGOWSKI, P. & KOWALCZYK, A. 2006a. Spectral optical coherence tomography: a new imaging technique in contact lens practice. *Ophthalmic Physiol Opt*, 26, 127-132.
- KALUZNY, B. J., SZKULMOWSKA, A., KALUZNY, J. J., BAJRASZEWSKI, T., SZKULMOWSKI, M., KOWALCZYK, A. & WOJTKOWSKI, M. 2006b. In vivo imaging of

- posterior capsule opacification using Spectral Optical Coherence Tomography. *J Cataract Refract Surg*, 32, 1892-1895.
- KEIR, N., WOODS, C. A., DUMBLETON, K. & JONES, L. 2010. Clinical performance of different care systems with silicone hydrogel contact lenses. *Cont Lens Ant Eye*, 33, 189-195.
- KERR, C. & MCPARLAND, M. (eds.) 2013. *ACLM Market Report 2012: The Association of Contact Lens Manufacturers Ltd.*
- KHNG, C. & OSHER, R. H. 2008. Evaluation of the relationship between corneal diameter and lens diameter. *J Cataract Refract Surg*, 34, 475-479.
- KIKKAWA, Y. 1979. Kinetics of soft contact lens fitting. *Contacto*, 23, 10-17.
- KNOLL, H. A. & CONWAY, H. D. 1987. Analysis of blink-induced vertical motion of contact lenses. *Am J Optom Physiol Opt*, 64, 153-155.
- KNOP, E. & BREWITT, H. 1992. Conjunctival cytology in asymptomatic wearers of soft contact lenses. *Graefe's Arch Clin Exp Ophthalmol*, 230, 340-347.
- KOCH, D. D., FOULKS, G. N., MORAN, C. T. & WAKIL, J. S. 1989. The Corneal EyeSys System: accuracy analysis and reproducibility of first-generation prototype. *Refract Corneal Surg*, 5, 424-429.
- KONSTANTOPOULOS, A., HOSSAIN, P. & ANDERSON, D. F. 2007. Recent advances in ophthalmic anterior segment imaging: a new era for ophthalmic diagnosis? *Br J Ophthalmol*, 91, 551-557.
- KORB, D. R., HERMAN, J. P., BLACKIE, C. A., SCAFFIDI, R. C., GREINER, J. V., EXFORD, J. M. & FINNEMORE, V. M. 2010. Prevalence of lid wiper epitheliopathy in subjects with dry eye signs and symptoms. *Cornea*, 29, 377-383.
- KORETZ, J. E., STRENK, S. A., STRENK, L. M. & SEMMLOW, J. L. 2004. Scheimpflug and high-resolution magnetic resonance imaging of the anterior segment: a comparative study. *J Opt Soc Am A Opt Image Sci*, 21, 346-354.
- KOUASSI, F. X., BLAIZEAU, M., BUESTEL, C., SCHWEITZER, C., GALLOIS, A., COLIN, J. & TOUBOUL, D. 2012. [Comparison of Lasik with femtosecond laser versus Lasik with mechanical microkeratome: predictability of flap depth, corneal biomechanical effects and optical aberrations]. *J Fr Ophtalmol*, 35, 2-8.
- KUCUMEN, B. R., YENEREL, N. M., GORGUN, E. & DINC, U. A. 2010. Anterior segment optical coherence tomography findings of acute hydrops in a patient with keratoconus. *Ophthalmic Surg Lasers Imaging*, 41 Suppl, S114-116.
- KWOK, L. S. 1990. Measurement of corneal diameter. *Br J Ophthalmol*, 74, 63-64 (Letter to the editor).

- LATTIMORE, M. R., JR., KAUPP, S., SCHALLHORN, S. & LEWIS, R. T. 1999. Orbscan pachymetry: implications of a repeated measures and diurnal variation analysis. *Ophthalmology*, 106, 977-981.
- LESTER, S., HARRIS, M., KELLER, S. & LARSEN, D. 1994. Clinical applications of corneal topography. *Int Cont Lens Clin*, 21, 170-174.
- LEUNG, C. K., CHEUNG, C. Y., LI, H., DORAIRAJ, S., YIU, C. K., WONG, A. L., LIEBMANN, J., RITCH, R., WEINREB, R. & LAM, D. S. 2007a. Dynamic analysis of dark-light changes of the anterior chamber angle with anterior segment OCT. *Invest Ophthalmol Vis Sci*, 48, 4116-4122.
- LEUNG, C. K., PALMIERO, P. M., WEINREB, R. N., LI, H., SBEITY, Z., DORAIRAJ, S., LEUNG, D., LIU, S., LIEBMANN, J. M., CONGDON, N., LAM, D. S. & RITCH, R. 2010. Comparisons of anterior segment biometry between Chinese and Caucasians using anterior segment optical coherence tomography. *Br J Ophthalmol*, 94, 1184-1189.
- LEUNG, C. K., YICK, D. W., KWONG, Y. Y., LI, F. C., LEUNG, D. Y., MOHAMED, S., THAM, C. C., CHUNG-CHAI, C. & LAM, D. S. 2007b. Analysis of bleb morphology after trabeculectomy with Visante anterior segment optical coherence tomography. *Br J Ophthalmol*, 91, 340-344.
- LIM, L. S., AUNG, H. T., AUNG, T. & TAN, D. T. 2008. Corneal imaging with anterior segment optical coherence tomography for lamellar keratoplasty procedures. *Am J Ophthalmol*, 145, 81-90.
- LITTLE, S. A. & BRUCE, A. S. 1994. Hydrogel (Acuvue) lens movement is influenced by the postlens tear film. *Optom Vis Sci*, 71, 364-370.
- LIU, Z., HUANG, A. J. & PFLUGFELDER, S. C. 1999. Evaluation of corneal thickness and topography in normal eyes using the Orbscan corneal topography system. *Br J Ophthalmol*, 83, 774-778.
- LONG, B. & MCNALLY, J. 2006. The clinical performance of a silicone hydrogel lens for daily wear in an Asian population. *Eye Cont Lens*, 32, 65-71.
- LOWTHER, G. E. & TOMLINSON, A. 1981. Critical base curve and diameter interval in the fitting of spherical soft contact lenses. *Am J Optom Physiol Opt*, 58, 355-360.
- LUMBA, J. D. & HERSH, P. S. 2000. Topography changes associated with sublamellar epithelial ingrowth after laser in situ keratomileusis. *J Cataract Refract Surg*, 26, 1413-1416.
- MAGUIRE, L. J. & BOURNE, W. M. 1989. Corneal topography of early keratoconus. *Am J Ophthalmol*, 108, 107-112.
- MAGUIRE, L. J., KLYCE, S. D., MCDONALD, M. B. & KAUFMAN, H. E. 1987a. Corneal topography of pellucid marginal degeneration. *Ophthalmology*, 94, 519-524.

- MAGUIRE, L. J., SINGER, D. E. & KLYCE, S. D. 1987b. Graphic presentation of computer-analyzed keratoscope photographs. *Arch Ophthalmol*, 105, 223-230.
- MAISSA, C., GUILLON, M. & GAROFALO, R. J. 2012. Contact lens-induced circumlimbal staining in silicone hydrogel contact lenses worn on a daily wear basis. *Eye Cont Lens*, 38, 16-26.
- MALDONADO-CODINA, C. & EFRON, N. 2004. Impact of manufacturing technology and material composition on the clinical performance of hydrogel lenses. *Optom Vis Sci*, 81, 442-454.
- MALDONADO, M. J., NIETO, J. C., DIEZ-CUENCA, M. & PINERO, D. P. 2006. Repeatability and reproducibility of posterior corneal curvature measurements by combined scanning-slit and placido-disc topography after LASIK. *Ophthalmology*, 113, 1918-26.
- MALLEN, E. A., WOLFFSOHN, J. S., GILMARTIN, B. & TSUJIMURA, S. 2001. Clinical evaluation of the Shin-Nippon SRW-5000 autorefractor in adults. *Ophthalmic Physiol Opt*, 21, 101-107.
- MANDELL, R. B. 1962. Morphometry model of the human cornea. Phd Thesis, Indiana University. Pg 155.
- MARRIOTT, P. J. 1966. An analysis of the global contours and haptic contact lens fitting. *Br J Physiol Opt*, 23, 1-40.
- MARTIN, D. K., BOULOS, J., GAN, J., GAVRIEL, K. & HARVEY, P. 1989. A unifying parameter to describe the clinical mechanics of hydrogel contact lenses. *Optom Vis Sci*, 66, 87-91.
- MARTIN, D. K. & HOLDEN, B. A. 1982. A new method for measuring the diameter of the in vivo human cornea. *Am J Optom Physiol Opt*, 59, 436-441.
- MARTIN, D. K. & HOLDEN, B. A. 1986. Forces developed beneath hydrogel contact lenses due to squeeze pressure. *Phys Med Biol*, 31, 635-649.
- MARUYAMA, K., YOKOI, N., TAKAMATA, A. & KINOSHITA, S. 2004. Effect of environmental conditions on tear dynamics in soft contact lens wearers. *Invest Ophthalmol Vis Sci*, 45, 2563-2568.
- MATSUDA, L. M., WOLDORFF, C. L., KAME, R. T. & HAYASHIDA, J. K. 1992. Clinical comparison of corneal diameter and curvature in Asian eyes with those of Caucasian eyes. *Optom Vis Sci*, 69, 51-54.
- MCMNAMARA, N. A., POLSE, K. A., BRAND, R. J., GRAHAM, A. D., CHAN, J. S. & MCKENNEY, C. D. 1999. Tear mixing under a soft contact lens: effects of lens diameter. *Am J Ophthalmol*, 127, 659-665.
- MEIER, D. 1992. [Das corneo-skleral-profil-ein kriterium individueller kontaktlinsenanpassung]. *Die Kontaklinse*, 26, 4-11.

- MEJIA-BARBOSA, Y. & MALACARA-HERNANDEZ, D. 2001. A review of methods for measuring corneal topography. *Optom Vis Sci*, 78, 240-253.
- MIHALTZ, K., KOVACS, I., TAKACS, A. & NAGY, Z. Z. 2009. Evaluation of keratometric, pachymetric, and elevation parameters of keratoconic corneas with pentacam. *Cornea*, 28, 976-980.
- MORGAN, A. J., HARPER, J., HOSKING, S. L. & GILMARTIN, B. 2002. The effect of corneal thickness and corneal curvature on pneumatonometer measurements. *Curr Eye Res*, 25, 107-112.
- MORGAN, P., WOODS, C., TRANOUDIS, I., HELLAND, M., EFRON, N. & TEUFL, I. 2014. International Contact Lens Prescribing in 2013. *Cont Lens Spect*, 29, 30-35.
- MORGAN, P. B. & EFRON, N. 2002. Comparative clinical performance of two silicone hydrogel contact lenses for continuous wear. *Clin Exp Optom*, 85, 183-192.
- NANGIA, V., JONAS, J. B., MATIN, A., KULKARNI, M., SINHA, A. & GUPTA, R. 2010. Body height and ocular dimensions in the adult population in rural Central India. The Central India Eye and Medical Study. *Graefe's Arch Clin Exp Ophthalmol*, 248, 1657-1666.
- NAROO, S. A. 2011. Soft lenses certainly have the dominant market share and have many advantages over other lens types. *Cont Lens Ant Eye*, 34, 1.
- NEMETH, G., HASSAN, Z., SZALAI, E., BERTA, A. & MODIS, L., JR. 2010. Comparative analysis of white-to-white and angle-to-angle distance measurements with partial coherence interferometry and optical coherence tomography. *J Cataract Refract Surg*, 36, 1862-1866.
- NICHOLS, J. 2011. Contact Lenses 2010 - Annual Report *Cont Lens Spect*, 26, 24-28.
- NICHOLS, J. 2014. Contact Lenses 2013 - Annual Report. *Cont Lens Spect*, 29, 22-28.
- PAPAS, E. 1998. On the relationship between soft contact lens oxygen transmissibility and induced limbal hyperaemia. *Exp Eye Res*, 67, 125-131.
- PASCOLINI, D. & MARIOTTI, S. P. 2012. Global estimates of visual impairment: 2010. *Br J Ophthalmol*, 96, 614-618.
- PETERSON, R. C. & WOLFFSOHN, J. S. 2007. Sensitivity and reliability of objective image analysis compared to subjective grading of bulbar hyperaemia. *Br J Ophthalmol*, 91, 1464-1466.
- PETERSON, R. C., WOLFFSOHN, J. S., NICK, J., WINTERTON, L. & LALLY, J. 2006. Clinical performance of daily disposable soft contact lenses using sustained release technology. *Cont Lens Ant Eye*, 29, 127-134.
- PIERONI, C. G., WITKIN, A. J., KO, T. H., FUJIMOTO, J. G., CHAN, A., SCHUMAN, J. S., ISHIKAWA, H., REICHEL, E. & DUKER, J. S. 2006. Ultrahigh resolution optical coherence tomography in non-exudative age related macular degeneration. *Br J Ophthalmol*, 90, 191-197.

- PINERO, D. P., PLAZA PUCHE, A. B. & ALIO, J. L. 2008. Corneal diameter measurements by corneal topography and angle-to-angle measurements by optical coherence tomography: evaluation of equivalence. *J Cataract Refract Surg*, 34, 126-131.
- POP, M., PAYETTE, Y. & MANSOUR, M. 2001. Predicting sulcus size using ocular measurements. *J Cataract Refract Surg*, 27, 1033-1038.
- POTGIETER, F. J., ROBERTS, C., COX, I. G., MAHMOUD, A. M., HERDERICK, E. E., ROETZ, M. & STEENKAMP, W. 2005. Prediction of flap response. *J Cataract Refract Surg*, 31, 106-114.
- PRITCHARD, N. & FONN, D. 1995. Dehydration, lens movement and dryness ratings of hydrogel contact lenses. *Ophthalmic Physiol Opt*, 15, 281-286.
- PRITCHARD, N., FONN, D. & BRAZEAU, D. 1999. Discontinuation of contact lens wear: a survey. *Int Cont Lens Clin*, 26, 157-162.
- QIN, B., TANG, M., LI, Y., ZHANG, X., CHU, R. & HUANG, D. 2012. Anterior segment dimensions in Asian and Caucasian eyes measured by optical coherence tomography. *Ophthalmic Surg Lasers Imaging*, 43, 135-142.
- QIN, B., ZHOU, X. T., HUANG, D. & CHU, R. Y. 2011. Effects of age on ocular anterior segment dimensions measured by optical coherence tomography. *Chin Med J (Engl)*, 124, 1829-1834.
- RABINOWITZ, Y. S. 1996. Tangential vs sagittal videokeratographs in the "early" detection of keratoconus. *Am J Ophthalmol*, 122, 887-889.
- RAMSDEN, J. 1779. The description of two micrometers. *Phil Trans Royal Soc Lond*. 69; 419.
- RAY, W. A. & O'DAY, D. M. 1985. Statistical analysis of multi-eye data in ophthalmic research. *Invest Ophthalmol Vis Sci*, 26, 1186-1188.
- READ, S. A., COLLINS, M. J., CARNEY, L. G. & FRANKLIN, R. J. 2006. The topography of the central and peripheral cornea. *Invest Ophthalmol Vis Sci*, 47, 1404-1415.
- REYNOLDS, A. 1958. Corneal topography as found by photo-electronic-keratoscopy. *Contacto*, 3, 229-233.
- RILEY, C., CHALMERS, R. L. & PENCE, N. 2005. The impact of lens choice in the relief of contact lens related symptoms and ocular surface findings. *Cont Lens Ant Eye*, 28, 13-9.
- RILEY, C., YOUNG, G. & CHALMERS, R. 2006. Prevalence of ocular surface symptoms, signs, and uncomfortable hours of wear in contact lens wearers: the effect of refitting with daily-wear silicone hydrogel lenses (senofilcon a). *Eye Cont Lens*, 32, 281-286.
- ROSEMAN, M. J., FROST, A. & LAWLEY, M. E. 1993. Effects of base curve on the fit of thin, mid-water contact lenses. *Int Cont Lens Clin*, 20, 95-101.

- ROWSEY, J., REYNOLDS, A. & BROWN, R. 1981. Corneal topography. Corneoscope. *Arch Ophthalmol*, 99, 1093-1100.
- RUFER, F., SCHRODER, A. & ERB, C. 2005. White-to-white corneal diameter: normal values in healthy humans obtained with the Orbscan II topography system. *Cornea*, 24, 259-261.
- SAKATA, L. M., WONG, T. T., WONG, H. T., KUMAR, R. S., HTOON, H. M., AUNG, H. T., HE, M. & AUNG, T. 2010. Comparison of Visante and slit-lamp anterior segment optical coherence tomography in imaging the anterior chamber angle. *Eye*, 24, 578-87.
- SANTODOMINGO-RUBIDO, J., BARRADO-NAVASCUES, E. & RUBIDO-CRESPO, M. J. 2010. Ocular surface comfort during the day assessed by instant reporting in different types of contact and non-contact lens wearers. *Eye Cont Lens*, 36, 96-100.
- SCHAFFER, J. & BERNTSEN, D. A. 2006. Build Your Practice with Today's Corneal Topographers. *Optometric Management*, 41, 26-34.
- SCHWALLIE, J. D. & BAUMAN, R. E. 1998. Fitting characteristics of Dailies daily disposable hydrogel contact lenses. *CLAO J*, 24, 102-6.
- SELLERS, E. 1967. Biomicroscopy in contact lens practice. *Aust J Optom*, 50, 18-24.
- SHEN, M., WANG, M. R., WANG, J., YUAN, Y. & CHEN, F. 2010. Entire contact lens imaged in vivo and in vitro with spectral domain optical coherence tomography. *Eye Cont Lens*, 36, 73-6.
- SHEPPARD, A. L. & DAVIES, L. N. 2011. The effect of ageing on in vivo human ciliary muscle morphology and contractility. *Invest Ophthalmol Vis Sci*, 52, 1809-1816.
- SHERIDAN, M. 1989. Keratometry and slit lamp biomicroscopy *Contact Lenses: A Textbook for Practitioner and Student*, 243-259. London, Butterworth.
- SNYDER, A. 1984. Cosmetic extended-wear lenses: considering sagittal differences between the lens and eye. *Int Cont Lens Clin*, 11, 613-624.
- SORBARA, L., MARAM, J., FONN, D., WOODS, C. & SIMPSON, T. 2010. Metrics of the normal cornea: anterior segment imaging with the Visante OCT. *Clin Exp Optom*, 93, 150-156.
- SORBARA, L., PETERSON, R., WOODS, C. & FONN, D. 2009. Multipurpose disinfecting solutions and their interactions with a silicone hydrogel lens. *Eye Cont Lens*, 35, 92-97.
- SOWKA, J. W., GURWOOD, A. S. & KABAT, A. G. 2000. *Understanding Corneal Topography* [Online]. Jobson Publishing L.L.C. Available: <http://cms.revoptom.com/handbook/authors.htm> [Accessed 29<sup>th</sup> September 2013].
- SRINIVAS, K. R. & SUBRAMANIAM, R. 2008. *Corneal Topography - An Overview* [Online]. Available: <http://www.ejournalofophthalmology.com/ejo/ejo27.html> [Accessed 30<sup>th</sup> August 2013].

- SRIVANNABOON, S. & CHOTIKAVANICH, S. 2005. Corneal characteristics in myopic patients. *J Med Assoc Thai*, 88, 1222-1227.
- SWARTZ, T., MARTEN, L. & WANG, M. 2007. Measuring the cornea: the latest developments in corneal topography. *Curr Opin Ophthalmol*, 18, 325-333.
- SZCZOTKA, L. B. 2003. Corneal topography and contact lenses. *Ophthalmol Clin* 16, 433-453.
- SZCZOTKA, L. B., ROBERTS, C., HERDERICK, E. E. & MAHMOUD, A. 2002. Quantitative descriptors of corneal topography that influence soft toric contact lens fitting. *Cornea*, 21, 249-255.
- TAHIRI, J., DUPONT, M., OUKACHA, G., MANTOUT, F., BENRABAH, R., HERON, E. & BAUDOQUIN, C. 2010. Acute bilateral angle-closure glaucoma induced by topiramate: contribution of Visante OCT. *J Fr Ophtalmol*, 33, 307-311.
- TANG, W., COLLINS, M. J., CARNEY, L. & DAVIS, B. 2000. The accuracy and precision performance of four videokeratoscopes in measuring test surfaces. *Optom Vis Sci*, 77, 483-491.
- THEODORFF, C. & LOWTHER, G. 1990. Quantitative effect of optic zone diameter changes on rigid gas permeable lens movement and centration. *Int Cont Lens Clin*, 17, 92-95.
- THIBOS, L. N., WHEELER, W. & HORNER, D. 1997. Power vectors: an application of Fourier analysis to the description and statistical analysis of refractive error. *Optom Vis Sci*, 74, 367-375.
- TKACHOV, S. I., LAUTENSCHLAGER, C., EHRICH, D. & STRUCK, H. G. 2006. Changes in the lens epithelium with respect to cataractogenesis: light microscopic and Scheimpflug densitometric analysis of the cataractous and the clear lens of diabetics and non-diabetics. *Graefes Arch Clin Exp Ophthalmol*, 244, 596-602.
- TRANOUDIS, I. & EFRON, N. 2004a. In-eye performance of soft contact lenses made from different materials. *Cont Lens Ant Eye*, 27, 133-148.
- TRANOUDIS, I. & EFRON, N. 2004b. Parameter stability of soft contact lenses made from different materials. *Cont Lens Ant Eye*, 27, 115-131.
- USUI, T., TOMIDOKORO, A., MISHIMA, K., MATAKI, N., MAYAMA, C., HONDA, N., AMANO, S. & ARAIE, M. 2011. Identification of Schlemm's canal and its surrounding tissues by anterior segment fourier domain optical coherence tomography. *Invest Ophthalmol Vis Sci*, 52, 6934-6939.
- VAN BUSKIRK, E. M. 1989. The anatomy of the limbus. *Eye*, 3 (Pt 2), 101-108.
- VAN DER WORP, E., DE BRABANDER, J., SWARBRICK, H., NUIJTS, R. & HENDRIKSE, F. 2003. Corneal desiccation in rigid contact lens wear: 3- and 9-o'clock staining. *Optom Vis Sci*, 80, 280-290.

- VAN DER WERP, E., GRAF, T. & CAROLINE, P. 2010. Exploring Beyond the Corneal Borders. *Cont Lens Spect*, 25, 27-32.
- WANG, F., XU, G. Z., WANG, W. J. & JIANG, C. H. 2010. [Clinical observations of macular hole with and without retinal detachment in high myopic eyes]. [*Zhonghua yan ke za zhi*] *Chinese journal of ophthalmology*, 46, 508-12.
- WERNER, L., IZAK, A. M., PANDEY, S. K., APPLE, D. J., TRIVEDI, R. H. & SCHMIDBAUER, J. M. 2004. Correlation between different measurements within the eye relative to phakic intraocular lens implantation. *J Cataract Refract Surg*, 30, 1982-1988.
- WILLCOX, M., PHILLIPS, B., OZKAN, J., JALBERT, I., MEAGHER, L., GENGENBACH, T., HOLDEN, B. & PAPAS, E. 2010. Interactions of lens care and silicone hydrogel lenses and effect on comfort. *Optom Vis Sci* 87, 839-846.
- WILSON, S. E., KLYCE, S. D. & HUSSEINI, Z. M. 1993. Standardized color-coded maps for corneal topography. *Ophthalmology*, 100, 1723-1727.
- WOLFFSOHN, J. (ed.) 2008. *Ophthalmic imaging*, Edinburgh, London, New York, Oxford, Philadelphia, St Louis, Sydney, Toronto: Butterworth Heinemann Elsevier.
- WOLFFSOHN, J. S. & DAVIES, L. N. 2007a. Advances in anterior segment imaging. *Curr Opin Ophthalmol*, 18, 32-8.
- WOLFFSOHN, J. S. & DAVIES, L. N. 2007b. Advances in ocular imaging. *Exp Rev Ophthalmol*, 2, 755-767.
- WOLFFSOHN, J. S., HUNT, O. A. & BASRA, A. K. 2009. Simplified recording of soft contact lens fit. *Cont Lens Ant Eye*, 32, 37-42.
- WOLFFSOHN, J. S., HUNT, O. A. & CHOWDHURY, A. 2010. Objective clinical performance of 'comfort-enhanced' daily disposable soft contact lenses. *Cont Lens Ant Eye*, 33, 88-92.
- WOLFFSOHN, J. S. & PETERSON, R. C. 2006. Anterior ophthalmic imaging. *Clin Exp Optom*, 89, 205-214.
- WOLFFSOHN, J. S. & PURSLOW, C. 2003. Clinical monitoring of ocular physiology using digital image analysis. *Cont Lens Ant Eye*, 26, 27-35.
- YOUNG, G. 1992. Ocular sagittal height and soft contact lens fit. *J Br Cont Lens Assoc*, 15, 45-49.
- YOUNG, G. 1996. Evaluation of soft contact lens fitting characteristics. *Optom Vis Sci*, 73, 247-254.
- YOUNG, G. 2004. Why one million contact lens wearers dropped out. *Cont Lens Ant Eye*, 27, 83-85.

YOUNG, G. & COLEMAN, S. 2001. Poorly fitting soft lenses affect ocular integrity. *CLAO J*, 27, 68-74.

YOUNG, G., HOLDEN, B. & COOKE, G. 1993. Influence of soft contact lens design on clinical performance. *Optom Vis Sci*, 70, 394-403.

YOUNG, G., SCHNIDER, C., HUNT, C. & EFRON, S. 2010. Corneal topography and soft contact lens fit. *Optom Vis Sci*, 87, 358-366.

ZAR, J. H. 1984. *Biostatistical Analysis*. B16, 570-571. New Jersey. Prentice-Hall

**Appendix 1:  
Published Papers**

**HALL, L. A., YOUNG, G., WOLFFSOHN, J. S. & RILEY, C.** 2011. The influence of corneoscleral topography on soft contact lens fit. *Invest Ophthalmol Vis Sci*, 52, 6801-6806.

**HALL, L. A., HUNT, C., YOUNG, G. & WOLFFSOHN, J.** 2013. Factors affecting corneoscleral topography. *Invest Ophthalmol Vis Sci*, 54, 3691-3701.